Incremental displacement-correction schemes for incompressible fluid-structure interaction — Source link

Miguel Angel Fernández

Institutions: French Institute for Research in Computer Science and Automation

Related papers:

- Stable loosely-coupled-type algorithm for fluid-structure interaction in blood flow

- Fluid-structure interaction in blood flow capturing non-zero longitudinal structure displacement

- Added-mass effect in the design of partitioned algorithms for fluid-structure problems

- Fluid-structure partitioned procedures based on Robin transmission conditions

- A semi-implicit approach for fluid-structure interaction based on an algebraic fractional step method

Incremental displacement-correction schemes for incompressible fluid-structure interaction: stability and convergence analysis

Miguel Angel Fernández

Incremental displacement-correction schemes for incompressible fluid-structure interaction: stability and convergence analysis

Miguel A. Fernández

Incremental displacement-correction schemes for incompressible fluid-structure interaction: stability and convergence analysis

Miguel A. Fernández*

Project-Team REO

Abstract: In this paper we introduce a class of incremental displacement-correction schemes for the explicit coupling of a thin-structure with an incompressible fluid. These methods enforce a specific Robin-Neumann explicit treatment of the interface coupling. We provide a general stability and convergence analysis that covers both the incremental and the non-incremental variants. Their stability properties are independent of the added-mass effect. The superior accuracy of the incremental schemes (with respect to the original non-incremental variant) is highlighted by the error estimates, and then confirmed in a benchmark by numerical experiments.

Key-words: Fluid-structure interaction, Stokes equation, thin-solid, time-discretization, explicit coupling schemes, Robin-Neumann schemes,finite element method, error estimates

* e-mail: miguel.fernandez@inria.fr

Schémas avec correction de déplacement incrémentale pour l'interaction fluide-structure: stabilité et convergence

Résumé : Dans cet article nous introduisons une classe de schémas avec correction de déplacement incrémentale pour le couplage explicite d'une structure mince et d'un fluide incompressible. Ces méthodes imposent un traitement spécifique Robin-Neumann explicite du couplage à l'interface. Nous proposons une analyse générale de stabilité et de convergence, qui traite à la fois les variantes incrémentales et non-incrémentale. Leurs propriétés de stabilité sont indépendants de l'effet de masse ajoutée. La précision supérieure des schémas incrémentaux (par rapport à la variante originale non-incrémentale) est mise en évidence par des estimations d'erreur *a priori*, puis confirmée par des expériences numériques dans un cas test connu.

Mots-clés : Interaction fluide-structure, équation de Stokes, structure mince, discrétisation en temps, couplage explicite, schémas Robin-Neumann, méthode des éléments finis, estimations d'erreur.

1 Introduction

The stability of the numerical approximations of fluid-structure interaction problems, involving an incompressible fluid and an elastic structure, is very sensitive to the way the interface coupling conditions (kinematic and kinetic continuity) are treated at the discrete level. For instance, it is well known that the stability of explicit Dirichlet-Neumann coupling (or conventional *loosely coupled* schemes, i.e., that only involve the solution of the fluid and the structure once, or just a few times, per time step) is dictated by the amount of *added-mass effect* in the system (see, e.g., [11, 24]). In other words, a large fluid/solid density ratio combined with a slender and lengthy geometry gives rise to numerical instability, irrespectively of the discretization parameters. Examples in hemodynamics simulations are popular (see, e.g., [23]).

Stable explicit coupling alternatives, circumventing these infamous instabilities, have only recently been proposed in the literature. In [7, 9], stability is achieved through an appropriate weak treatment of the interface coupling and the addition of a weakly consistent interface compressibility term. For thin-solid models, the explicit coupling procedure introduced in [30, 29] combines the splitting of the time-marching in the solid with an implicit treatment of the fluid pressure and the hydrodynamic solid contributions (fully embedded into the fluid sub-step through a Robin boundary condition). Since the solid displacement is ignored in the fluid sub-step, this procedure can be interpreted as a *non-incremental* displacement-correction scheme (borrowing the terminology used for projection methods in fluids, see [28] for instance).

In this paper, we introduce a class of *incremental* displacement-correction schemes for the explicit coupling of a thin-structure with an incompressible fluid (the displacement is extrapolated in the first step and then corrected in the second). A salient feature of these schemes is that they can be formulated as Robin-Neumann explicit coupling schemes. In this sense, they have an intrinsic connexion with the Robin-Neumann implicit coupling solution framework introduced in [2]. Another remarkable property of these schemes is that they can be interpreted as interface kinematic perturbations of an underlying implicit coupling scheme. Thus, we present a general stability and convergence analysis that covers both the non-incremental and incremental variants and, also, the fully implicit case. The analysis shows, in particular, that the non-incremental scheme is expected to yield sub-optimal time-convergence in the energy norm; on the contrary, optimal accuracy is achieved with the proposed incremental schemes, without compromising stability. This enhanced accuracy is also illustrated with numerical experiments in a benchmark.

Although a number of works have been devoted to the convergence analysis of the numerical approximations of linear incompressible fluid-structure interaction problems (see [35, 15, 1]), none of them addresses the time-marching via an explicit coupling scheme. This is not surprising since, as remarked above, stable procedures of this kind have only recently been reported in the literature. Regarding the discretization in space, all the aforesaid works consider *inf-sup* stable finite element approximations for the fluid. Our analysis is also valid for pressure stabilized operators that are symmetric and weakly consistent (see [8]). This feature, besides its practical interest, requires the generalization of some valuable results from [31] that we report in appendix B.

This paper is organized as follows. The considered linear fluid-structure interaction model problem is described in Section 2. Its numerical approximation is introduced in Section 3. We present the space semi-discrete finite element setting in Subsection 3.1. Subsection 3.2 is devoted to the discretization in time. Here, a brief review of the available time-marching procedures precedes the introduction of our incremental displacement-correction schemes. Section 4 is devoted to the energy stability analysis. The *a priori* error estimates are derived in Section 5. Numerical experiments illustrating the theoretical results are presented in Section 6. At last, Section 7 contains some conclusions together with a few lines of future reserach.

Some preliminary results of this work have been announced, without proof, in [18].

2   A linear model problem

We consider a low Reynolds regime and assume that the structure undergoes infinitesimal displacements. The fluid is described by the Stokes equations in a polyhedral fixed domain $\Omega \subset \mathbb{R}^d$ ($d = 2, 3$). We consider a partition $\partial\Omega = \Gamma^{\mathrm{d}} \cup \Gamma^{\mathrm{n}} \cup \Sigma$ of the fluid boundary, where Σ stands for the fluid-structure interface. The structure is assumed to behave as a linear thin-solid (e.g., string, membrane) represented by the $(d-1)$-manifold Σ. Our simplified coupled problem reads therefore as follows: find the fluid velocity $\boldsymbol{u} : \Omega^{\mathrm{f}} \times \mathbb{R}^+ \to \mathbb{R}^d$, the fluid pressure $p : \Omega^{\mathrm{f}} \times \mathbb{R}^+ \to \mathbb{R}$, the solid displacement $\boldsymbol{d} : \Sigma \times \mathbb{R}^+ \to \mathbb{R}^d$ and the solid velocity $\dot{\boldsymbol{d}} : \Sigma \times \mathbb{R}^+ \to \mathbb{R}^d$ such that

$$\begin{cases} \rho^{\mathrm{f}} \partial_t \boldsymbol{u} - \mathbf{div}\boldsymbol{\sigma}(\boldsymbol{u}, p) = \boldsymbol{0} & \text{in} \quad \Omega, \\ \mathrm{div}\boldsymbol{u} = 0 & \text{in} \quad \Omega, \\ \boldsymbol{u} = \boldsymbol{0} & \text{on} \quad \Gamma^{\mathrm{d}}, \\ \boldsymbol{\sigma}(\boldsymbol{u}, p)\boldsymbol{n} = \boldsymbol{h} & \text{on} \quad \Gamma^{\mathrm{n}}, \end{cases} \tag{1}$$

$$\begin{cases} \boldsymbol{u} = \dot{\boldsymbol{d}} & \text{on} \quad \Sigma, \\ \dot{\boldsymbol{d}} = \partial_t \boldsymbol{d} & \text{on} \quad \Sigma, \\ \boldsymbol{d}(t) \in \boldsymbol{W}, \\ \rho^{\mathrm{s}}\epsilon \displaystyle\int_\Sigma \partial_t \dot{\boldsymbol{d}} \cdot \boldsymbol{w} + a^{\mathrm{e}}(\boldsymbol{d}, \boldsymbol{w}) = -\int_\Sigma \boldsymbol{\sigma}(\boldsymbol{u}, p)\boldsymbol{n} \cdot \boldsymbol{w} & \forall \boldsymbol{w} \in \boldsymbol{W}, \end{cases} \tag{2}$$

complemented with the initial conditions

$$\boldsymbol{u}(0) = \boldsymbol{u}^0, \quad \boldsymbol{d}(0) = \boldsymbol{d}^0, \quad \dot{\boldsymbol{d}}(0) = \dot{\boldsymbol{d}}^0.$$

Here, ρ^{f} and ρ^{s} respectively denote the fluid and solid densities, and ϵ the solid thickness. The fluid Cauchy-stress tensor is given by

$$\boldsymbol{\sigma}(\boldsymbol{u}, p) \stackrel{\mathrm{def}}{=} -p\boldsymbol{I} + 2\mu\boldsymbol{\epsilon}(\boldsymbol{u}), \quad \boldsymbol{\epsilon}(\boldsymbol{u}) \stackrel{\mathrm{def}}{=} \frac{1}{2}\left(\boldsymbol{\nabla}\boldsymbol{u} + \boldsymbol{\nabla}\boldsymbol{u}^{\mathrm{T}}\right),$$

where μ stands for the fluid dynamic viscosity. The exterior unit-vector normal to $\partial\Omega$ is denoted by $\boldsymbol{n}$ and $\boldsymbol{h}$ represents a given surface force. At last, the abstract bilinear form $a^{\mathrm{e}} : \boldsymbol{W} \times \boldsymbol{W} \to \mathbb{R}$ describes the elastic behavior of the structure and $\boldsymbol{W}$ stands for its space of admissible displacements.

The relations $(2)_1$ and $(2)_4$ enforce the so-called kinematic and kinetic interface coupling conditions, respectively. Note that the latter represents also the variational formulation of the structure. Though simplified, problem (1)-(2) features some of the main numerical issues that appear in complex nonlinear fluid-structure interaction problems involving an incompressible fluid (see, e.g., [11, 17]).

2.1   Monolithic variational formulation

In what follows, we will consider the usual Sobolev spaces $H^m(\omega)$ ($m \geq 0$), with norm $\|\cdot\|_{m,\omega}$. The closed subspaces $H_0^1(\omega)$, consisting of functions in $H^1(\omega)$ with zero trace on $\partial\omega$, and $L_0^2(\omega)$, consisting of function in $L^2(\omega)$ with zero mean in ω, will also be used. The scalar product

in $L^2(\omega)$ is denoted by $(\cdot, \cdot)_\omega$ and its norm by $\|\cdot\|_{0,\omega}$. In order to ease the notation, we set $(\cdot, \cdot) \stackrel{\text{def}}{=} (\cdot, \cdot)_\Omega$.

We assume that a^{e} is an inner-product into $\boldsymbol{W} \subset [H^1_0(\Sigma)]^d$ and that, endowed with this inner-product, $\boldsymbol{W}$ is a Hilbert space. We set

$$\|\boldsymbol{w}\|_{\mathrm{e}} \stackrel{\text{def}}{=} \left(a^{\mathrm{e}}(\boldsymbol{w}, \boldsymbol{w})\right)^{\frac{1}{2}}$$

and we assume that the following continuity estimate holds

$$\|\boldsymbol{w}\|^2_{\mathrm{e}} \leq \beta^{\mathrm{e}} \|\boldsymbol{w}\|^2_{1,\Sigma} \tag{3}$$

for all $\boldsymbol{w} \in \boldsymbol{W}$. The strong formulation of the thin-solid elastic contribution is supposed to be given in terms of a densely defined, self-adjoint and unbounded linear operator $\boldsymbol{L}^{\mathrm{e}} : \boldsymbol{D}^{\mathrm{e}} \subset [L^2(\Sigma)]^d \to [L^2(\Sigma)]^d$, such that

$$\left(\boldsymbol{L}^{\mathrm{e}}\boldsymbol{d}, \boldsymbol{w}\right)_\Sigma = a^{\mathrm{e}}\left(\boldsymbol{d}, \boldsymbol{w}\right) \tag{4}$$

for all $\boldsymbol{d} \in \boldsymbol{D}^{\mathrm{e}}$ and $\boldsymbol{w} \in \boldsymbol{W}$. We recall that, endowed with the graph-norm

$$\|\boldsymbol{d}\|_{\boldsymbol{D}^{\mathrm{e}}} \stackrel{\text{def}}{=} \left(\|\boldsymbol{d}\|^2_{0,\Sigma} + \|\boldsymbol{L}^{\mathrm{e}}\boldsymbol{d}\|^2_{0,\Sigma}\right)^{\frac{1}{2}},$$

the subspace $\boldsymbol{D}^{\mathrm{e}}$ is a Banach space.

We also introduce the fluid velocity and pressure functional spaces

$$\boldsymbol{V} \stackrel{\text{def}}{=} \left\{\boldsymbol{v} \in [H^1(\Omega)]^d \,/\, \boldsymbol{v}|_{\Gamma^{\mathrm{d}}} = \boldsymbol{0}\right\}, \quad \boldsymbol{V}_\Sigma \stackrel{\text{def}}{=} \left\{\boldsymbol{v} \in \boldsymbol{V} \,/\, \boldsymbol{v}|_\Sigma = \boldsymbol{0}\right\}$$

and $Q \stackrel{\text{def}}{=} L^2(\Omega)$, equipped with the norms

$$\|\boldsymbol{v}\|_{\boldsymbol{V}} \stackrel{\text{def}}{=} \|\mu^{\frac{1}{2}} \boldsymbol{\nabla} \boldsymbol{v}\|_{0,\Omega}, \quad \|q\|_Q = \|\mu^{-\frac{1}{2}} q\|_{0,\Omega}.$$

At last, the standard bilinear forms for the Stokes problem, $a : \boldsymbol{V} \times \boldsymbol{V} \to \mathbb{R}$ and $b : Q \times \boldsymbol{V} \to \mathbb{R}$, given by

$$a(\boldsymbol{u}, \boldsymbol{v}) \stackrel{\text{def}}{=} 2\mu\left(\boldsymbol{\epsilon}(\boldsymbol{u}), \boldsymbol{\epsilon}(\boldsymbol{v})\right), \quad b(q, \boldsymbol{v}) \stackrel{\text{def}}{=} -(q, \mathrm{div}\boldsymbol{v}),$$

will be used.

Problem (1)-(2) can then be rewritten in variational form as follows: for $t > 0$, find

$$\left(\boldsymbol{u}(t), p(t), \dot{\boldsymbol{d}}(t), \boldsymbol{d}(t)\right) \in \boldsymbol{V} \times Q \times [L^2(\Sigma)]^d \times \boldsymbol{W},$$

such that

$$\begin{cases} \boldsymbol{u}|_\Sigma = \dot{\boldsymbol{d}}, \\ \dot{\boldsymbol{d}} = \partial_t \boldsymbol{d}, \\ \rho^{\mathrm{f}}\left(\partial_t \boldsymbol{u}, \boldsymbol{v}\right) + a(\boldsymbol{u}, \boldsymbol{v}) + b(p, \boldsymbol{v}) - b(q, \boldsymbol{u}) + \rho^{\mathrm{s}}\epsilon\left(\partial_t \dot{\boldsymbol{d}}, \boldsymbol{w}\right)_\Sigma + a^{\mathrm{e}}(\boldsymbol{d}, \boldsymbol{w}) \\ \qquad = (\boldsymbol{h}, \boldsymbol{v})_{\Gamma^{\mathrm{n}}} \end{cases} \tag{5}$$

for all $(\boldsymbol{v}, q, \boldsymbol{w}) \in \boldsymbol{V} \times Q \times \boldsymbol{W}$ with $\boldsymbol{v}|_\Sigma = \boldsymbol{w}$.

Well-posedness results for this type of linear fluid-structure interaction problems can be found in [35] (see also [14]).

3   Displacement-correction explicit coupling schemes

In this section we address the numerical approximation of the coupled problem (5). The proposed time-marching procedures (Algorithms 4–5 below) allow an uncoupled sequential computation of the fluid and solid discrete approximations (explicit coupling scheme). Finite elements are used for the discretization in space. Through this paper, the symbols $\lesssim$ and $\gtrsim$ will indicate inequalities up to a multiplicative constant (independent of the physical and discretization parameters).

3.1   Space discretization

Let $\{\mathcal{T}_h\}_{0<h\leq 1}$ denote a family of triangulations of Ω. For each triangulation $\mathcal{T}_h$, the subscript $h \in (0,1]$ refers to the level of refinement of the triangulation, which is defined by $h \stackrel{\mathrm{def}}{=} \max_{K\in\mathcal{T}_h} h_K$, with h_K the diameter of K. In order to simplify the presentation, we assume that the family of triangulations is quasi-uniform. In what follows, we let X_h and M_h denote, respectively, the standard spaces of continuous and (possibly) discontinuous piecewise polynomial functions of degree $k \geq 1$ and $l \geq 0$ ($k-1 \leq l \leq k$):

$$\begin{aligned}
X_h &\stackrel{\mathrm{def}}{=} \left\{ v_h \in C^0(\overline{\Omega}) \,/\, v_{h|K} \in \mathbb{P}_k(K) \quad \forall K \in \mathcal{T}_h \right\}, \\
M_h &\stackrel{\mathrm{def}}{=} \left\{ q_h \in Q \,/\, q_{h|K} \in \mathbb{P}_l(K) \quad \forall K \in \mathcal{T}_h \right\}.
\end{aligned} \tag{6}$$

For the approximation of the fluid velocity we will consider the space $\boldsymbol{V}_h \stackrel{\mathrm{def}}{=} [X_h]^d \cap \boldsymbol{V}$ and for the pressure we will use either $Q_h \stackrel{\mathrm{def}}{=} M_h$ or $Q_h \stackrel{\mathrm{def}}{=} M_h \cap C^0(\overline{\Omega})$. We also set $\boldsymbol{V}_{\Sigma,h} \stackrel{\mathrm{def}}{=} \boldsymbol{V}_h \cap \boldsymbol{V}_\Sigma$. Whenever the considered velocity/pressure pair fails to satisfy the standard inf-sup condition (see, e.g., [27]), we assume that there exists a pressure stabilization operator,

$$s_h : Q_h \times Q_h \to \mathbb{R}, \tag{7}$$

satisfying the properties stated in Section 3.1.1 below. The discrete space for the solid displacement and velocity is chosen as the trace space

$$\boldsymbol{W}_h \stackrel{\mathrm{def}}{=} \left\{ \boldsymbol{v}_h|_\Sigma \,/\, \boldsymbol{v}_h \in \boldsymbol{V}_h \right\} \cap \boldsymbol{W}.$$

Hence, the fluid and solid space discretizations match at the interface. At last, we introduce the standard fluid-sided discrete lifting operator $\boldsymbol{\mathcal{L}}_h : \boldsymbol{W}_h \to \boldsymbol{V}_h$, such that, the nodal values of $\boldsymbol{\mathcal{L}}_h \boldsymbol{w}_h$ vanish out of Σ and $(\boldsymbol{\mathcal{L}}_h \boldsymbol{w}_h)|_\Sigma = \boldsymbol{w}_h$, for all $\boldsymbol{w}_h \in \boldsymbol{W}_h$.

Our space semi-discrete approximation of (5) reads as follows: for $t > 0$, find

$$\left(\boldsymbol{u}_h(t), p_h(t), \dot{\boldsymbol{d}}_h(t), \boldsymbol{d}_h(t) \right) \in \boldsymbol{V}_h \times Q_h \times \boldsymbol{W}_h \times \boldsymbol{W}_h,$$

such that

$$\begin{cases}
\boldsymbol{u}_h|_\Sigma = \dot{\boldsymbol{d}}_h, \\
\dot{\boldsymbol{d}}_h = \partial_t \boldsymbol{d}_h, \\
\rho^{\mathrm{f}}\left(\partial_t \boldsymbol{u}_h, \boldsymbol{v}_h\right) + a(\boldsymbol{u}_h, \boldsymbol{v}_h) + b(p_h, \boldsymbol{v}_h) - b(q_h, \boldsymbol{u}_h) + s_h(p_h, q_h) \\
\quad + \rho^{\mathrm{s}}\epsilon\left(\partial_t \dot{\boldsymbol{d}}_h, \boldsymbol{w}_h\right)_\Sigma + a^{\mathrm{e}}(\boldsymbol{d}_h, \boldsymbol{w}_h) = (\boldsymbol{h}, \boldsymbol{v}_h)_{\Gamma^{\mathrm{n}}}
\end{cases} \tag{8}$$

for all $(\boldsymbol{v}_h, q_h, \boldsymbol{w}_h) \in \boldsymbol{V}_h \times Q_h \times \boldsymbol{W}_h$ with $\boldsymbol{v}_h|_\Sigma = \boldsymbol{w}_h$.

Equivalently, using the following decomposition of the test space

$$\begin{aligned}
\left\{ (\boldsymbol{v}_h, \boldsymbol{w}_h) \in \boldsymbol{V}_h \times \boldsymbol{W}_h \,/\, \boldsymbol{v}_h|_\Sigma = \boldsymbol{w}_h \right\} = {}& \left\{ (\boldsymbol{v}_h, \boldsymbol{0}) \,/\, \boldsymbol{v}_h \in \boldsymbol{V}_{\Sigma,h} \right\} \\
& \oplus \left\{ (\boldsymbol{\mathcal{L}}_h \boldsymbol{w}_h, \boldsymbol{w}_h) \,/\, \boldsymbol{w}_h \in \boldsymbol{W}_h \right\},
\end{aligned}$$

the monolithic formulation (8) can be reformulated in a partitioned Dirichlet-Neumann fashion as: for $t > 0$,

- Fluid: find $\big(\boldsymbol{u}_h(t), p_h(t)\big) \in \boldsymbol{V}_h \times Q_h$, such that

$$
\begin{cases}
\boldsymbol{u}_h|_\Sigma = \dot{\boldsymbol{d}}_h, \\
\rho^{\mathrm{f}}\big(\partial_t \boldsymbol{u}_h, \boldsymbol{v}_h\big) + a(\boldsymbol{u}_h, \boldsymbol{v}_h) + b(p_h, \boldsymbol{v}_h) - b(q_h, \boldsymbol{u}_h) + s_h(p_h, q_h) \\
\quad = (\boldsymbol{h}, \boldsymbol{v}_h)_{\Gamma^{\mathrm{n}}}
\end{cases}
\tag{9}
$$

for all $(\boldsymbol{v}_h, q_h) \in \boldsymbol{V}_{\Sigma,h} \times Q_h$.

- Solid: find $\big(\dot{\boldsymbol{d}}_h(t), \boldsymbol{d}_h(t)\big) \in \boldsymbol{W}_h \times \boldsymbol{W}_h$, such that

$$
\begin{cases}
\dot{\boldsymbol{d}}_h = \partial_t \boldsymbol{d}_h, \\
\rho^{\mathrm{s}} \epsilon \big(\partial_t \dot{\boldsymbol{d}}_h, \boldsymbol{w}_h\big)_\Sigma + a^{\mathrm{e}}(\boldsymbol{d}_h, \boldsymbol{w}_h) \\
\quad = -\rho^{\mathrm{f}}\big(\partial_t \boldsymbol{u}_h, \boldsymbol{\mathcal{L}}_h \boldsymbol{w}_h\big) - a(\boldsymbol{u}_h, \boldsymbol{\mathcal{L}}_h \boldsymbol{w}_h) - b(p_h, \boldsymbol{\mathcal{L}}_h \boldsymbol{w}_h)
\end{cases}
\tag{10}
$$

for all $\boldsymbol{w}_h \in \boldsymbol{W}_h$.

3.1.1 Symmetric pressure stabilizations

We assume that the pressure stabilization bilinear form (7) satisfies the following properties (see [8]):

- Symmetry and positiveness:

$$
s_h(p_h, q_h) = s_h(q_h, p_h), \quad s_h(q_h, q_h) \geq 0 \quad \forall p_h, q_h \in Q_h.
\tag{11}
$$

In particular, we set $|q_h|_{s_h} \overset{\mathrm{def}}{=} \sqrt{s_h(q_h, q_h)}$.

- Continuity:

$$
|s_h(p_h, q_h)| \leq |p_h|_{s_h} |q_h|_{s_h} \quad \forall p_h, q_h \in Q_h.
\tag{12}
$$

- Consistency:

$$
|\Pi_h q|_{s_h} \lesssim \mu^{-\frac{1}{2}} h^{\tilde{l}} \|q\|_{\tilde{l},\Omega} \quad \forall q \in H^{\tilde{l}}(\Omega),
\tag{13}
$$

with $l \leq \tilde{l} \leq l + 1$ denoting the order of weak consistency of the stabilization operator, and $\Pi_h : Q \to Q_h$ a given projection operator such that

$$
\|q - \Pi_h q\|_Q \lesssim \mu^{-\frac{1}{2}} h^{l+1} \|q\|_{l+1,\Omega} \quad \forall q \in H^{l+1}(\Omega).
\tag{14}
$$

- Generalized Fortin's criterion: there exists a projection operator $\boldsymbol{\mathcal{F}}_h : [H_0^1(\Omega)]^d \to \boldsymbol{V}_h \cap [H_0^1(\Omega)]^d$ such that:

$$
\|\boldsymbol{\mathcal{F}}_h \boldsymbol{v}\|_{\boldsymbol{V}} \lesssim \|\boldsymbol{v}\|_{\boldsymbol{V}}, \quad b(q_h, \boldsymbol{v} - \boldsymbol{\mathcal{F}}_h \boldsymbol{v}) \lesssim |q_h|_{s_h} \|\boldsymbol{v}\|_{\boldsymbol{V}}
\tag{15}
$$

for all $\boldsymbol{v} \in [H_0^1(\Omega)]^d$ and $q_h \in Q_h \cap L_0^2(\Omega)$.

Examples of stabilization methods entering this abstract framework are discussed in [8, Section 3.1.1] (see also Section 6 below). Among them, we can mention the Orthogonal Sub-scales Stabilization [13], the Local Projection Stabilization [4] and the Continuous Interior Penalty method [10], which are optimal for arbitrary polynomial order.

Remark 3.1 *If the velocity/pressure finite-element pair is inf-sup stable, we can take $s_h = 0$ in (8), as usual. Obviously, this choice is compatible with the hypothesis (11)-(15), in this case (15) becomes the so-called Fortin criterion (see, e.g, [5]). Hence, the results reported in Sections 4 and 5 below will also apply.* $\diamondsuit$

3.1.2   Discrete solid operators

Through this paper, we will make extensive use of the discrete reconstruction of the solid elastic operator, $\boldsymbol{L}_h^{\mathrm{e}} : \boldsymbol{W} \to \boldsymbol{W}_h$, defined, for all $\boldsymbol{w} \in \boldsymbol{W}$, as

$$
\begin{cases}
\boldsymbol{L}_h^{\mathrm{e}} \boldsymbol{w} \in \boldsymbol{W}_h, \\
\left(\boldsymbol{L}_h^{\mathrm{e}} \boldsymbol{w}, \boldsymbol{w}_h \right)_\Sigma = a^{\mathrm{e}}(\boldsymbol{w}, \boldsymbol{w}_h) \quad \forall \boldsymbol{w}_h \in \boldsymbol{W}_h.
\end{cases}
\tag{16}
$$

We introduce also the Ritz-projector, $\boldsymbol{\pi}_h^{\mathrm{e}} : \boldsymbol{W} \to \boldsymbol{W}_h$, such that, for all $\boldsymbol{w} \in \boldsymbol{W}$, we have

$$
\begin{cases}
\boldsymbol{\pi}_h^{\mathrm{e}} \boldsymbol{w} \in \boldsymbol{W}_h, \\
a^{\mathrm{e}}\!\left(\boldsymbol{\pi}_h^{\mathrm{e}} \boldsymbol{w}, \boldsymbol{w}_h \right) = a^{\mathrm{e}}\!\left(\boldsymbol{w}, \boldsymbol{w}_h \right) \quad \forall \boldsymbol{w}_h \in \boldsymbol{W}_h.
\end{cases}
\tag{17}
$$

For further reference in the paper, some standard properties of these two operators are stated in the next lemma.

Lemma 3.2   • *For all $\boldsymbol{w} \in \boldsymbol{W}$, there holds*

$$
\|\boldsymbol{\pi}_h^{\mathrm{e}} \boldsymbol{w}\|_{\mathrm{e}} \leq \|\boldsymbol{w}\|_{\mathrm{e}}.
\tag{18}
$$

Moreover, under the regularity assumption $\boldsymbol{w} \in \boldsymbol{D}^{\mathrm{e}}$, we have

$$
\|\boldsymbol{L}_h^{\mathrm{e}} \boldsymbol{w}\|_{0,\Sigma} \leq \|\boldsymbol{L}^{\mathrm{e}} \boldsymbol{w}\|_{0,\Sigma}.
\tag{19}
$$

• *There holds:*

$$
\boldsymbol{L}_h^{\mathrm{e}} \boldsymbol{\pi}_h^{\mathrm{e}} = \boldsymbol{L}_h^{\mathrm{e}}.
\tag{20}
$$

• *For all $\boldsymbol{w}_h \in \boldsymbol{W}_h$, we have*

$$
\|\boldsymbol{w}_h\|_{\mathrm{e}}^2 \leq \frac{\beta^{\mathrm{e}} C_{\mathrm{inv}}^2}{h^2} \|\boldsymbol{w}_h\|_{0,\Sigma}^2,
\tag{21}
$$

where $C_{\mathrm{inv}} > 0$ is the constant of an inverse estimate.

• *For all $\boldsymbol{w}_h \in \boldsymbol{W}_h$, we have*

$$
\|\boldsymbol{L}_h^{\mathrm{e}} \boldsymbol{w}_h\|_{\mathrm{e}} \leq \frac{\beta^{\mathrm{e}} C_{\mathrm{inv}}^2}{h^2} \|\boldsymbol{w}_h\|_{\mathrm{e}},
\tag{22}
$$

$$
\|\boldsymbol{L}_h^{\mathrm{e}} \boldsymbol{w}_h\|_{0,\Sigma} \leq \frac{(\beta^{\mathrm{e}})^{\frac{1}{2}} C_{\mathrm{inv}}}{h} \|\boldsymbol{w}_h\|_{\mathrm{e}}.
\tag{23}
$$

Proof. The details are given in appendix A.◇

3.2   Time discretization

This section is devoted to the time discretization of the space semi-discrete formulation (8). We first briefly review the different coupling schemes that can be found in the literature. The proposed incremental displacement-correction explicit coupling schemes are then introduced in Subsection 3.2.2. In what follows, the parameter τ denotes the time-step size, $t_n \stackrel{\mathrm{def}}{=} n\tau$, for $n \in \mathbb{N}$, and

$$
\partial_\tau x^n \stackrel{\mathrm{def}}{=} \frac{1}{\tau}\big(x^n - x^{n-1} \big),
$$

stands for the first-order backward difference.

3.2.1 State-of-the-art at a glance

One of the most elementary time-marching procedures (perhaps the most popular in the aero-elastic community, see, e.g., [39]) is the Dirichlet-Neumann explicit coupling scheme reported in Algorithm 1. It is based on the explicit treatment of the kinematic constraint in (9) and the fully implicit time discretization of the kinetic relation (10). For the sake of simplicity, a backward-Euler time-discretization has been considered for both the fluid and the structure. Algorithm 1 is very appealing in terms of computational cost, since it allows a fully uncoupled (sequential) solution of the discrete problem. It is well known, however, that this kind of time-marching procedure is unstable under certain choices of the physical parameters (see, e.g., [37, 36, 11, 24]). Typically, this happens when the fluid and solid densities are comparable or when the domain has a slender shape (strong added-mass effect), irrespectively of the time-step size τ. Blood flows are a popular example of such a situation. Theoretical explanations of this issue can be found in [11] (see also [24]).

Algorithm 1 Dirichlet-Neumann explicit coupling scheme.

For $n \geq 1$:

1. Fluid: find $\left(\boldsymbol{u}_h^n, p_h^n\right) \in \boldsymbol{V}_h \times Q_h$, such that

$$
\begin{cases}
\boldsymbol{u}_h^n|_\Sigma = \dot{\boldsymbol{d}}_h^{n-1}, \\
\rho^{\mathrm{f}}\left(\partial_\tau \boldsymbol{u}_h^n, \boldsymbol{v}_h\right) + a(\boldsymbol{u}_h^n, \boldsymbol{v}_h) + b(p_h^n, \boldsymbol{v}_h) - b(q_h, \boldsymbol{u}_h^n) + s_h(p_h^n, q_h) \\
\quad = (\boldsymbol{h}(t_n), \boldsymbol{v}_h)_{\Gamma^{\mathrm{n}}}
\end{cases}
\tag{24}
$$

   for all $(\boldsymbol{v}_h, q_h) \in \boldsymbol{V}_{\Sigma,h} \times Q_h$.

2. Solid: find $\left(\dot{\boldsymbol{d}}_h^n, \boldsymbol{d}_h^n\right) \in \boldsymbol{W}_h \times \boldsymbol{W}_h$, such that

$$
\begin{cases}
\dot{\boldsymbol{d}}_h^n = \partial_\tau \boldsymbol{d}_h^n, \\
\rho^{\mathrm{s}}\epsilon\left(\partial_\tau \dot{\boldsymbol{d}}_h^n, \boldsymbol{w}_h\right)_\Sigma + a^{\mathrm{e}}(\boldsymbol{d}_h^n, \boldsymbol{w}_h) \\
\quad = -\rho^{\mathrm{f}}\left(\partial_\tau \boldsymbol{u}_h^n, \boldsymbol{\mathcal{L}}_h \boldsymbol{w}_h\right) - a(\boldsymbol{u}_h^n, \boldsymbol{\mathcal{L}}_h \boldsymbol{w}_h) - b(p_h^n, \boldsymbol{\mathcal{L}}_h \boldsymbol{w}_h)
\end{cases}
\tag{25}
$$

   for all $\boldsymbol{w}_h \in \boldsymbol{W}_h$.

Traditionally, these numerical instabilities have been circumvented by considering fully implicit time-discretizations of (8). For instance, as shown in Algorithm 2. The payoff of the enhanced stability is, however, the resolution of the coupled system (28) at each time-step, which can be computationally demanding. Particularly, due to the hybrid characteristics of the system, since general thin-solid models discretized by finite elements are known to lead to ill-conditioned system matrices requiring specific solvers (see, e.g. [26]).

Remark 3.3 *Note that* (28) *involves the following implicit time discretization of* (2)$_4$:

$$
\boldsymbol{\sigma}(\boldsymbol{u}^n, p^n)\boldsymbol{n} + \frac{\rho^{\mathrm{s}}\epsilon}{\tau}\boldsymbol{u}^n = \frac{\rho^{\mathrm{s}}\epsilon}{\tau}\dot{\boldsymbol{d}}^{n-1} - \boldsymbol{L}^{\mathrm{e}}\boldsymbol{d}^n \quad on \quad \Sigma.
\tag{26}
$$

As noticed in [38], we can eliminate $\boldsymbol{d}^n$ *via the identity* $\boldsymbol{d}^n = \boldsymbol{d}^{n-1} + \tau\boldsymbol{u}^n|_\Sigma$ *from* (28)$_{1,2}$, *yielding*

$$
\boldsymbol{\sigma}(\boldsymbol{u}^n, p^n)\boldsymbol{n} + \left(\frac{\rho^{\mathrm{s}}\epsilon}{\tau} + \tau\boldsymbol{L}^{\mathrm{e}}\right)\boldsymbol{u}^n = \frac{\rho^{\mathrm{s}}\epsilon}{\tau}\dot{\boldsymbol{d}}^{n-1} - \boldsymbol{L}^{\mathrm{e}}\boldsymbol{d}^{n-1} \quad on \quad \Sigma.
\tag{27}
$$

This relation is a non-standard Robin boundary condition for the fluid, unless the operator $\boldsymbol{L}^{\mathrm{e}}$ is purely algebraic (see [38]). ◇

Alternative stable (and less computationally onerous) time-marching procedures are the semi-implicit coupling schemes reported in [19, 20, 41, 3]. These methods, based on the use of a fractional-step scheme in the fluid, treat explicitly the viscous-structure coupling (which reduces computational cost) and implicitly the pressure-structure coupling (which guarantees stability).

Algorithm 2 Implicit coupling scheme.

For $n \geq 1$, find $\left(\boldsymbol{u}_h^n, p_h^n, \dot{\boldsymbol{d}}_h^n, \boldsymbol{d}_h^n\right) \in \boldsymbol{V}_h \times Q_h \times \boldsymbol{W}_h \times \boldsymbol{W}_h$, such that

$$
\begin{cases}
\boldsymbol{u}_h^n|_\Sigma = \dot{\boldsymbol{d}}_h^n, \\
\dot{\boldsymbol{d}}_h^n = \partial_\tau \boldsymbol{d}_h^n, \\
\rho^{\mathrm{f}}\left(\partial_\tau \boldsymbol{u}_h^n, \boldsymbol{v}_h\right) + a(\boldsymbol{u}_h^n, \boldsymbol{v}_h) + b(p_h^n, \boldsymbol{v}_h) - b(q_h, \boldsymbol{u}_h^n) + s_h(p_h^n, q_h) \\
\quad + \rho^{\mathrm{s}}\epsilon\left(\partial_\tau \dot{\boldsymbol{d}}_h^n, \boldsymbol{w}_h\right)_\Sigma + a^{\mathrm{e}}(\boldsymbol{d}_h^n, \boldsymbol{w}_h) = (\boldsymbol{h}(t_n), \boldsymbol{v}_h)_{\Gamma^{\mathrm{n}}}
\end{cases} \tag{28}
$$

for all $(\boldsymbol{v}_h, q_h, \boldsymbol{w}_h) \in \boldsymbol{V}_h \times Q_h \times \boldsymbol{W}_h$ with $\boldsymbol{v}_h|_\Sigma = \boldsymbol{w}_h$.

In the *stabilized* explicit coupling scheme reported in [7, 9], stability is achieved via a specific Robin-Robin explicit treatment of the interface coupling conditions (derived from the Nitsche interface method, see [32]) and the addition of a time penalty on the interface pressure fluctuations (weakly consistent interface compressibility). The stability of the scheme is independent of the fluid and solid time discretizations (and of the added-mass effect). The price to pay is a perturbation of the truncation error, whose leading term scales as $\mathcal{O}(\tau/h)$. Defect-correction iterations are therefore needed to enhance accuracy, under restrictive constraints on the discretization parameters.

In the framework of the coupling with a thin-solid model, a second stable explicit coupling alternative is given by the *kinematically coupled* scheme introduced in [30, 29]. Applied to (8), this procedure yields the fully discrete formulation reported in Algorithm 3. Instead of $(24)_1$, the fluid sub-step (29) involves the following explicit interface Robin condition:

$$
\boldsymbol{\sigma}(\boldsymbol{u}^n, p^n)\boldsymbol{n} + \frac{\rho^{\mathrm{s}}\epsilon}{\tau}\boldsymbol{u}^n = \frac{\rho^{\mathrm{s}}\epsilon}{\tau}\dot{\boldsymbol{d}}^{n-1} \quad \text{on} \quad \Sigma. \tag{31}
$$

Note that (31) and (30) correspond to the following fractional-step time discretization of the solid momentum equation $(2)_4$:

$$
\begin{cases}
\dfrac{\rho^{\mathrm{s}}\epsilon}{\tau}(\boldsymbol{u}^n - \dot{\boldsymbol{d}}^{n-1}) = -\boldsymbol{\sigma}(\boldsymbol{u}^n, p^n)\boldsymbol{n} \quad \text{on} \quad \Sigma, \\[2mm]
\dfrac{\rho^{\mathrm{s}}\epsilon}{\tau}(\dot{\boldsymbol{d}}^n - \boldsymbol{u}^n) + \boldsymbol{L}^{\mathrm{e}}\boldsymbol{d}^n = \boldsymbol{0} \quad \text{on} \quad \Sigma,
\end{cases} \tag{32}
$$

where $\boldsymbol{u}^n|_\Sigma$ and $\dot{\boldsymbol{d}}^n$ stand for the intermediate and the end-of-step solid velocities, respectively. This solid time splitting allows to:

1. treat implicitly the fluid-solid hydrodynamic coupling (fluid stresses and solid inertia contributions), via (29) (or $(32)_1$);

2. explicitly couple the solid end-of-step velocity and elastic contributions with the fluid, via (30) (or $(32)_2$).

Algorithm 3 Kinematically coupled scheme (from [30, 29]).

For $n \geq 1$:

1. Fluid: find $(\boldsymbol{u}_h^n, p_h^n) \in \boldsymbol{V}_h \times Q_h$ with $\boldsymbol{u}_h^n|_\Sigma \in \boldsymbol{W}_h$, such that

$$\rho^{\mathrm{f}}\big(\partial_\tau \boldsymbol{u}_h^n, \boldsymbol{v}_h\big) + a\big(\boldsymbol{u}_h^n, \boldsymbol{v}_h\big) + b\big(p_h^n, \boldsymbol{v}_h\big) - b\big(q_h, \boldsymbol{u}_h^n\big) + s_h\big(p_h^n, q_h\big)$$
$$+ \frac{\rho^{\mathrm{s}}\epsilon}{\tau}\big(\boldsymbol{u}_h^n, \boldsymbol{v}_h\big)_\Sigma = \frac{\rho^{\mathrm{s}}\epsilon}{\tau}\big(\dot{\boldsymbol{d}}_h^{n-1}, \boldsymbol{v}_h\big)_\Sigma + \big(\boldsymbol{h}(t_n), \boldsymbol{v}_h\big)_{\Gamma^{\mathrm{n}}} \quad (29)$$

   for all $(\boldsymbol{v}_h, q_h) \in \boldsymbol{V}_h \times Q_h$ with $\boldsymbol{v}_h|_\Sigma \in \boldsymbol{W}_h$.

2. Solid: find $\big(\dot{\boldsymbol{d}}_h^n, \boldsymbol{d}_h^n\big) \in \boldsymbol{W}_h \times \boldsymbol{W}_h$, such that

$$\begin{cases} \dot{\boldsymbol{d}}_h^n = \partial_\tau \boldsymbol{d}_h^n, \\ \dfrac{\rho^{\mathrm{s}}\epsilon}{\tau}\big(\dot{\boldsymbol{d}}_h^n, \boldsymbol{w}_h\big)_\Sigma + a^{\mathrm{e}}(\boldsymbol{d}_h^n, \boldsymbol{w}_h) = \dfrac{\rho^{\mathrm{s}}\epsilon}{\tau}\big(\boldsymbol{u}_h^n, \boldsymbol{w}_h\big)_\Sigma \end{cases} \quad (30)$$

   for all $\boldsymbol{w}_h \in \boldsymbol{W}_h$.

The first point guarantees stability, while the second reduces the computational complexity.

It is worth noting that, contrary to (26), the displacement (or elastic contribution) is ignored in the fluid sub-step (29) through the explicit Robin condition (31) (or (32)$_1$). As a result, Algorithm 3 can be interpreted as a *non-incremental* displacement-correction scheme, borrowing the terminology used for projection methods in fluids (see [28, Section 3], for instance). This observation indicates that the accuracy of the scheme might be sub-optimal in time (see Remark 3.8 below). In the next subsection, we introduce and discuss two incremental variants of Algorithm 3 that yield optimal accuracy, without compromising stability.

Remark 3.4 *From the above discussion, Algorithm 3 can also be considered a semi-implicit coupling scheme (e.g., in the spirit of [20]), in the sense that it performs an implicit-explicit splitting of the fluid-solid coupling via a fractional-step time-marching of the solid (instead of the fluid as, e.g., in [20]). Nevertheless, since the solid is thin, the implicit part (32) of the coupling can be fully embedded into the fluid sub-step through a Robin boundary condition and, hence, the coupling scheme becomes fully explicit. An extension of this explicit coupling paradigm to the case of thick-solid models can be found in [21].* ◊

Remark 3.5 *In the interface terms of (29), we have made a slight abuse of notation by using $\boldsymbol{u}_h^n$ and $\boldsymbol{v}_h$, instead of $\boldsymbol{u}_h^n|_\Sigma$ and $\boldsymbol{v}_h|_\Sigma$.* ◊

3.2.2 Incremental displacement-correction schemes

In this paper, we propose to discretize in time the finite element formulation (8) via an incremental displacement-correction scheme. In these time-marching procedures, the approximation of (8) is split into two sequential sub-steps: the solid displacement is treated explicitly in the first and it is then corrected in the second. The proposed fully discrete schemes are detailed in Algorithm 4, where

$$\boldsymbol{d}_h^\star = \boldsymbol{d}_h^{n-1}, \quad \boldsymbol{d}_h^\star = \boldsymbol{d}_h^{n-1} + \tau \dot{\boldsymbol{d}}_h^{n-1}, \quad (35)$$

are the first- and second-order displacement extrapolations, respectively.

Algorithm 4 Incremental displacement-correction explicit coupling schemes.

For $n \geq 1$:

1. Fluid: find $(\boldsymbol{u}_h^n, p_h^n) \in \boldsymbol{V}_h \times Q_h$ with $\boldsymbol{u}_h^n|_\Sigma \in \boldsymbol{W}_h$, such that

$$\rho^{\mathrm{f}}\big(\partial_\tau \boldsymbol{u}_h^n, \boldsymbol{v}_h\big) + a\big(\boldsymbol{u}_h^n, \boldsymbol{v}_h\big) + b\big(p_h^n, \boldsymbol{v}_h\big) - b\big(q_h, \boldsymbol{u}_h^n\big) + s_h\big(p_h^n, q_h\big)$$
$$+ \frac{\rho^{\mathrm{s}}\epsilon}{\tau}\big(\boldsymbol{u}_h^n, \boldsymbol{v}_h\big)_\Sigma = \frac{\rho^{\mathrm{s}}\epsilon}{\tau}\big(\dot{\boldsymbol{d}}_h^{n-1}, \boldsymbol{v}_h\big)_\Sigma - a^{\mathrm{e}}(\boldsymbol{d}_h^\star, \boldsymbol{v}_h) + (\boldsymbol{h}(t_n), \boldsymbol{v}_h)_{\Gamma^{\mathrm{n}}} \quad (33)$$

   for all $(\boldsymbol{v}_h, q_h) \in \boldsymbol{V}_h \times Q_h$ with $\boldsymbol{v}_h|_\Sigma \in \boldsymbol{W}_h$.

2. Solid: $\big(\dot{\boldsymbol{d}}_h^n, \boldsymbol{d}_h^n\big) \in \boldsymbol{W}_h \times \boldsymbol{W}_h$, such that

$$\begin{cases} \dot{\boldsymbol{d}}_h^n = \partial_\tau \boldsymbol{d}_h^n, \\ \dfrac{\rho^{\mathrm{s}}\epsilon}{\tau}\big(\dot{\boldsymbol{d}}_h^n, \boldsymbol{w}_h\big)_\Sigma + a^{\mathrm{e}}(\boldsymbol{d}_h^n, \boldsymbol{w}_h) = \dfrac{\rho^{\mathrm{s}}\epsilon}{\tau}\big(\boldsymbol{u}_h^n, \boldsymbol{w}_h\big)_\Sigma + a^{\mathrm{e}}(\boldsymbol{d}_h^\star, \boldsymbol{w}_h) \end{cases} \quad (34)$$

   for all $\boldsymbol{w}_h \in \boldsymbol{W}_h$.

Without displacement extrapolation, that is, $\boldsymbol{d}_h^\star = \boldsymbol{0}$, Algorithm 4 yields the non-incremental scheme reported in Algorithm 3. As mentioned above, this scheme was termed kinematically coupled, since it treats implicitly the hydro-dynamic fluid-solid coupling (the so-called added-mass effect) and explicitly the solid elastic contribution. Algorithm 4 admits, in addition, two alternative interpretations which are discussed thereafter.

Robin-Neumann explicit coupling schemes. Taking $\boldsymbol{v}_h = \boldsymbol{\mathcal{L}}_h \boldsymbol{w}_h$ and $q_h = 0$ in (33) and adding the resulting expression to (34) yields the Neumann-like solid problem (25). Therefore, Algorithm 4 can be reformulated in a equivalent manner by replacing (34) with the solid sub-step (25). This yields the genuine Robin-Neumann explicit coupling scheme reported in Algorithm 5.

Although Algorithms 4 and 5 are exactly the same explicit coupling scheme, the latter formulation is preferred in practice since it involves a more standard solid problem (i.e., displacement extrapolations are only present in the fluid sub-step). In fact, Algorithm 5 involves the following Robin-Neumann time-marching on the interface:

$$\begin{cases} \boldsymbol{\sigma}(\boldsymbol{u}^n, p^n)\boldsymbol{n} + \dfrac{\rho^{\mathrm{s}}\epsilon}{\tau}\boldsymbol{u}^n = \dfrac{\rho^{\mathrm{s}}\epsilon}{\tau}\dot{\boldsymbol{d}}^{n-1} - \boldsymbol{L}^{\mathrm{e}}\boldsymbol{d}^\star & \text{on} \quad \Sigma, \\ \rho^{\mathrm{s}}\epsilon\partial_\tau \dot{\boldsymbol{d}}^n + \boldsymbol{L}^{\mathrm{e}}\boldsymbol{d}^n = -\boldsymbol{\sigma}(\boldsymbol{u}^n, p^n)\boldsymbol{n} & \text{on} \quad \Sigma. \end{cases} \quad (36)$$

Obviously, for $\boldsymbol{d}^\star = \boldsymbol{0}$, we recover (31) from $(36)_1$ and Algorithm 3 is also equivalent to Algorithm 5. In passing, it is worth mentioning that this feature has been disregarded in [30, 29].

Note that, by introducing the velocity prediction

$$\partial_\tau \boldsymbol{d}^\star \overset{\text{def}}{=} \frac{1}{\tau}(\boldsymbol{d}^\star - \dot{\boldsymbol{d}}^{n-1}),$$

the Robin condition $(36)_1$ can be equivalently rewritten as

$$\boldsymbol{\sigma}(\boldsymbol{u}^n, p^n)\boldsymbol{n} + \alpha\boldsymbol{u}^n = \alpha\partial_\tau \boldsymbol{d}^\star - \left[\frac{\rho^{\mathrm{s}}\epsilon}{\tau}\left(\partial_\tau \boldsymbol{d}^\star - \dot{\boldsymbol{d}}^{n-1}\right) + \boldsymbol{L}^{\mathrm{e}}\boldsymbol{d}^\star\right] \quad \text{on} \quad \Sigma,$$

Algorithm 5 Robin-Neumann formulation of Algorithm 4.

For $n \geq 1$:

1. Fluid: find $(\boldsymbol{u}_h^n, p_h^n) \in \boldsymbol{V}_h \times Q_h$ with $\boldsymbol{u}_h^n|_\Sigma \in \boldsymbol{W}_h$, such that

$$\rho^{\mathrm{f}}\big(\partial_\tau \boldsymbol{u}_h^n, \boldsymbol{v}_h\big) + a\big(\boldsymbol{u}_h^n, \boldsymbol{v}_h\big) + b\big(p_h^n, \boldsymbol{v}_h\big) - b\big(q_h, \boldsymbol{u}_h^n\big) + s_h\big(p_h^n, q_h\big)$$
$$+ \frac{\rho^{\mathrm{s}}\epsilon}{\tau}\big(\boldsymbol{u}_h^n, \boldsymbol{v}_h\big)_\Sigma = \frac{\rho^{\mathrm{s}}\epsilon}{\tau}\big(\dot{\boldsymbol{d}}_h^{n-1}, \boldsymbol{v}_h\big)_\Sigma - a^{\mathrm{e}}(\boldsymbol{d}_h^\star, \boldsymbol{v}_h) + (\boldsymbol{h}(t_n), \boldsymbol{v}_h)_{\Gamma^{\mathrm{n}}}$$

for all $(\boldsymbol{v}_h, q_h) \in \boldsymbol{V}_h \times Q_h$ with $\boldsymbol{v}_h|_\Sigma \in \boldsymbol{W}_h$.

2. Solid: find $\big(\dot{\boldsymbol{d}}_h^n, \boldsymbol{d}_h^n\big) \in \boldsymbol{W}_h \times \boldsymbol{W}_h$, such that

$$\begin{cases} \dot{\boldsymbol{d}}_h^n = \partial_\tau \boldsymbol{d}_h^n, \\ \rho^{\mathrm{s}}\epsilon\big(\partial_\tau \dot{\boldsymbol{d}}_h^n, \boldsymbol{w}_h\big)_\Sigma + a^{\mathrm{e}}(\boldsymbol{d}_h^n, \boldsymbol{w}_h) = -\rho^{\mathrm{f}}\big(\partial_\tau \boldsymbol{u}_h^n, \boldsymbol{\mathcal{L}}_h \boldsymbol{w}_h\big) - a(\boldsymbol{u}_h^n, \boldsymbol{\mathcal{L}}_h \boldsymbol{w}_h) - b(p_h^n, \boldsymbol{\mathcal{L}}_h \boldsymbol{w}_h) \end{cases}$$

for all $\boldsymbol{w}_h \in \boldsymbol{W}_h$.

---

with

$$\alpha \overset{\mathrm{def}}{=} \frac{\rho^{\mathrm{s}}\epsilon}{\tau}. \tag{37}$$

Therefore, each step of Algorithm 5 corresponds to the first iteration, initialized with $\boldsymbol{d}^\star$, of the Robin-Neumann iterative procedure reported in [2], with an alternative Robin-parameter α. In fact, only inertial effects are present in (37) since Algorithm 5 treats explicit the whole elastic contribution of the solid, as usual in explicit coupling schemes.

Remark 3.6 *It is worth emphasizing that the Robin-Neumann procedures introduced in [2] have been originally devised to iterate until convergence, with the aim of retrieving (in a partitioned fashion) the numerical solution of implicit coupling schemes (e.g., of the coupled problem (28)). To the best of our knowledge, this is the first time that these kind of solution procedures are considered as explicit coupling schemes (i.e., only one iteration is performed per time-step) with sound mathematical foundations.* $\diamond$

Kinematic perturbations of implicit coupling. Taking $\boldsymbol{v}_h|_\Sigma = \boldsymbol{w}_h$ in (33) and adding the resulting expression to (34), yields

$$\begin{cases} \dot{\boldsymbol{d}}_h^n = \partial_\tau \boldsymbol{d}_h^n, \\ \rho^{\mathrm{f}}\big(\partial_\tau \boldsymbol{u}_h^n, \boldsymbol{v}_h\big) + a\big(\boldsymbol{u}_h^n, \boldsymbol{v}_h\big) + b\big(p_h^n, \boldsymbol{v}_h\big) - b\big(q_h, \boldsymbol{u}_h^n\big) + s_h(p_h^n, q_h) \\ \quad + \rho^{\mathrm{s}}\epsilon\big(\partial_\tau \dot{\boldsymbol{d}}_h^n, \boldsymbol{w}_h\big)_\Sigma + a^{\mathrm{e}}\big(\boldsymbol{d}_h^n, \boldsymbol{w}_h\big) = (\boldsymbol{h}(t_n), \boldsymbol{v}_h)_{\Gamma^{\mathrm{n}}} \end{cases} \tag{38}$$

for all $(\boldsymbol{v}_h, q_h, \boldsymbol{w}_h) \in \boldsymbol{V}_h \times Q_h \times \boldsymbol{W}_h$ with $\boldsymbol{v}_h|_\Sigma = \boldsymbol{w}_h$. On the other hand, using the definition (16) of $\boldsymbol{L}_h^{\mathrm{e}}$, the solid sub-step $(34)_2$ can be reformulated as

$$\boldsymbol{u}_h^n = \dot{\boldsymbol{d}}_h^n + \frac{\tau}{\rho^{\mathrm{s}}\epsilon}\boldsymbol{L}_h^{\mathrm{e}}\big(\boldsymbol{d}_h^n - \boldsymbol{d}_h^\star\big) \quad \text{on} \quad \Sigma. \tag{39}$$

In short, Algorithms 4–5 are an interface kinematic perturbation of Algorithm 2. They involve the implicit time discretization (38), of (8), with the perturbed interface kinematic continuity (39)

(instead of $(28)_1$). This observation is crucial for the derivation of the stability and convergence results reported in Sections 4 and 5 below. Indeed, it suffices to analyze how the perturbation

$$\frac{\tau}{\rho^{\mathrm{s}}\epsilon}\boldsymbol{L}_h^{\mathrm{e}}\left(\boldsymbol{d}_h^n-\boldsymbol{d}_h^\star\right),\tag{40}$$

in (39), affects the stability and the consistency of the underlying implicit coupling scheme (Algorithm 2).

Remark 3.7 *It is precisely the perturbed kinematic continuity* (39) *that allows the decoupled computation of the fluid* $(\boldsymbol{u}_h^n, p_h^n)$ *and the solid* $(\boldsymbol{d}_h^n, \dot{\boldsymbol{d}}_h^n)$ *states in Algorithms 4–5.* $\diamondsuit$

Remark 3.8 *Note that the order of the perturbation* (40) *introduced by the non-incremental variant* $(\boldsymbol{d}_h^\star = \boldsymbol{0})$ *is lower than for the incremental schemes* $(\boldsymbol{d}_h^\star$ *given by* (35)*). Indeed, as we shall see in Section 5, for the non-incremental variant the consistency of this perturbation scales as* $\mathcal{O}(\tau^{\frac{1}{2}})$ *in the energy-norm, whereas for the proposed incremental schemes we get* $\mathcal{O}(\tau)$ *and* $\mathcal{O}(\tau^2)$*, respectively.* $\diamondsuit$

Remark 3.9 *If damping effects are present in the solid model, namely, through a viscous term* $a^{\mathrm{v}}(\dot{\boldsymbol{d}}, \boldsymbol{w})$ *in* $(2)_3$*, we can incorporate this contribution into Algorithm 4 by adding the term* $a^{\mathrm{v}}(\boldsymbol{u}_h^n, \boldsymbol{v}_h)$ *to the left hand-side of* (33)*. This corresponds to the implicit treatment of the whole fluid-solid hydrodynamic coupling, as originally suggested in [30, 29] for the non-incremental variant. The extension of the stability and convergence results reported in the next sections to this framework is straightforward. It is worth noting, however, that in this case the resulting coupling scheme is not necessarily explicit, since the solid-damping term introduces a perturbation of the explicit Robin-condition* $(36)_1$ *(see Remark 3.3). Alternatively, we can treat explicitly this contribution in* (33) *and implicitly in* (34)*, which is one of the ingredients of the displacement-velocity correction schemes recently introduced in [21] for the coupling with general thick-solids.* $\diamondsuit$

4   Stability analysis

This section is devoted to the stability analysis of the incremental displacement corrections schemes introduced in §3.2.2. In what follows, we will refer to these explicit coupling schemes as Algorithm 5.

   We first recall a version of the discrete Gronwall lemma, from [33], that will be useful.

Lemma 4.1 ([33, Lemma 5.1]) *Let* τ*,* B *and* a_m*,* b_m*,* c_m*,* γ_m *(for integers* $m \geq 1$*) be non-negative numbers such that*

$$a_n + \tau \sum_{m=1}^{n} b_m \leq \tau \sum_{m=1}^{n} \gamma_m a_m + \tau \sum_{m=1}^{n} c_m + B$$

for $n \geq 1$*. Suppose that* $\tau\gamma_m < 1$ *for all* $m \geq 1$*. Then, there holds*

$$a_n + \tau \sum_{m=1}^{n} b_m \leq \exp\left(\tau \sum_{m=1}^{n} \frac{\gamma_m}{1 - \tau\gamma_m}\right)\left(\tau \sum_{m=1}^{n} c_m + B\right)$$

for $n \geq 1$*.*

For $n \geq 0$, we define the discrete energy and dissipation of the fluid-structure system, at time level n, as

$$E_h^n \overset{\text{def}}{=} \rho^{\text{f}} \|\boldsymbol{u}_h^n\|_{0,\Omega}^2 + \rho^{\text{s}} \epsilon \|\dot{\boldsymbol{d}}_h^n\|_{0,\Sigma}^2 + \|\boldsymbol{d}_h^n\|_{\text{e}}^2,$$

$$D_h^n \overset{\text{def}}{=} \tau \sum_{m=1}^{n} \left(\|\boldsymbol{u}_h^m\|_{\boldsymbol{V}}^2 + |p_h^m|_{s_h}^2 \right)$$

$$+ \tau^2 \sum_{m=1}^{n} \left(\rho^{\text{f}} \|\partial_\tau \boldsymbol{u}_h^m\|_{0,\Omega}^2 + \rho^{\text{s}} \epsilon \|\partial_\tau \dot{\boldsymbol{d}}_h^m\|_{0,\Sigma}^2 + \|\partial_\tau \boldsymbol{d}_h^m\|_{\text{e}}^2 \right).$$

We then have the following energy stability result.

Theorem 4.2 *Assume that $\boldsymbol{h} = \boldsymbol{0}$ (free system) and let*

$$\left\{ (\boldsymbol{u}_h^n, p_h^n, \boldsymbol{d}_h^n, \dot{\boldsymbol{d}}_h^n) \right\}_{n \geq 1} \subset \boldsymbol{V}_h \times Q_h \times \boldsymbol{W}_h \times \boldsymbol{W}_h$$

be given by Algorithm 5. Then, the following a priori energy estimates hold for $n \geq 1$:

- *Non-incremental scheme ($\boldsymbol{d}_h^\star = \boldsymbol{0}$):*

$$E_h^n + D_h^n + \frac{\tau^2}{\rho^{\text{s}} \epsilon} \sum_{m=1}^{n} \|\boldsymbol{L}_h^{\text{e}} \boldsymbol{d}_h^m\|_{0,\Sigma}^2 \lesssim E_h^0. \tag{41}$$

- *Incremental scheme with $\boldsymbol{d}_h^\star = \boldsymbol{d}_h^{n-1}$:*

$$E_h^n + D_h^n + \tau^2 \|\dot{\boldsymbol{d}}_h^n\|_{\text{e}}^2 + \frac{\tau^2}{\rho^{\text{s}} \epsilon} \|\boldsymbol{L}_h^{\text{e}} \boldsymbol{d}_h^n\|_{0,\Sigma}^2$$

$$+ \tau^2 \sum_{m=1}^{n} \|\dot{\boldsymbol{d}}_h^m - \dot{\boldsymbol{d}}_h^{m-1}\|_{\text{e}}^2 + \frac{\tau^2}{\rho^{\text{s}} \epsilon} \sum_{m=0}^{n-1} \|\boldsymbol{L}_h^{\text{e}} (\boldsymbol{d}_h^m - \boldsymbol{d}_h^{m-1})\|_{0,\Sigma}^2 \tag{42}$$

$$\lesssim E_h^0 + \tau^2 \|\dot{\boldsymbol{d}}_h^0\|_{\text{e}}^2 + \frac{\tau^2}{\rho^{\text{s}} \epsilon} \|\boldsymbol{L}_h^{\text{e}} \boldsymbol{d}_h^0\|_{0,\Sigma}^2.$$

- *Incremental scheme with $\boldsymbol{d}_h^\star = \boldsymbol{d}_h^{n-1} + \tau \dot{\boldsymbol{d}}_h^{n-1}$, under the $\frac{6}{5}$-CFL condition*

$$\tau (\omega^{\text{e}} C_{\text{inv}})^{\frac{6}{5}} \leq \alpha h^{\frac{6}{5}} \tag{43}$$

and with $2\tau \alpha^5 < 1$:

$$E_h^n + D_h^n + \tau^2 \sum_{m=1}^{n} \|\dot{\boldsymbol{d}}_h^m - \dot{\boldsymbol{d}}_h^{m-1}\|_{\text{e}}^2 \lesssim \exp\left(\frac{2 t_n}{\alpha^{-5} - 2\tau} \right) E_h^0. \tag{44}$$

Here,

$$\omega^{\text{e}} \overset{\text{def}}{=} \left(\frac{\beta^{\text{e}}}{\rho^{\text{s}} \epsilon} \right)^{\frac{1}{2}} \tag{45}$$

represents a maximum solid elastic wave-speed and $\alpha > 0$ is the $\frac{6}{5}$-CFL constant.

Proof. We first test (38) with

$$(\boldsymbol{v}_h, q_h) = \tau(\boldsymbol{u}_h^n, p_h^n), \quad \boldsymbol{w}_h = \tau \dot{\boldsymbol{d}}_h^n + \frac{\tau^2}{\rho^{\mathrm{s}}\epsilon} \boldsymbol{L}_h^{\mathrm{e}}\left(\boldsymbol{d}_h^n - \boldsymbol{d}_h^\star\right).$$

These are admissible test functions since, thanks to (39), we do have $\boldsymbol{v}_h|_\Sigma = \boldsymbol{w}_h$. Hence, using (11), $(38)_1$, the symmetry of the bilinear form a^{e} and (16), we get the following energy identity:

$$\begin{aligned}
&\frac{\rho^{\mathrm{f}}}{2}\left(\|\boldsymbol{u}_h^n\|_{0,\Omega}^2 - \|\boldsymbol{u}_h^{n-1}\|_{0,\Omega}^2 + \|\boldsymbol{u}_h^n - \boldsymbol{u}_h^{n-1}\|_{0,\Omega}^2\right) + 2\mu\tau\|\boldsymbol{\epsilon}(\boldsymbol{u}_h^n)\|_{0,\Omega}^2 \\
&\quad + \tau|p_h^n|_{s_h}^2 + \frac{\rho^{\mathrm{s}}\epsilon}{2}\left(\|\dot{\boldsymbol{d}}_h^n\|_{0,\Sigma}^2 - \|\dot{\boldsymbol{d}}_h^{n-1}\|_{0,\Sigma}^2 + \|\dot{\boldsymbol{d}}_h^n - \dot{\boldsymbol{d}}_h^{n-1}\|_{0,\Sigma}^2\right) \\
&\quad + \frac{1}{2}\left(\|\boldsymbol{d}_h^n\|_{\mathrm{e}}^2 - \|\boldsymbol{d}_h^{n-1}\|_{\mathrm{e}}^2 + \|\boldsymbol{d}_h^n - \boldsymbol{d}_h^{n-1}\|_{\mathrm{e}}^2\right) \\
&\quad + \underbrace{\tau^2\left(\partial_\tau \dot{\boldsymbol{d}}_h^n, \boldsymbol{L}_h^{\mathrm{e}}(\boldsymbol{d}_h^n - \boldsymbol{d}_h^\star)\right)_\Sigma}_{T_1} + \underbrace{\frac{\tau^2}{\rho^{\mathrm{s}}\epsilon}\left(\boldsymbol{L}_h^{\mathrm{e}}\boldsymbol{d}_h^n, \boldsymbol{L}_h^{\mathrm{e}}(\boldsymbol{d}_h^n - \boldsymbol{d}_h^\star)\right)_\Sigma}_{T_2} = 0.
\end{aligned} \tag{46}$$

Therefore, it only remains to estimate the terms T_1 and T_2. Each choice of $\boldsymbol{d}_h^\star$ will be treated separately.

Case $\boldsymbol{d}_h^\star = \boldsymbol{0}$. We have

$$T_2 = \frac{\tau^2}{\rho^{\mathrm{s}}\epsilon}\left(\boldsymbol{L}_h^{\mathrm{e}}\boldsymbol{d}_h^n, \boldsymbol{L}_h^{\mathrm{e}}\boldsymbol{d}_h^n\right)_\Sigma = \frac{\tau^2}{\rho^{\mathrm{s}}\epsilon}\|\boldsymbol{L}_h^{\mathrm{e}}\boldsymbol{d}_h^n\|_{0,\Sigma}^2$$

and

$$T_1 = \tau\left(\dot{\boldsymbol{d}}_h^n - \dot{\boldsymbol{d}}_h^{n-1}, \boldsymbol{L}_h^{\mathrm{e}}\boldsymbol{d}_h^n\right)_\Sigma \geq -\varepsilon\frac{\rho^{\mathrm{s}}\epsilon}{2}\|\dot{\boldsymbol{d}}_h^n - \dot{\boldsymbol{d}}_h^{n-1}\|_{0,\Sigma}^2 - \frac{1}{2\varepsilon}\frac{\tau^2}{\rho^{\mathrm{s}}\epsilon}\|\boldsymbol{L}_h^{\mathrm{e}}\boldsymbol{d}_h^n\|_{0,\Sigma}^2,$$

with $\varepsilon > 0$. So that,

$$T_1 + T_2 \geq \frac{\tau^2}{\rho^{\mathrm{s}}\epsilon}\left(1 - \frac{1}{2\varepsilon}\right)\|\boldsymbol{L}_h^{\mathrm{e}}\boldsymbol{d}_h^n\|_{0,\Sigma}^2 - \varepsilon\frac{\rho^{\mathrm{s}}\epsilon}{2}\|\dot{\boldsymbol{d}}_h^n - \dot{\boldsymbol{d}}_h^{n-1}\|_{0,\Sigma}^2. \tag{47}$$

Therefore, by inserting this inequality (with $\varepsilon = \frac{3}{4}$) into (46), using Korn's inequality (see, e.g., [12]) and summing over $m = 1, \ldots, n$, we recover the energy estimate (41).

Case $\boldsymbol{d}_h^\star = \boldsymbol{d}_h^{n-1}$. For the first term, using (16) and $(38)_1$, we have

$$\begin{aligned}
T_1 &= \tau\left(\dot{\boldsymbol{d}}_h^n - \dot{\boldsymbol{d}}_h^{n-1}, \boldsymbol{L}_h^{\mathrm{e}}(\boldsymbol{d}_h^n - \boldsymbol{d}_h^{n-1})\right)_\Sigma = \tau^2 a^{\mathrm{e}}\left(\dot{\boldsymbol{d}}_h^n - \dot{\boldsymbol{d}}_h^{n-1}, \dot{\boldsymbol{d}}_h^n\right) \\
&= \frac{\tau^2}{2}\left(\|\dot{\boldsymbol{d}}_h^n\|_{\mathrm{e}}^2 - \|\dot{\boldsymbol{d}}_h^{n-1}\|_{\mathrm{e}}^2 + \|\dot{\boldsymbol{d}}_h^n - \dot{\boldsymbol{d}}_h^{n-1}\|_{\mathrm{e}}^2\right),
\end{aligned}$$

while, for the second, we get

$$\begin{aligned}
T_2 &= \frac{\tau^2}{\rho^{\mathrm{s}}\epsilon}\left(\boldsymbol{L}_h^{\mathrm{e}}\boldsymbol{d}_h^n, \boldsymbol{L}_h^{\mathrm{e}}(\boldsymbol{d}_h^n - \boldsymbol{d}_h^{n-1})\right)_\Sigma \\
&= \frac{\tau^2}{2\rho^{\mathrm{s}}\epsilon}\left(\|\boldsymbol{L}_h^{\mathrm{e}}\boldsymbol{d}_h^n\|_{0,\Sigma}^2 - \|\boldsymbol{L}_h^{\mathrm{e}}\boldsymbol{d}_h^{n-1}\|_{0,\Sigma}^2 + \|\boldsymbol{L}_h^{\mathrm{e}}(\boldsymbol{d}_h^n - \boldsymbol{d}_h^{n-1})\|_{0,\Sigma}^2\right).
\end{aligned}$$

Therefore, by inserting these equalities into (46), using Korn's inequality and summing over $m = 0, \ldots, n-1$, we recover the energy estimate (42).

Case $\boldsymbol{d}_h^\star = \boldsymbol{d}_h^{n-1} + \tau \dot{\boldsymbol{d}}_h^{n-1}$. For the first term, we have

$$
\begin{aligned}
T_1 &= \tau \big(\dot{\boldsymbol{d}}_h^n - \dot{\boldsymbol{d}}_h^{n-1}, \boldsymbol{L}_h^{\mathrm{e}}(\boldsymbol{d}_h^n - \boldsymbol{d}_h^{n-1} - \tau \dot{\boldsymbol{d}}_h^{n-1}) \big)_\Sigma \\
&= \tau a^{\mathrm{e}} \big(\dot{\boldsymbol{d}}_h^n - \dot{\boldsymbol{d}}_h^{n-1}, \tau(\dot{\boldsymbol{d}}_h^n - \dot{\boldsymbol{d}}_h^{n-1}) \big) \\
&= \tau^2 \| \dot{\boldsymbol{d}}_h^n - \dot{\boldsymbol{d}}_h^{n-1} \|_{\mathrm{e}}^2
\end{aligned}
\tag{48}
$$

and, for the second,

$$
\begin{aligned}
T_2 &= \frac{\tau^2}{\rho^{\mathrm{s}}\epsilon} \big(\boldsymbol{L}_h^{\mathrm{e}} \boldsymbol{d}_h^n, \boldsymbol{L}_h^{\mathrm{e}}(\boldsymbol{d}_h^n - \boldsymbol{d}_h^{n-1} - \tau \dot{\boldsymbol{d}}_h^{n-1}) \big)_\Sigma = \frac{\tau^3}{\rho^{\mathrm{s}}\epsilon} \big(\boldsymbol{L}_h^{\mathrm{e}} \boldsymbol{d}_h^n, \boldsymbol{L}_h^{\mathrm{e}}(\dot{\boldsymbol{d}}_h^n - \dot{\boldsymbol{d}}_h^{n-1}) \big)_\Sigma \\
&= \frac{\tau^3}{\rho^{\mathrm{s}}\epsilon} a^{\mathrm{e}} \big(\boldsymbol{L}_h^{\mathrm{e}} \boldsymbol{d}_h^n, \dot{\boldsymbol{d}}_h^n - \dot{\boldsymbol{d}}_h^{n-1} \big) \le \frac{\tau^3}{\rho^{\mathrm{s}}\epsilon} \| \boldsymbol{L}_h^{\mathrm{e}} \boldsymbol{d}_h^n \|_{\mathrm{e}} \| \dot{\boldsymbol{d}}_h^n - \dot{\boldsymbol{d}}_h^{n-1} \|_{\mathrm{e}}.
\end{aligned}
$$

On the other hand, thanks to the inverse estimates (21) and (22), the $\frac{6}{5}$-CFL condition (43) and (45), we obtain the following bounds

$$
\begin{aligned}
T_2 &\le \frac{\tau^3}{\rho^{\mathrm{s}}\epsilon} \frac{(\beta^{\mathrm{e}})^{\frac{1}{2}} C_{\mathrm{inv}}}{h} \| \boldsymbol{L}_h^{\mathrm{e}} \boldsymbol{d}_h^n \|_{\mathrm{e}} \| \dot{\boldsymbol{d}}_h^n - \dot{\boldsymbol{d}}_h^{n-1} \|_{0,\Sigma} \\
&\le \frac{\tau^3}{(\rho^{\mathrm{s}}\epsilon)^{\frac{3}{2}}} \frac{(\beta^{\mathrm{e}})^{\frac{3}{2}} C_{\mathrm{inv}}^3}{h^3} \| \boldsymbol{d}_h^n \|_{\mathrm{e}} (\rho^{\mathrm{s}}\epsilon)^{\frac{1}{2}} \| \dot{\boldsymbol{d}}_h^n - \dot{\boldsymbol{d}}_h^{n-1} \|_{0,\Sigma} \\
&\le \tau^6 \frac{(\omega^{\mathrm{e}} C_{\mathrm{inv}})^6}{h^6} \| \boldsymbol{d}_h^n \|_{\mathrm{e}}^2 + \frac{\rho^{\mathrm{s}}\epsilon}{4} \| \dot{\boldsymbol{d}}_h^n - \dot{\boldsymbol{d}}_h^{n-1} \|_{0,\Sigma}^2, \\
&\le \tau \alpha^5 \| \boldsymbol{d}_h^n \|_{\mathrm{e}}^2 + \frac{\rho^{\mathrm{s}}\epsilon}{4} \| \dot{\boldsymbol{d}}_h^n - \dot{\boldsymbol{d}}_h^{n-1} \|_{0,\Sigma}^2.
\end{aligned}
\tag{49}
$$

The energy estimate (44) follows by inserting the estimates (48) and (49) into (46), using Korn's inequality, summing over $m = 1, \dots, n$ and applying Lemma 4.1 with

$$
a_m = \frac{\rho^{\mathrm{f}}}{2} \| \boldsymbol{u}_h^m \|_{0,\Omega}^2 + \frac{\rho^{\mathrm{s}}\epsilon}{2} \| \dot{\boldsymbol{d}}_h^m \|_{0,\Sigma}^2 + \frac{1}{2} \| \boldsymbol{d}_h^m \|_{\mathrm{e}}^2, \quad \gamma_m = 2\alpha^5.
$$

Hence, the proof is complete.$\diamond$

Some observations are now in order:

1. The estimate (41) shows that the non-incremental displacement-correction scheme is unconditionally stable in the energy norm. For this variant (Algorithm 3), an alternative energy estimate was obtained in [29], yielding unconditional stability as well.

2. The estimate (42) shows that the incremental scheme with first-order extrapolation, $\boldsymbol{d}_h^\star = \boldsymbol{d}_h^{n-1}$, is unconditionally stable in the energy norm. Indeed, under the additional regularity assumptions on the initial data, $\boldsymbol{d}^0 \in \boldsymbol{D}^{\mathrm{e}}$ and $\dot{\boldsymbol{d}}^0 \in \boldsymbol{W}$, we can consider the finite element approximations

$$
\boldsymbol{d}_h^0 = \boldsymbol{\pi}_h^{\mathrm{e}} \boldsymbol{d}^0, \quad \dot{\boldsymbol{d}}_h^0 = \boldsymbol{\pi}_h^{\mathrm{e}} \dot{\boldsymbol{d}}^0.
$$

It then follows, from Lemma 3.2, that

$$
\| \dot{\boldsymbol{d}}_h^0 \|_{\mathrm{e}} \le \| \dot{\boldsymbol{d}}^0 \|_{\mathrm{e}}, \quad \| \boldsymbol{L}_h^{\mathrm{e}} \boldsymbol{d}_h^0 \|_{0,\Sigma} = \| \boldsymbol{L}_h^{\mathrm{e}} \boldsymbol{d}^0 \|_{0,\Sigma} \le \| \boldsymbol{L}^{\mathrm{e}} \boldsymbol{d}^0 \|_{0,\Sigma},
$$

which guarantees that the right hand-side of (42) remains uniformly bounded with respect to h and τ.

3. Theorem 4.2 also shows that the incremental scheme with $\boldsymbol{d}_h^\star = \boldsymbol{d}_h^n + \tau \dot{\boldsymbol{d}}_h^{n-1}$ is energy stable under the $\frac{6}{5}$-CFL constraint (43).

4. Note that the energy estimates (41), (42) and (44) and the $\frac{6}{5}$-CFL constraint (43) are independent of the fluid-solid density ratio and of the slender characteristics of the domain. Therefore, all these variants are energy stable, irrespectively of the amount of added-mass effect in the system. This is a major advantage with respect to Algorithm 1, whose (in)stability precisely relies on these quantities, irrespectively of the discretization parameters (see [11, 24]).

Remark 4.3 *It is worth noting that, in the case $\boldsymbol{d}_h^\star = \boldsymbol{0}$, the above proof makes use of the solid time-marching numerical dissipation*

$$\frac{\rho^s \epsilon}{2} \| \dot{\boldsymbol{d}}_h^n - \dot{\boldsymbol{d}}_h^{n-1} \|_{0,\Sigma}^2,$$

to control the last term of (47). This is not the case for the incremental scheme with $\boldsymbol{d}_h^\star = \boldsymbol{d}_h^{n-1}$. Moreover, in the case $\boldsymbol{d}_h^\star = \boldsymbol{d}_h^n + \tau \dot{\boldsymbol{d}}_h^{n-1}$, we can also avoid the use of this dissipation in the bound (49), which could be useful for the development of high-order schemes. Indeed, alternatively to (49), term T_2 can be bounded as follows, using the inverse estimate (22) and the high-order dissipation given by (48):

$$\begin{aligned} T_2 &\leq \frac{\tau^4}{2(\rho^s \epsilon)^2} \| L_h^e \boldsymbol{d}_h^n \|_e^2 + \frac{\tau^2}{2} \| \dot{\boldsymbol{d}}_h^n - \dot{\boldsymbol{d}}_h^{n-1} \|_e^2 \\ &\leq \frac{\tau^4 (\omega^e C_{\mathrm{inv}})^4}{2h^4} \| \boldsymbol{d}_h^n \|_e^2 + \frac{\tau^2}{2} \| \dot{\boldsymbol{d}}_h^n - \dot{\boldsymbol{d}}_h^{n-1} \|_e^2. \end{aligned}$$

We then conclude as in the proof of Theorem 4.2, by applying Lemma 4.1, but now under the strengthened $\frac{4}{3}$-CFL condition

$$\tau (\omega^e C_{\mathrm{inv}})^{\frac{4}{3}} \leq \alpha h^{\frac{4}{3}}. \tag{50}$$

$\Diamond$

Remark 4.4 *Theorem 4.2 can be viewed as a generalization of the energy-stability of Algorithm 2 to the case of the perturbed kinematic condition (39). Indeed, in the implicit scheme, thanks to $(28)_1$, we can test (38) with*

$$(\boldsymbol{v}_h, q_h) = \tau(\boldsymbol{u}_h^n, p_h^n), \quad \boldsymbol{w}_h = \tau \dot{\boldsymbol{d}}_h^n,$$

so that (46) holds with $T_1 = T_2 = 0$. The following standard energy estimate is then recovered

$$E_h^n + D_h^n \lesssim E_h^0$$

for $n \geq 1$, which guarantees the unconditional stability of the implicit coupling scheme. $\Diamond$

5   Convergence analysis

This section is devoted to the convergence analysis of the explicit coupling schemes reported in §3.2.2.

5.1 Preliminaries

For the sake of simplicity, we assume that the interface Σ is flat. We also suppose that the elastic Ritz-projector (17) satisfies the standard approximation property

$$\|\boldsymbol{w} - \pi_h^{\mathrm{e}}\boldsymbol{w}\|_{\mathrm{e}} \lesssim h^k (\beta^{\mathrm{e}})^{\frac{1}{2}} \|\boldsymbol{w}\|_{k+1,\Sigma} \tag{51}$$

for all $\boldsymbol{w} \in [H^{k+1}(\Sigma)]^d \cap \boldsymbol{W}$. In addition, we shall make use of the standard Lagrange-interpolant onto the solid discrete space, $\boldsymbol{\mathcal{I}}_h : \boldsymbol{W} \cap [C^0(\overline{\Sigma})]^d \to \boldsymbol{W}_h$, for which there holds

$$\|\boldsymbol{w} - \boldsymbol{\mathcal{I}}_h\boldsymbol{w}\|_{0,\Sigma} + h\|\boldsymbol{w} - \boldsymbol{\mathcal{I}}_h\boldsymbol{w}\|_{1,\Sigma} \lesssim h^{k+1}\|\boldsymbol{w}\|_{k+1,\Sigma} \tag{52}$$

for all $\boldsymbol{w} \in [H^{k+1}(\Sigma)]^d \cap \boldsymbol{W}$.

For the fluid velocities we introduce the following Stokes-like projection operator, $(\boldsymbol{P}_h, R_h) : \boldsymbol{V} \to \boldsymbol{V}_h \times Q_h$, defined for all $\boldsymbol{v} \in \boldsymbol{V}$ by

$$\begin{cases} (\boldsymbol{P}_h\boldsymbol{v}, R_h\boldsymbol{v}) \in \boldsymbol{V}_h \times Q_h, \\ (\boldsymbol{P}_h\boldsymbol{v})|_\Sigma = \boldsymbol{\mathcal{I}}_h(\boldsymbol{v}|_\Sigma), \\ a(\boldsymbol{P}_h\boldsymbol{v}, \boldsymbol{v}_h) + b(R_h\boldsymbol{v}, \boldsymbol{v}_h) = a(\boldsymbol{v}, \boldsymbol{v}_h) \quad \forall \boldsymbol{v}_h \in \boldsymbol{V}_{\Sigma,h}, \\ b(q_h, \boldsymbol{P}_h\boldsymbol{v}) = s_h(R_h\boldsymbol{v}, q_h) \quad \forall q_h \in Q_h. \end{cases} \tag{53}$$

The approximation properties of $\boldsymbol{P}_h$ are stated in the next lemma.

Lemma 5.1 *Assume that $\boldsymbol{v} \in [H^{k+1}(\Omega)]^d$ and $\mathrm{div}\boldsymbol{v} = 0$. There holds*

$$\|\boldsymbol{v} - \boldsymbol{P}_h\boldsymbol{v}\|_{\boldsymbol{V}} + |R_h\boldsymbol{v}|_{s_h} \lesssim \mu^{\frac{1}{2}} h^k \|\boldsymbol{v}\|_{k+1,\Omega}.$$

Assume, in addition, that $\boldsymbol{v}|_\Sigma \in [H^{k+1}(\Sigma)]^d$ and that the solution of the steady Stokes problem

$$\begin{cases} -\mathbf{div}\boldsymbol{\sigma}(\boldsymbol{z}, r) = \boldsymbol{f} & in \quad \Omega, \\ \mathrm{div}\boldsymbol{z} = 0 & in \quad \Omega, \\ \boldsymbol{z} = \boldsymbol{0} & on \quad \Gamma^{\mathrm{d}} \cup \Sigma, \\ \boldsymbol{\sigma}(\boldsymbol{z}, r)\boldsymbol{n} = \boldsymbol{0} & on \quad \Gamma^{\mathrm{n}}, \end{cases}$$

satisfies the regularity estimates

$$\mu^{\frac{1}{2}}\|\boldsymbol{z}\|_{2,\Omega} + \mu^{-\frac{1}{2}}\|r\|_{1,\Omega} \leq c_\mu \|\boldsymbol{f}\|_{0,\Omega}, \quad \|\boldsymbol{\sigma}(\boldsymbol{z}, r)\boldsymbol{n}\|_{0,\Sigma} \leq \tilde{c}_\mu \|\boldsymbol{f}\|_{0,\Omega}, \tag{54}$$

with $c_\mu, \tilde{c}_\mu > 0$ depending only on Ω and μ. Then, there holds

$$\|\boldsymbol{v} - \boldsymbol{P}_h\boldsymbol{v}\|_{0,\Omega} \lesssim h^{k+1}\big(c_\mu \mu^{\frac{1}{2}}\|\boldsymbol{v}\|_{k+1,\Omega} + \tilde{c}_\mu\|\boldsymbol{v}\|_{k+1,\Sigma}\big).$$

Proof. Both estimates follow from Theorem B.5 in appendix B.$\diamond$

For the convergence analysis, we shall assume that the solution of (5) has the following regularity, for a given final time $T > \tau$:

$$\begin{aligned} &\boldsymbol{u} \in H^1(0, T; [H^{k+1}(\Omega)]^d), \quad \boldsymbol{u} \in H^1(0, T; [H^{k+1}(\Sigma)]^d), \\ &\partial_{tt}\boldsymbol{u} \in L^2(0, T; [L^2(\Omega)]^d), \quad \partial_{tt}\boldsymbol{u} \in L^2(0, T; [L^2(\Sigma)]^d), \\ &p \in C^0([0, T]; H^{\tilde{l}}(\Omega)) \end{aligned} \tag{55}$$

and

$$\begin{cases} \boldsymbol{d} \in C^0([0, T]; \boldsymbol{D}^{\mathrm{e}}) & \text{if} \quad \boldsymbol{d}_h^\star = \boldsymbol{0}, \\ \boldsymbol{d} \in H^1(0, T; \boldsymbol{D}^{\mathrm{e}}) & \text{if} \quad \boldsymbol{d}_h^\star = \boldsymbol{d}_h^{n-1}, \\ \boldsymbol{d} \in H^2(0, T; \boldsymbol{D}^{\mathrm{e}}) & \text{if} \quad \boldsymbol{d}_h^\star = \boldsymbol{d}_h^{n-1} + \tau \dot{\boldsymbol{d}}_h^{n-1}. \end{cases} \tag{56}$$

5.2 *A priori* energy-error estimate

For a given time-dependent function $x(t)$, the notation $x^n \stackrel{\text{def}}{=} x(t_n)$ will be used. The convergence analysis below is based on the following decompositions of the error, between the solution of (5) and the fully discrete approximations provided by Algorithm 5:

$$
\begin{aligned}
\boldsymbol{u}^n - \boldsymbol{u}_h^n &= \underbrace{\boldsymbol{u}^n - \boldsymbol{P}_h \boldsymbol{u}^n}_{\boldsymbol{\theta}_\pi^n} + \underbrace{\boldsymbol{P}_h \boldsymbol{u}^n - \boldsymbol{u}_h^n}_{\boldsymbol{\theta}_h^n}, \\
p^n - p_h^n &= \underbrace{p^n - \Pi_h p^n}_{y_\pi^n} + \underbrace{\Pi_h p^n - p_h^n}_{y_h^n},
\end{aligned}
\tag{57}
$$

for the velocity and pressure of the fluid (the operator Π_h is that of Section 3.1.1); and

$$
\begin{aligned}
\boldsymbol{d}^n - \boldsymbol{d}_h^n &= \underbrace{\boldsymbol{d}^n - \boldsymbol{\pi}_h^{\text{e}} \boldsymbol{d}^n}_{\boldsymbol{\xi}_\pi^n} + \underbrace{\boldsymbol{\pi}_h^{\text{e}} \boldsymbol{d}^n - \boldsymbol{d}_h^n}_{\boldsymbol{\xi}_h^n}, \\
\dot{\boldsymbol{d}}^n - \dot{\boldsymbol{d}}_h^n &= \underbrace{\dot{\boldsymbol{d}}^n - \boldsymbol{\mathcal{I}}_h \dot{\boldsymbol{d}}^n}_{\dot{\boldsymbol{\xi}}_\pi^n} + \underbrace{\boldsymbol{\mathcal{I}}_h \dot{\boldsymbol{d}}^n - \dot{\boldsymbol{d}}_h^n}_{\dot{\boldsymbol{\xi}}_h^n}.
\end{aligned}
\tag{58}
$$

for the displacement and velocity of the solid.

For $n \geq 1$, we define the energy-norm of the discrete error, at time level n, as

$$
\begin{aligned}
\mathcal{E}_h^n \stackrel{\text{def}}{=} (\rho^{\text{f}})^{\frac{1}{2}} \|\boldsymbol{\theta}_h^n\|_{0,\Omega} &+ \left(\sum_{m=1}^n \tau \|\boldsymbol{\theta}_h^m\|_{\boldsymbol{V}}^2 \right)^{\frac{1}{2}} + \left(\sum_{m=1}^n \tau |y_h^m|_{s_h}^2 \right)^{\frac{1}{2}} \\
&+ (\rho^{\text{s}} \epsilon)^{\frac{1}{2}} \|\dot{\boldsymbol{\xi}}_h^n\|_{0,\Sigma} + \|\boldsymbol{\xi}_h^n\|_{\text{e}}.
\end{aligned}
$$

The main result of this section is stated in the next theorem, which provides an a priori estimate for $\mathcal{E}_h^n$, in terms of the different choices of the extrapolation $\boldsymbol{d}_h^\star$.

Theorem 5.2 *Let $(\boldsymbol{u}, p, \boldsymbol{d}, \dot{\boldsymbol{d}})$ be the solution of (5) and*

$$
\left\{ (\boldsymbol{u}_h^n, p_h^n, \boldsymbol{d}_h^n, \dot{\boldsymbol{d}}_h^n) \right\}_{n \geq 1} \subset \boldsymbol{V}_h \times Q_h \times \boldsymbol{W}_h \times \boldsymbol{W}_h
$$

be given by Algorithm 5, with discrete initial data

$$
\left(\boldsymbol{u}_h^0, \dot{\boldsymbol{d}}_h^0, \boldsymbol{d}_h^0 \right) = \left(\boldsymbol{P}_h \boldsymbol{u}_0, \boldsymbol{\mathcal{I}}_h \dot{\boldsymbol{d}}^0, \boldsymbol{\pi}_h^{\text{e}} \boldsymbol{d}^0 \right).
\tag{59}
$$

Suppose that (54) holds and that the exact solution has the regularity (55)-(56). For $\boldsymbol{d}_h^\star = \boldsymbol{d}_h^{n-1} + \tau \dot{\boldsymbol{d}}_h^{n-1}$ we assume, in addition, that the $\frac{6}{5}$-CFL condition (43) holds and that

$$
\max \left\{ 2\alpha^5, \frac{\alpha^{\frac{10}{3}} \tau^{\frac{2}{3}} + \alpha^{\frac{5}{3}} \tau^{\frac{1}{3}}}{T} \right\} \tau < 1.
$$

Then, for $n \geq 1$ and $n\tau \leq T$, we have the following discrete error estimate:

$$
\mathcal{E}_h^n \lesssim c^\star \left(c_1 h^k + c_2 h^{\tilde{l}} + c_3 \tau + e_\tau^\star \right),
\tag{60}
$$

where the term $e_\tau^\star$ stands for the time-consistency of the displacement-correction in Algorithm 5, given by

$$
e_\tau^\star \overset{\text{def}}{=} \begin{cases}
\tau^{\frac{1}{2}} \left(\dfrac{T}{\rho^{\mathrm{s}} \epsilon} \right)^{\frac{1}{2}} \|\boldsymbol{d}\|_{L^\infty(0,T;\boldsymbol{D}^{\mathrm{e}})} & \text{if} \quad \boldsymbol{d}_h^\star = \boldsymbol{0}, \\[3mm]
\tau \left(\dfrac{T}{\rho^{\mathrm{s}} \epsilon} \right)^{\frac{1}{2}} \|\partial_t \boldsymbol{d}\|_{L^2(0,T;\boldsymbol{D}^{\mathrm{e}})} & \text{if} \quad \boldsymbol{d}_h^\star = \boldsymbol{d}_h^{n-1}, \\[3mm]
\tau^2 \left(\dfrac{T}{\rho^{\mathrm{s}} \epsilon} \right)^{\frac{1}{2}} \|\partial_{tt} \boldsymbol{d}\|_{L^2(0,T;\boldsymbol{D}^{\mathrm{e}})} & \text{if} \quad \boldsymbol{d}_h^\star = \boldsymbol{d}_h^{n-1} + \tau \dot{\boldsymbol{d}}_h^{n-1}.
\end{cases}
\tag{61}
$$

The multiplying constants in (60) are given by

$$
c^\star \overset{\text{def}}{=} \begin{cases}
\exp\left(\dfrac{T}{T - \tau} \right) & \text{if} \quad \boldsymbol{d}_h^\star = \boldsymbol{0} \quad \text{or} \quad \boldsymbol{d}_h^\star = \boldsymbol{d}_h^{n-1}, \\[5mm]
\exp\left(\dfrac{\max\left\{ 1, 2\alpha^5 T, \alpha^{\frac{10}{3}} \tau^{\frac{2}{3}} + \alpha^{\frac{5}{3}} \tau^{\frac{1}{3}} \right\}}{1 - \frac{\tau}{T} \max\left\{ 1, 2\alpha^5 T, \alpha^{\frac{10}{3}} \tau^{\frac{2}{3}} + \alpha^{\frac{5}{3}} \tau^{\frac{1}{3}} \right\}} \right) & \text{if} \quad \boldsymbol{d}_h^\star = \boldsymbol{d}_h^{n-1} + \tau \dot{\boldsymbol{d}}_h^{n-1},
\end{cases}
$$

$$
c_1 \overset{\text{def}}{=} \frac{\rho^{\mathrm{f}} C_{\mathrm{P}}}{\mu^{\frac{1}{2}}} \left(c_\mu \mu^{\frac{1}{2}} h \|\partial_t \boldsymbol{u}\|_{L^2(0,T;H^{k+1}(\Omega))} + \tilde{c}_\mu h \|\partial_t \boldsymbol{u}\|_{L^2(0,T;H^{k+1}(\Sigma))} \right)
$$
$$
+ \frac{\rho^{\mathrm{s}} \epsilon C_{\mathrm{T}}}{\mu^{\frac{1}{2}}} h \|\partial_t \boldsymbol{u}\|_{L^2(0,T;H^{k+1}(\Sigma))} + (\mu T)^{\frac{1}{2}} \|\boldsymbol{u}\|_{L^\infty(0,T;H^{k+1}(\Omega))}
$$
$$
+ (\beta^{\mathrm{e}})^{\frac{1}{2}} T \|\boldsymbol{u}\|_{L^\infty(0,T;H^{k+1}(\Sigma))},
$$

$$
c_2 \overset{\text{def}}{=} \left(\frac{T}{\mu} \right)^{\frac{1}{2}} \|p\|_{L^\infty(0,T;H^l(\Omega))},
$$

$$
c_3 \overset{\text{def}}{=} \frac{\rho^{\mathrm{f}} C_{\mathrm{P}}}{\mu^{\frac{1}{2}}} \|\partial_{tt} \boldsymbol{u}\|_{L^2(0,T;L^2(\Omega))} + \frac{\rho^{\mathrm{s}} \epsilon C_{\mathrm{T}}}{\mu^{\frac{1}{2}}} \|\partial_{tt} \boldsymbol{u}\|_{L^2(0,T;L^2(\Sigma))}
$$
$$
+ (\beta^{\mathrm{e}} T)^{\frac{1}{2}} \|\partial_t \boldsymbol{u}\|_{L^2(0,T;H^1(\Sigma))},
\tag{62}
$$

where $C_{\mathrm{P}}, C_{\mathrm{T}} > 0$ stand for the constants of the Poincaré and trace inequalities, respectively.

Proof. The proof is split into two main parts.

(i) Modified Galerkin orthogonality and discrete errors equation. We first subtract (38) from (5) to get the following modified Galerkin orthogonality:

$$
\rho^{\mathrm{f}} \left(\partial_\tau (\boldsymbol{u}^n - \boldsymbol{u}_h^n), \boldsymbol{v}_h \right) + a\left(\boldsymbol{u}^n - \boldsymbol{u}_h^n, \boldsymbol{v}_h \right) + b\left(p^n - p_h^n, \boldsymbol{v}_h \right) - b\left(q_h, \boldsymbol{u}^n - \boldsymbol{u}_h^n \right)
$$
$$
+ \rho^{\mathrm{s}} \epsilon \left(\partial_\tau (\dot{\boldsymbol{d}}^{n+1} - \dot{\boldsymbol{d}}_h^n), \boldsymbol{w}_h \right)_\Sigma + a^{\mathrm{e}} \left(\boldsymbol{d}^n - \boldsymbol{d}_h^n, \boldsymbol{w}_h \right)
$$
$$
= s_h\left(p_h^n, q_h \right) - \rho^{\mathrm{f}} \left(\partial_t \boldsymbol{u}(t_n) - \partial_\tau \boldsymbol{u}^n, \boldsymbol{v}_h \right) - \rho^{\mathrm{s}} \epsilon \left(\partial_t \dot{\boldsymbol{d}}(t_n) - \partial_\tau \dot{\boldsymbol{d}}^n, \boldsymbol{w}_h \right)_\Sigma \tag{63}
$$

for all $(\boldsymbol{v}_h, q_h, \boldsymbol{w}_h) \in \boldsymbol{V}_h \times Q_h \times \boldsymbol{W}_h$ with $\boldsymbol{v}_h|_\Sigma = \boldsymbol{w}_h$. Moreover, by inserting (57)-(58) into (63), we infer the following equation for the discrete errors:

$$
\begin{aligned}
&\rho^{\mathrm{f}}\big(\partial_\tau \boldsymbol{\theta}_h^n, \boldsymbol{v}_h\big) + a\big(\boldsymbol{\theta}_h^n, \boldsymbol{v}_h\big) + b(y_h^n, \boldsymbol{v}_h) - b(q_h, \boldsymbol{\theta}_h^n) + s_h\big(y_h^n, q_h\big) \\
&\quad + \rho^{\mathrm{s}}\epsilon\big(\partial_\tau \dot{\boldsymbol{\xi}}_h^n, \boldsymbol{w}_h\big)_\Sigma + a^{\mathrm{e}}(\boldsymbol{\xi}_h^n, \boldsymbol{w}_h) \\
&= \underbrace{-\rho^{\mathrm{f}}\big(\partial_t \boldsymbol{u}(t_n) - \partial_\tau \boldsymbol{u}^n, \boldsymbol{v}_h\big) - \rho^{\mathrm{f}}\big(\partial_\tau \boldsymbol{\theta}_\pi^n, \boldsymbol{v}_h\big)}_{T_1(\boldsymbol{v}_h)} \\
&\quad \underbrace{-\rho^{\mathrm{s}}\epsilon\big(\partial_t \dot{\boldsymbol{d}}(t_n) - \partial_\tau \dot{\boldsymbol{d}}^n, \boldsymbol{v}_h\big)_\Sigma - \rho^{\mathrm{s}}\epsilon\big(\partial_\tau \dot{\boldsymbol{\xi}}_\pi^n, \boldsymbol{v}_h\big)_\Sigma}_{T_2(\boldsymbol{v}_h)} \\
&\quad \underbrace{-a\big(\boldsymbol{\theta}_\pi^n, \boldsymbol{v}_h\big) - b\big(y_\pi^n, \boldsymbol{v}_h\big) + b\big(q_h, \boldsymbol{\theta}_\pi^n\big) + s_h\big(\Pi_h p^n, q_h\big)}_{T_3(\boldsymbol{v}_h, q_h)} - \underbrace{a^{\mathrm{e}}\big(\boldsymbol{\xi}_\pi^n, \boldsymbol{w}_h\big)}_{=\,0}
\end{aligned}
\tag{64}
$$

for all $(\boldsymbol{v}_h, q_h, \boldsymbol{w}_h) \in \boldsymbol{V}_h \times Q_h \times \boldsymbol{W}_h$ with $\boldsymbol{v}_h|_\Sigma = \boldsymbol{w}_h$. Note that the last term vanishes due to the definition of the projection operator (17) involved in (58).

We need to derive the discrete error counterpart of $(38)_1$ and (39). By combining $(38)_1$ with (58), the following perturbed velocity-displacement relation for the solid discrete errors holds

$$
\dot{\boldsymbol{\xi}}_h^n = \partial_\tau \boldsymbol{\xi}_h^n + \boldsymbol{\mathcal{I}}_h \dot{\boldsymbol{d}}^n - \boldsymbol{\pi}_h^{\mathrm{e}} \partial_\tau \boldsymbol{d}^n.
\tag{65}
$$

Similarly, owing to (39), (57) and (58), we get

$$
\boldsymbol{\theta}_h^n|_\Sigma = \dot{\boldsymbol{\xi}}_h^n + \frac{\tau}{\rho^{\mathrm{s}}\epsilon} \boldsymbol{L}_h^{\mathrm{e}}\big(\boldsymbol{\xi}_h^n - \boldsymbol{\xi}_h^\star\big) - \frac{\tau}{\rho^{\mathrm{s}}\epsilon} \boldsymbol{L}_h^{\mathrm{e}} \boldsymbol{\pi}_h^{\mathrm{e}}\big(\boldsymbol{d}^n - \boldsymbol{d}^\star\big) + (\boldsymbol{P}_h \boldsymbol{u}^n)|_\Sigma - \boldsymbol{\mathcal{I}}_h \dot{\boldsymbol{d}}^n,
\tag{66}
$$

with the natural notations

$$
\boldsymbol{\xi}_h^\star \overset{\mathrm{def}}{=} \boldsymbol{\pi}_h^{\mathrm{e}} \boldsymbol{d}^\star - \boldsymbol{d}_h^\star, \quad \boldsymbol{d}^\star \overset{\mathrm{def}}{=} \boldsymbol{0}, \boldsymbol{d}^{n-1}, \boldsymbol{d}^{n-1} + \tau \dot{\boldsymbol{d}}^{n-1},
\tag{67}
$$

accordingly with the choice of $\boldsymbol{d}_h^\star$. On the other hand, from $(53)_2$ and $(5)_1$, we have

$$
(\boldsymbol{P}_h \boldsymbol{u}^n)|_\Sigma = \boldsymbol{\mathcal{I}}_h(\boldsymbol{u}^n|_\Sigma) = \boldsymbol{\mathcal{I}}_h \dot{\boldsymbol{d}}^n.
\tag{68}
$$

Hence, using (20) and (68), the perturbed kinematic condition for the discrete errors (66) reduces to

$$
\boldsymbol{\theta}_h^n = \dot{\boldsymbol{\xi}}_h^n + \frac{\tau}{\rho^{\mathrm{s}}\epsilon} \boldsymbol{L}_h^{\mathrm{e}}\big(\boldsymbol{\xi}_h^n - \boldsymbol{\xi}_h^\star\big) - \frac{\tau}{\rho^{\mathrm{s}}\epsilon} \boldsymbol{L}_h^{\mathrm{e}}\big(\boldsymbol{d}^n - \boldsymbol{d}^\star\big) \quad \text{on} \quad \Sigma.
\tag{69}
$$

In summary, the dynamics of the discrete errors are given by (65), (69) and (64).

(ii) Stability and consistency. We can now proceed as in the proof of Theorem 4.2, by testing (64) with

$$
(\boldsymbol{v}_h, q_h) = \tau(\boldsymbol{\theta}_h^n, y_h^n), \quad \boldsymbol{w}_h = \tau \dot{\boldsymbol{\xi}}_h^n + \frac{\tau^2}{\rho^{\mathrm{s}}\epsilon} \boldsymbol{L}_h^{\mathrm{e}}\big(\boldsymbol{\xi}_h^n - \boldsymbol{\xi}_h^\star\big) - \frac{\tau^2}{\rho^{\mathrm{s}}\epsilon} \boldsymbol{L}_h^{\mathrm{e}}\big(\boldsymbol{d}^n - \boldsymbol{d}^\star\big).
$$

These are admissible test functions since (69) yields $\boldsymbol{v}_h|_\Sigma = \boldsymbol{w}_h$. Therefore, using (11), (65) and (69), we obtain the following identity for the energy-norm of the discrete errors:

$$
\begin{aligned}
\frac{\rho^{\mathrm{f}}}{2} & \left(\|\boldsymbol{\theta}_h^n\|_{0,\Omega}^2 - \|\boldsymbol{\theta}_h^{n-1}\|_{0,\Omega}^2 + \|\boldsymbol{\theta}_h^n - \boldsymbol{\theta}_h^{n-1}\|_{0,\Omega}^2 \right) + 2\mu\tau\|\boldsymbol{\epsilon}(\boldsymbol{\theta}_h^n)\|_{0,\Omega}^2 + \tau|y_h^n|_{s_h}^2 \\
& + \frac{\rho^{\mathrm{s}}\epsilon}{2} \left(\|\dot{\boldsymbol{\xi}}_h^n\|_{0,\Sigma}^2 - \|\dot{\boldsymbol{\xi}}_h^{n-1}\|_{0,\Sigma}^2 + \|\dot{\boldsymbol{\xi}}_h^n - \dot{\boldsymbol{\xi}}_h^{n-1}\|_{0,\Sigma}^2 \right) \\
& + \frac{1}{2} \left(\|\boldsymbol{\xi}_h^n\|_{\mathrm{e}}^2 - \|\boldsymbol{\xi}_h^{n-1}\|_{\mathrm{e}}^2 + \|\boldsymbol{\xi}_h^n - \boldsymbol{\xi}_h^{n-1}\|_{\mathrm{e}}^2 \right) \\
& + \tau^2 \big(\partial_\tau \dot{\boldsymbol{\xi}}_h^n, \boldsymbol{L}_h^{\mathrm{e}}(\boldsymbol{\xi}_h^n - \boldsymbol{\xi}_h^\star) \big)_\Sigma + \underbrace{\frac{\tau^2}{\rho^{\mathrm{s}}\epsilon} \big(\boldsymbol{L}_h^{\mathrm{e}}\boldsymbol{\xi}_h^n, \boldsymbol{L}_h^{\mathrm{e}}(\boldsymbol{\xi}_h^n - \boldsymbol{\xi}_h^\star) \big)_\Sigma}_{T_5} \\
= & \; T_1(\tau\boldsymbol{\theta}_h^n) + T_2(\tau\boldsymbol{\theta}_h^n) + T_3(\tau\boldsymbol{\theta}_h^n, \tau y_h^n) - \underbrace{\tau a^{\mathrm{e}}\big(\boldsymbol{\xi}_h^n, \boldsymbol{\mathcal{I}}_h \dot{\boldsymbol{d}}^n - \boldsymbol{\pi}_h^{\mathrm{e}} \partial_\tau \boldsymbol{d}^n \big)}_{T_4} \\
& + \underbrace{\tau^2 \big(\partial_\tau \dot{\boldsymbol{\xi}}_h^n, \boldsymbol{L}_h^{\mathrm{e}}(\boldsymbol{d}^n - \boldsymbol{d}^\star) \big)_\Sigma}_{T_6} + \underbrace{\frac{\tau^2}{\rho^{\mathrm{s}}\epsilon} \big(\boldsymbol{L}_h^{\mathrm{e}}\boldsymbol{\xi}_h^n, \boldsymbol{L}_h^{\mathrm{e}}(\boldsymbol{d}^n - \boldsymbol{d}^\star) \big)_\Sigma}_{T_7} .
\end{aligned}
\tag{70}
$$

We now estimate each term T_i separately, for $i = 1, \ldots, 7$. At this point, it is worth noticing that the terms T_i, for $i = 1, \ldots, 4$, are already present in the analysis of Algorithm 2. On the contrary, the terms T_5, T_6 and T_7 come from the perturbation of the interface kinematic constraint (69) (see also (39)) and, therefore, are inherent to Algorithm 5.

The first term can be bounded, in a standard fashion (see, e.g., [42]), using a Taylor expansion, Lemma 5.1 and the Poincaré inequality. This yields

$$
\begin{aligned}
T_1(\tau\boldsymbol{\theta}_h^n) & \leq \rho^{\mathrm{f}}\tau \left(\|\partial_t\boldsymbol{u}(t_n) - \partial_\tau\boldsymbol{u}^n\|_{0,\Omega} + \|\partial_\tau\boldsymbol{\theta}_\pi^n\|_{0,\Omega} \right) \|\boldsymbol{\theta}_h^n\|_{0,\Omega} \\
& \leq \rho^{\mathrm{f}}\tau \left(\tau^{\frac{1}{2}}\|\partial_{tt}\boldsymbol{u}\|_{L^2(t_{n-1},t_n;L^2(\Omega))} + \tau^{-\frac{1}{2}}\|\partial_t\boldsymbol{\theta}_\pi\|_{L^2(t_{n-1},t_n;L^2(\Omega))} \right) \|\boldsymbol{\theta}_h^n\|_{0,\Omega} \\
& \leq \frac{(\rho^{\mathrm{f}}C_{\mathrm{P}})^2}{2\varepsilon_1\mu} \left(\tau^2\|\partial_{tt}\boldsymbol{u}\|_{L^2(t_{n-1},t_n;L^2(\Omega))}^2 + \|\partial_t\boldsymbol{\theta}_\pi\|_{L^2(t_{n-1},t_n;L^2(\Omega))}^2 \right) + \frac{\varepsilon_1}{2}\tau\|\boldsymbol{\theta}_h^n\|_{\boldsymbol{V}}^2 \\
& \lesssim \frac{(\rho^{\mathrm{f}}C_{\mathrm{P}})^2}{\varepsilon_1\mu} \left(\tau^2\|\partial_{tt}\boldsymbol{u}\|_{L^2(t_{n-1},t_n;L^2(\Omega))}^2 + c_\mu^2 h^{2k+2}\|\partial_t\boldsymbol{u}\|_{L^2(t_{n-1},t_n;H^{k+1}(\Omega))}^2 \right) \\
& \qquad + \frac{(\rho^{\mathrm{f}}C_{\mathrm{P}})^2}{\varepsilon_1\mu} \tilde{c}_\mu^2 h^{2k+2}\|\partial_t\boldsymbol{u}\|_{L^2(t_{n-1},t_n;H^{k+1}(\Sigma))}^2 + \varepsilon_1\tau\|\boldsymbol{\theta}_h^n\|_{\boldsymbol{V}}^2, \quad (71)
\end{aligned}
$$

with $\varepsilon_1 > 0$. Note that, by applying the Korn inequality and by choosing ε_1 small enough, the last term of (71) can be absorbed into the left-hand side of (70).

Similarly, for the second term, using (52), (2)$_1$ and the trace inequality, we have

$$
\begin{aligned}
T_2(\tau\boldsymbol{\theta}_h^n) & \leq \rho^{\mathrm{s}}\epsilon\tau \big(\|\partial_t\dot{\boldsymbol{d}}(t_n) - \partial_\tau\dot{\boldsymbol{d}}^n\|_{0,\Sigma} + \|\partial_\tau\dot{\boldsymbol{\xi}}_\pi^n\|_{0,\Sigma} \big) \|\boldsymbol{\theta}_h^n\|_{0,\Sigma} \\
& \leq \rho^{\mathrm{s}}\epsilon\tau \big(\tau^{\frac{1}{2}}\|\partial_{tt}\dot{\boldsymbol{d}}\|_{L^2(t_{n-1},t_n;L^2(\Sigma))} + \tau^{-\frac{1}{2}}\|\partial_t\dot{\boldsymbol{\xi}}_\pi\|_{L^2(t_{n-1},t_n;L^2(\Sigma))} \big) \|\boldsymbol{\theta}_h^n\|_{0,\Sigma} \\
& \lesssim \frac{(\rho^{\mathrm{s}}\epsilon C_{\mathrm{T}})^2}{\varepsilon_2\mu} \left(\tau^2\|\partial_{tt}\boldsymbol{u}\|_{L^2(t_{n-1},t_n;L^2(\Sigma))}^2 + h^{2k+2}\|\partial_t\boldsymbol{u}\|_{L^2(t_{n-1},t_n;H^{k+1}(\Sigma))} \right) \\
& \qquad\qquad\qquad\qquad\qquad\qquad\qquad\qquad\qquad + \varepsilon_2\tau\|\boldsymbol{\theta}_h^n\|_{\boldsymbol{V}}^2, \quad (72)
\end{aligned}
$$

with $\varepsilon_2 > 0$. The last term can be absorbed into the left-hand side of (70) as in (71).

Using (12), $(53)_4$ and the fact that $\mathrm{div}\boldsymbol{u}^n = 0$, for the third term we have

$$
\begin{aligned}
T_3(\tau\boldsymbol{\theta}_h^n, \tau y_h^n) = & -\tau a\big(\boldsymbol{\theta}_\pi^n, \boldsymbol{\theta}_h^n\big) - \tau b\big(y_\pi^n, \boldsymbol{\theta}_h^n\big) + \tau s_h\big(R_h\boldsymbol{u}^n, y_h^n\big) + \tau s_h\big(\Pi_h p^n, y_h^n\big) \\
\leq & \frac{\tau}{2\varepsilon_3}\big(\|\boldsymbol{\theta}_\pi^n\|_{\boldsymbol{V}}^2 + \|y_\pi^n\|_Q^2 + |R_h\boldsymbol{u}^n|_{s_h}^2 + |\Pi_h p^n|_{s_h}^2\big) \\
& + \frac{\varepsilon_3\tau}{2}\big(2\|\boldsymbol{\theta}_h^n\|_{\boldsymbol{V}}^2 + 2|y_h^n|_{s_h}^2\big),
\end{aligned}
$$

with $\varepsilon_3 > 0$. Hence, using Lemma 5.1, (13) and (14) we get

$$
\begin{aligned}
T_3(\tau\boldsymbol{\theta}_h^n, \tau y_h^n) \lesssim & \frac{\tau}{\varepsilon_3}\Big(\mu h^{2k}\|\boldsymbol{u}^n\|_{k+1,\Omega}^2 + \mu^{-1}h^{2\tilde{l}}\|p^n\|_{\tilde{l},\Omega}^2\Big) \\
& + \varepsilon_3\tau\big(\|\boldsymbol{\theta}_h^n\|_{\boldsymbol{V}}^2 + |y_h^n|_{s_h}^2\big).
\end{aligned}
\tag{73}
$$

Once more, the last term is absorbed into the left-hand side of (70) by choosing ε_3 sufficiently small.

For the term T_4, we apply (17), (3), (52) and a Taylor expansion to obtain

$$
\begin{aligned}
T_4 = & a^{\mathrm{e}}\big(\boldsymbol{\xi}_h^n, \boldsymbol{\mathcal{I}}_h\dot{\boldsymbol{d}}^n - \partial_\tau\boldsymbol{d}^n\big) \leq \tau\|\boldsymbol{\xi}_h^n\|_{\mathrm{e}}\|\boldsymbol{\mathcal{I}}_h\dot{\boldsymbol{d}}^n - \partial_\tau\boldsymbol{d}^n\|_{\mathrm{e}} \\
\leq & \frac{\tau T}{2}\Big(\|\boldsymbol{\mathcal{I}}_h\dot{\boldsymbol{d}}^n - \dot{\boldsymbol{d}}^n\|_{\mathrm{e}}^2 + \|\dot{\boldsymbol{d}}^n - \partial_\tau\boldsymbol{d}^n\|_{\mathrm{e}}^2\Big) + \frac{\tau}{T}\|\boldsymbol{\xi}_h^n\|_{\mathrm{e}}^2 \\
\lesssim & h^{2k}\beta^{\mathrm{e}}T\tau\|\boldsymbol{u}^n\|_{k+1,\Sigma}^2 + \tau^2\beta^{\mathrm{e}}T\|\partial_t\boldsymbol{u}\|_{L^2(t_{n-1},t_n;H^1(\Sigma))}^2 + \frac{\tau}{2T}\|\boldsymbol{\xi}_h^n\|_{\mathrm{e}}^2.
\end{aligned}
\tag{74}
$$

The last term can be controlled thanks to (70) via Lemma 4.1.

The term T_5 can be estimated using basically the same arguments than in the proof of Theorem 4.2. The consistency terms T_6 and T_7 also need specific treatments that depend on the choice of the extrapolation $\boldsymbol{d}_h^\star$. We analyze below each case separately.

Case $\boldsymbol{d}_h^\star = \boldsymbol{0}$. As in (47), we have

$$
T_5 \geq \frac{\tau^2}{\rho^{\mathrm{s}}\epsilon}\left(1 - \frac{1}{2\varepsilon_4}\right)\|\boldsymbol{L}_h^{\mathrm{e}}\boldsymbol{\xi}_h^n\|_{0,\Sigma}^2 - \varepsilon_4\frac{\rho^{\mathrm{s}}\epsilon}{2}\|\dot{\boldsymbol{\xi}}_h^n - \dot{\boldsymbol{\xi}}_h^{n-1}\|_{0,\Sigma}^2,
$$

with $\varepsilon_4 > 0$. On the other hand, using (19), we have the bound

$$
\begin{aligned}
T_6 = & \tau\big(\dot{\boldsymbol{\xi}}_h^n - \dot{\boldsymbol{\xi}}_h^{n-1}, \boldsymbol{L}_h^{\mathrm{e}}\boldsymbol{d}^n\big)_\Sigma \leq \tau\|\dot{\boldsymbol{\xi}}_h^n - \dot{\boldsymbol{\xi}}_h^{n-1}\|_{0,\Sigma}\|\boldsymbol{L}_h^{\mathrm{e}}\boldsymbol{d}^n\|_{0,\Sigma} \\
\leq & \frac{\varepsilon_5\rho^{\mathrm{s}}\epsilon}{2}\|\dot{\boldsymbol{\xi}}_h^n - \dot{\boldsymbol{\xi}}_h^{n-1}\|_{0,\Sigma}^2 + \frac{\tau^2}{2\varepsilon_5\rho^{\mathrm{s}}\epsilon}\|\boldsymbol{L}^{\mathrm{e}}\boldsymbol{d}^n\|_{0,\Sigma}^2,
\end{aligned}
$$

with $\varepsilon_5 > 0$. Similarly, for the last term, we obtain

$$
T_7 = \frac{\tau^2}{\rho^{\mathrm{s}}\epsilon}\big(\boldsymbol{L}_h^{\mathrm{e}}\boldsymbol{\xi}_h^n, \boldsymbol{L}_h^{\mathrm{e}}\boldsymbol{d}^n\big)_\Sigma \geq -\frac{\varepsilon_6\tau^2}{2\rho^{\mathrm{s}}\epsilon}\|\boldsymbol{L}_h^{\mathrm{e}}\boldsymbol{\xi}_h^n\|_{0,\Sigma}^2 - \frac{\tau^2}{2\varepsilon_6\rho^{\mathrm{s}}\epsilon}\|\boldsymbol{L}^{\mathrm{e}}\boldsymbol{d}^n\|_{0,\Sigma}^2,
$$

with $\varepsilon_6 > 0$. Hence, by collecting these three estimates, we get

$$
\begin{aligned}
T_5 + T_6 + T_7 \geq & \frac{\tau^2}{\rho^{\mathrm{s}}\epsilon}\left(1 - \frac{1}{2\varepsilon_4} - \frac{\varepsilon_6}{2}\right)\|\boldsymbol{L}_h^{\mathrm{e}}\boldsymbol{\xi}_h^n\|_{0,\Sigma}^2 \\
& - \frac{\tau^2}{2\rho^{\mathrm{s}}\epsilon}\left(\frac{1}{\varepsilon_5} + \frac{1}{\varepsilon_6}\right)\|\boldsymbol{L}^{\mathrm{e}}\boldsymbol{d}^n\|_{0,\Sigma}^2 - \frac{\rho^{\mathrm{s}}\epsilon}{2}(\varepsilon_4 + \varepsilon_5)\|\dot{\boldsymbol{\xi}}_h^n - \dot{\boldsymbol{\xi}}_h^{n-1}\|_{0,\Sigma}^2.
\end{aligned}
\tag{75}
$$

In particular, by taking $\varepsilon_4 = \frac{3}{4}$, $\varepsilon_5 = \frac{1}{8}$ and $\varepsilon_6 = \frac{1}{3}$, we have

$$1 - \frac{1}{2\varepsilon_4} - \frac{\varepsilon_6}{2} > 0$$

and the last term of (75) can be absorbed into the left-hand side of (70).

In summary, the estimate (60) follows by inserting the estimates (71)-(75) into (70), using Korn's inequality, summing over $m = 1, \ldots, n$, and applying Lemma 4.1 with

$$a_m = \frac{\rho^{\mathrm{f}}}{2}\|\boldsymbol{\theta}_h^m\|_{0,\Omega}^2 + \frac{\rho^{\mathrm{s}}\epsilon}{2}\|\dot{\boldsymbol{\xi}}_h^m\|_{0,\Sigma}^2 + \frac{1}{2}\|\boldsymbol{\xi}_h^m\|_{\mathrm{e}}^2, \quad \gamma_m = \frac{1}{T}.$$

Note in particular that, owing to (57)-(58) and (59), we have

$$\boldsymbol{\theta}_h^0 = \mathbf{0}, \quad \dot{\boldsymbol{\xi}}_h^0 = \boldsymbol{\xi}_h^0 = \mathbf{0}. \tag{76}$$

Case $\boldsymbol{d}_h^\star = \boldsymbol{d}_h^{n-1}$. For the term T_5 we proceed as in the proof of Theorem 4.2 and use (65) and (20) to obtain

$$
\begin{aligned}
T_5 = {} & \frac{\tau^2}{2}\left(\|\dot{\boldsymbol{\xi}}_h^n\|_{\mathrm{e}}^2 - \|\dot{\boldsymbol{\xi}}_h^{n-1}\|_{\mathrm{e}}^2 + \|\dot{\boldsymbol{\xi}}_h^n - \dot{\boldsymbol{\xi}}_h^{n-1}\|_{\mathrm{e}}^2\right) \\
& - \underbrace{\tau^2\big(\dot{\boldsymbol{\xi}}_h^n - \dot{\boldsymbol{\xi}}_h^{n-1}, \boldsymbol{L}_h^{\mathrm{e}}(\mathcal{I}_h\dot{\boldsymbol{d}}^n - \partial_\tau \boldsymbol{d}^n)\big)_\Sigma}_{T_{5,1}} \\
& + \frac{\tau^2}{2\rho^{\mathrm{s}}\epsilon}\left(\|\boldsymbol{L}_h^{\mathrm{e}}\boldsymbol{\xi}_h^n\|_{0,\Sigma}^2 - \|\boldsymbol{L}_h^{\mathrm{e}}\boldsymbol{\xi}_h^{n-1}\|_{0,\Sigma}^2 + \|\boldsymbol{L}_h^{\mathrm{e}}(\boldsymbol{\xi}_h^n - \boldsymbol{\xi}_h^{n-1})\|_{0,\Sigma}^2\right).
\end{aligned}
$$

On the other hand, from (16) and similarly to (74), we get

$$
\begin{aligned}
T_{5,1} = {} & \tau^2 a^{\mathrm{e}}\big(\dot{\boldsymbol{\xi}}_h^n - \dot{\boldsymbol{\xi}}_h^{n-1}, \mathcal{I}_h\dot{\boldsymbol{d}}^n - \partial_\tau \boldsymbol{d}^n\big) \\
\lesssim {} & \frac{\tau^2}{4}\|\dot{\boldsymbol{\xi}}_h^n - \dot{\boldsymbol{\xi}}_h^{n-1}\|_{\mathrm{e}}^2 + h^{2k}\beta^{\mathrm{e}}\tau^2\|\boldsymbol{u}^n\|_{k+1,\Sigma}^2 + \tau^3\beta^{\mathrm{e}}\|\partial_t\boldsymbol{u}\|_{L^2(t_{n-1},t_n;H^1(\Sigma))}^2,
\end{aligned}
$$

so that

$$
\begin{aligned}
T_5 \gtrsim {} & \frac{\tau^2}{2}\left(\|\dot{\boldsymbol{\xi}}_h^n\|_{\mathrm{e}}^2 - \|\dot{\boldsymbol{\xi}}_h^{n-1}\|_{\mathrm{e}}^2\right) + \frac{\tau^2}{4}\|\dot{\boldsymbol{\xi}}_h^n - \dot{\boldsymbol{\xi}}_h^{n-1}\|_{\mathrm{e}}^2 \\
& + \frac{\tau^2}{2\rho^{\mathrm{s}}\epsilon}\left(\|\boldsymbol{L}_h^{\mathrm{e}}\boldsymbol{\xi}_h^n\|_{0,\Sigma}^2 - \|\boldsymbol{L}_h^{\mathrm{e}}\boldsymbol{\xi}_h^{n-1}\|_{0,\Sigma}^2 + \|\boldsymbol{L}_h^{\mathrm{e}}(\boldsymbol{\xi}_h^n - \boldsymbol{\xi}_h^{n-1})\|_{0,\Sigma}^2\right) \\
& - h^{2k}\beta^{\mathrm{e}}\tau^2\|\boldsymbol{u}^n\|_{k+1,\Sigma}^2 - \tau^3\beta^{\mathrm{e}}\|\partial_t\boldsymbol{u}\|_{L^2(t_{n-1},t_n;H^1(\Sigma))}^2.
\end{aligned}
\tag{77}
$$

Using (19) and a Taylor expansion, we get the following bound for T_6:

$$
\begin{aligned}
T_6 = {} & \tau\big(\dot{\boldsymbol{\xi}}_h^n - \dot{\boldsymbol{\xi}}_h^{n-1}, \boldsymbol{L}_h^{\mathrm{e}}(\boldsymbol{d}^n - \boldsymbol{d}^{n-1})\big)_\Sigma \leq \tau\|\dot{\boldsymbol{\xi}}_h^n - \dot{\boldsymbol{\xi}}_h^{n-1}\|_{0,\Sigma}\|\boldsymbol{L}_h^{\mathrm{e}}(\boldsymbol{d}^n - \boldsymbol{d}^{n-1})\|_{0,\Sigma} \\
\leq {} & \tau\frac{\rho^{\mathrm{s}}\epsilon}{2T}\left(\|\dot{\boldsymbol{\xi}}_h^n\|_{0,\Sigma}^2 + \|\dot{\boldsymbol{\xi}}_h^{n-1}\|_{0,\Sigma}^2\right) + \frac{\tau T}{\rho^{\mathrm{s}}\epsilon}\|\boldsymbol{L}^{\mathrm{e}}(\boldsymbol{d}^n - \boldsymbol{d}^{n-1})\|_{0,\Sigma}^2 \\
\leq {} & \tau\frac{\rho^{\mathrm{s}}\epsilon}{2T}\left(\|\dot{\boldsymbol{\xi}}_h^n\|_{0,\Sigma}^2 + \|\dot{\boldsymbol{\xi}}_h^{n-1}\|_{0,\Sigma}^2\right) + \frac{\tau^2 T}{\rho^{\mathrm{s}}\epsilon}\|\boldsymbol{L}^{\mathrm{e}}\partial_t\boldsymbol{d}\|_{L^2(t_{n-1},t_n;L^2(\Sigma))}^2.
\end{aligned}
\tag{78}
$$

The first term of this bound is controlled thanks to (70) via Lemma 4.1.

Similarly, for the last term, we obtain

$$
\begin{aligned}
T_7 =& \frac{\tau^2}{\rho^{\mathrm{s}}\epsilon}\big(\boldsymbol{L}_h^{\mathrm{e}}\boldsymbol{\xi}_h^n, \boldsymbol{L}_h^{\mathrm{e}}(\boldsymbol{d}^n - \boldsymbol{d}^{n-1})\big)_\Sigma \\
\leq& \frac{\tau^3}{2T\rho^{\mathrm{s}}\epsilon}\|\boldsymbol{L}_h^{\mathrm{e}}\boldsymbol{\xi}_h^n\|_{0,\Sigma}^2 + \frac{\tau T}{2\rho^{\mathrm{s}}\epsilon}\|\boldsymbol{L}^{\mathrm{e}}(\boldsymbol{d}^n - \boldsymbol{d}^{n-1})\|_{0,\Sigma}^2 \\
\leq& \frac{\tau^3}{2T\rho^{\mathrm{s}}\epsilon}\|\boldsymbol{L}_h^{\mathrm{e}}\boldsymbol{\xi}_h^n\|_{0,\Sigma}^2 + \frac{\tau^2 T}{2\rho^{\mathrm{s}}\epsilon}\|\boldsymbol{L}^{\mathrm{e}}\partial_t\boldsymbol{d}\|_{L^2(t_{n-1},t_n;L^2(\Sigma))}^2.
\end{aligned}
\tag{79}
$$

Here, the first term of the left-hand side is treated through the control provided by (77) and Lemma 4.1.

In summary, the estimate (60) follows by inserting the estimates (71)-(74) and (77)-(79) into (70), using Korn's inequality, summing over $m = 1, \ldots, n$, using (76) and applying Lemma 4.1 with

$$
a_m = \frac{\rho^{\mathrm{f}}}{2}\|\boldsymbol{\theta}_h^m\|_{0,\Omega}^2 + \frac{\rho^{\mathrm{s}}\epsilon}{2}\|\dot{\boldsymbol{\xi}}_h^m\|_{0,\Sigma}^2 + \frac{1}{2}\|\boldsymbol{\xi}_h^m\|_{\mathrm{e}}^2 + \frac{\tau^2}{2\rho^{\mathrm{s}}\epsilon}\|\boldsymbol{L}_h^{\mathrm{e}}\boldsymbol{\xi}_h^m\|_{0,\Sigma}^2, \quad \gamma_m = \frac{1}{T}.
$$

Case $\boldsymbol{d}_h^\star = \boldsymbol{d}^{n-1} + \tau\dot{\boldsymbol{d}}^{n-1}$. We first consider the term T_6. Using (19) and a Taylor expansion, we obtain

$$
\begin{aligned}
T_6 =& \tau^2\big(\dot{\boldsymbol{\xi}}_h^n - \dot{\boldsymbol{\xi}}_h^{n-1}, \boldsymbol{L}_h^{\mathrm{e}}(\partial_\tau\boldsymbol{d}^n - \dot{\boldsymbol{d}}^{n-1})\big)_\Sigma \\
\leq& \tau\frac{\rho^{\mathrm{s}}\epsilon}{2T}\big(\|\dot{\boldsymbol{\xi}}_h^n\|_{0,\Sigma}^2 + \|\dot{\boldsymbol{\xi}}_h^{n-1}\|_{0,\Sigma}^2\big) + \frac{\tau^3 T}{2\rho^{\mathrm{s}}\epsilon}\|\boldsymbol{L}^{\mathrm{e}}(\partial_\tau\boldsymbol{d}^n - \dot{\boldsymbol{d}}^{n-1})\|_{0,\Sigma}^2 \\
\leq& \tau\frac{\rho^{\mathrm{s}}\epsilon}{2T}\big(\|\dot{\boldsymbol{\xi}}_h^n\|_{0,\Sigma}^2 + \|\dot{\boldsymbol{\xi}}_h^{n-1}\|_{0,\Sigma}^2\big) + \frac{\tau^4 T}{2\rho^{\mathrm{s}}\epsilon}\|\boldsymbol{L}^{\mathrm{e}}\partial_{tt}\boldsymbol{d}\|_{L^2(t_{n-1},t_n;L^2(\Sigma))}^2,
\end{aligned}
\tag{80}
$$

where the first term of the bound is controlled via Lemma 4.1 and (70).

Similarly, using the inverse estimate (23) and the $\frac{6}{5}$-CFL condition (43), for the term T_7 we get

$$
\begin{aligned}
T_7 =& \frac{\tau^3}{\rho^{\mathrm{s}}\epsilon}\big(\boldsymbol{L}_h^{\mathrm{e}}\boldsymbol{\xi}_h^n, \boldsymbol{L}_h^{\mathrm{e}}(\partial_\tau\boldsymbol{d}^n - \dot{\boldsymbol{d}}^{n-1})\big)_\Sigma \\
\leq& \frac{\tau^3}{2T\rho^{\mathrm{s}}\epsilon}\|\boldsymbol{L}_h^{\mathrm{e}}\boldsymbol{\xi}_h^n\|_{0,\Sigma}^2 + \frac{\tau^3 T}{2\rho^{\mathrm{s}}\epsilon}\|\boldsymbol{L}^{\mathrm{e}}(\partial_\tau\boldsymbol{d}^n - \dot{\boldsymbol{d}}^{n-1})\|_{0,\Sigma}^2 \\
\leq& \frac{\tau^3}{2T\rho^{\mathrm{s}}\epsilon}\|\boldsymbol{L}_h^{\mathrm{e}}\boldsymbol{\xi}_h^n\|_{0,\Sigma}^2 + \frac{\tau^4 T}{2\rho^{\mathrm{s}}\epsilon}\|\partial_{tt}\boldsymbol{L}^{\mathrm{e}}\boldsymbol{d}\|_{L^2(t_{n-1},t_n;L^2(\Sigma))}^2 \\
\leq& \frac{\tau^3(\omega^{\mathrm{e}}C_{\mathrm{inv}})^2}{2Th^2}\|\boldsymbol{\xi}_h^n\|_{\mathrm{e}}^2 + \frac{\tau^4 T}{2\rho^{\mathrm{s}}\epsilon}\|\partial_{tt}\boldsymbol{L}^{\mathrm{e}}\boldsymbol{d}\|_{L^2(t_{n-1},t_n;L^2(\Sigma))}^2 \\
\leq& \frac{\tau\alpha^{\frac{5}{3}}\tau^{\frac{1}{3}}}{2T}\|\boldsymbol{\xi}_h^n\|_{\mathrm{e}}^2 + \frac{\tau^4 T}{2\rho^{\mathrm{s}}\epsilon}\|\partial_{tt}\boldsymbol{L}^{\mathrm{e}}\boldsymbol{d}\|_{L^2(t_{n-1},t_n;L^2(\Sigma))}^2.
\end{aligned}
\tag{81}
$$

Once more, the first term of the bound is controlled via Lemma 4.1 and (70).

For the term T_5 we first note that, from (67) and (58), we have

$$
\boldsymbol{\xi}_h^\star = \boldsymbol{\xi}_h^{n-1} + \tau\dot{\boldsymbol{\xi}}_h^{n-1} + \tau(\boldsymbol{\pi}_h^{\mathrm{e}}\dot{\boldsymbol{d}}^{n-1} - \boldsymbol{\mathcal{I}}_h\dot{\boldsymbol{d}}^{n-1}).
$$

Thus, from (65) and (20), it follows that

$$
\begin{aligned}
T_5 =& \tau^2\big(\dot{\boldsymbol{\xi}}_h^n - \dot{\boldsymbol{\xi}}_h^{n-1}, \boldsymbol{L}_h^{\mathrm{e}}(\dot{\boldsymbol{\xi}}_h^n - \dot{\boldsymbol{\xi}}_h^{n-1})\big)_\Sigma + \frac{\tau^3}{\rho^{\mathrm{s}}\epsilon}\big(\boldsymbol{L}_h^{\mathrm{e}}\boldsymbol{\xi}_h^n, \boldsymbol{L}_h^{\mathrm{e}}(\dot{\boldsymbol{\xi}}_h^n - \dot{\boldsymbol{\xi}}_h^{n-1})\big)_\Sigma \\
&- \underbrace{\tau^2\left(\dot{\boldsymbol{\xi}}_h^n - \dot{\boldsymbol{\xi}}_h^{n-1}, \boldsymbol{L}_h^{\mathrm{e}}\big(\mathcal{I}_h(\dot{\boldsymbol{d}}^n - \dot{\boldsymbol{d}}^{n-1}) - \partial_\tau \boldsymbol{d}^n + \dot{\boldsymbol{d}}^{n-1}\big)\right)_\Sigma}_{T_{5,1}} \\
&- \underbrace{\frac{\tau^3}{\rho^{\mathrm{s}}\epsilon}\left(\boldsymbol{L}_h^{\mathrm{e}}\boldsymbol{\xi}_h^n, \boldsymbol{L}_h^{\mathrm{e}}\big(\mathcal{I}_h(\dot{\boldsymbol{d}}^n - \dot{\boldsymbol{d}}^{n-1}) - \partial_\tau \boldsymbol{d}^n + \dot{\boldsymbol{d}}^{n-1}\big)\right)_\Sigma}_{T_{5,2}}.
\end{aligned}
$$

Proceeding similarly to (48) and (49), we then have

$$
T_5 \geq \tau^2\|\dot{\boldsymbol{\xi}}_h^n - \dot{\boldsymbol{\xi}}_h^{n-1}\|_{\mathrm{e}}^2 - \frac{\rho^{\mathrm{s}}}{4}\|\dot{\boldsymbol{\xi}}_h^n - \dot{\boldsymbol{\xi}}_h^{n-1}\|_{0,\Sigma}^2 - \tau\alpha^5\|\boldsymbol{\xi}_h^n\|_{\mathrm{e}}^2 - T_{5,1} - T_{5,2}, \tag{82}
$$

under the $\frac{6}{5}$-CFL condition (43). Moreover, using (16) and adding and subtracting $\dot{\boldsymbol{d}}^n$ in $T_{5,1}$ yields

$$
\begin{aligned}
T_{5,1} =& \tau^2 a^{\mathrm{e}}\big(\dot{\boldsymbol{\xi}}_h^n - \dot{\boldsymbol{\xi}}_h^{n-1}, \mathcal{I}_h(\dot{\boldsymbol{d}}^n - \dot{\boldsymbol{d}}^{n-1}) - (\dot{\boldsymbol{d}}^n - \dot{\boldsymbol{d}}^{n-1})\big) \\
&+ \tau^2\big(\dot{\boldsymbol{\xi}}_h^n - \dot{\boldsymbol{\xi}}_h^{n-1}, \boldsymbol{L}_h^{\mathrm{e}}(\dot{\boldsymbol{d}}^n - \partial_\tau \boldsymbol{d}^n)\big)_\Sigma,
\end{aligned}
$$

with the second term in the right-hand side similar to (80). For the first we apply (3) and (52), so that we infer the bound

$$
\begin{aligned}
T_{5,1} \lesssim& \frac{\tau^2}{2}\|\dot{\boldsymbol{\xi}}_h^n - \dot{\boldsymbol{\xi}}_h^{n-1}\|_{\mathrm{e}}^2 + h^{2k}\beta^{\mathrm{e}}\tau^2\|\boldsymbol{u}^n - \boldsymbol{u}^{n-1}\|_{k+1,\Sigma}^2 \\
&+ \tau\frac{\rho^{\mathrm{s}}\epsilon}{2T}\left(\|\dot{\boldsymbol{\xi}}_h^n\|_{0,\Sigma}^2 + \|\dot{\boldsymbol{\xi}}_h^{n-1}\|_{0,\Sigma}^2\right) + \frac{\tau^4 T}{2\rho^{\mathrm{s}}\epsilon}\|\boldsymbol{L}^{\mathrm{e}}\partial_{tt}\boldsymbol{d}\|_{L^2(t_{n-1},t_n;L^2(\Sigma))}^2.
\end{aligned} \tag{83}
$$

Analogously, for the term $T_{5,2}$ we have

$$
\begin{aligned}
T_{5,2} =& \frac{\tau^3}{\rho^{\mathrm{s}}\epsilon}a^{\mathrm{e}}\big(\boldsymbol{L}_h^{\mathrm{e}}\boldsymbol{\xi}_h^n, \mathcal{I}_h(\dot{\boldsymbol{d}}^n - \dot{\boldsymbol{d}}^{n-1}) - (\dot{\boldsymbol{d}}^n - \dot{\boldsymbol{d}}^{n-1})\big) \\
&+ \frac{\tau^3}{\rho^{\mathrm{s}}\epsilon}\big(\boldsymbol{L}_h^{\mathrm{e}}\boldsymbol{\xi}_h^n, \boldsymbol{L}_h^{\mathrm{e}}(\dot{\boldsymbol{d}}^n - \partial_\tau \boldsymbol{d}^n)\big)_\Sigma,
\end{aligned}
$$

with the second term of the right-hand side similar to (81). In the first, we apply the inverse estimates (22), (23) and the $\frac{6}{5}$-CFL condition (43), so that

$$
\begin{aligned}
T_{5,2} \leq& \frac{\tau^5}{2T(\rho^{\mathrm{s}}\epsilon)^2}\|\boldsymbol{L}_h^{\mathrm{e}}\boldsymbol{\xi}_h^n\|_{\mathrm{e}}^2 + \frac{\tau T}{2}\|\mathcal{I}_h(\dot{\boldsymbol{d}}^n - \dot{\boldsymbol{d}}^{n-1}) - (\dot{\boldsymbol{d}}^n - \dot{\boldsymbol{d}}^{n-1})\|_{\mathrm{e}}^2 \\
&+ \frac{\tau\alpha^{\frac{5}{3}}\tau^{\frac{1}{3}}}{2T}\|\boldsymbol{\xi}_h^n\|_{\mathrm{e}}^2 + \frac{\tau^4 T}{2\rho^{\mathrm{s}}\epsilon}\|\partial_{tt}\boldsymbol{L}^{\mathrm{e}}\boldsymbol{d}\|_{L^2(t_{n-1},t_n;L^2(\Sigma))}^2 \\
\lesssim& \left(\frac{\tau\alpha^{\frac{10}{3}}\tau^{\frac{2}{3}}}{2T} + \frac{\tau\alpha^{\frac{5}{3}}\tau^{\frac{1}{3}}}{2T}\right)\|\boldsymbol{\xi}_h^n\|_{\mathrm{e}}^2 + h^{2k}\beta^{\mathrm{e}}\tau T\|\boldsymbol{u}^n - \boldsymbol{u}^{n-1}\|_{k+1,\Sigma}^2 \\
&+ \frac{\tau^4 T}{2\rho^{\mathrm{s}}\epsilon}\|\partial_{tt}\boldsymbol{L}^{\mathrm{e}}\boldsymbol{d}\|_{L^2(t_{n-1},t_n;L^2(\Sigma))}^2.
\end{aligned} \tag{84}
$$

In short, by inserting the estimates (84) and (83) into (82), we finally get

$$T_5 \gtrsim \frac{\tau^2}{2} \|\dot{\boldsymbol{\xi}}_h^n - \dot{\boldsymbol{\xi}}_h^{n-1}\|_{\mathrm{e}}^2 - \frac{\rho^{\mathrm{s}}}{4} \|\dot{\boldsymbol{\xi}}_h^n - \dot{\boldsymbol{\xi}}_h^{n-1}\|_{0,\Sigma}^2 - \tau \frac{\rho^{\mathrm{s}}\epsilon}{2T} \left(\|\dot{\boldsymbol{\xi}}_h^n\|_{0,\Sigma}^2 + \|\dot{\boldsymbol{\xi}}_h^{n-1}\|_{0,\Sigma}^2 \right)$$

$$- \tau \left(\alpha^5 + \frac{\alpha^{\frac{10}{3}}\tau^{\frac{2}{3}}}{2T} + \frac{\alpha^{\frac{5}{3}}\tau^{\frac{1}{3}}}{2T} \right) \|\boldsymbol{\xi}_h^n\|_{\mathrm{e}}^2 - \frac{\tau^4 T}{2\rho^{\mathrm{s}}\epsilon} \|\boldsymbol{L}^{\mathrm{e}} \partial_{tt} \boldsymbol{d}\|_{L^2(t_{n-1},t_n;L^2(\Sigma))}^2$$

$$- h^{2k}\beta^{\mathrm{e}}(T+\tau)\tau\|\boldsymbol{u}^n - \boldsymbol{u}^{n-1}\|_{k+1,\Sigma}^2. \quad (85)$$

The first negative term is absorbed into the left-hand side of (70) and, the two following treated via Lemma 4.1.

The estimate (60) then follows by inserting (71)-(74), (79), (81) and (85) into (70), using Korn's inequality, summing over $m = 1, \ldots, n$, using (76) and applying Lemma 4.1 with

$$a_m = \frac{\rho^{\mathrm{f}}}{2} \|\boldsymbol{\theta}_h^m\|_{0,\Omega}^2 + \frac{\rho^{\mathrm{s}}\epsilon}{2} \|\dot{\boldsymbol{\xi}}_h^m\|_{0,\Sigma}^2 + \frac{1}{2} \|\boldsymbol{\xi}_h^m\|_{\mathrm{e}}^2,$$

$$\gamma_m = \max \left\{ \frac{1}{T}, 2\alpha^5, \frac{\alpha^{\frac{10}{3}}\tau^{\frac{2}{3}} + \alpha^{\frac{5}{3}}\tau^{\frac{1}{3}}}{T} \right\}.$$

Hence, the proof is complete. $\diamond$

Remark 5.3 *As for the stability (see Remark 4.3) in the case $\boldsymbol{d}_h^\star = \boldsymbol{0}$, the error estimate (60) makes use of the solid time-marching numerical dissipation, which is needed to absorb the last term of (75). On the contrary, for the incremental scheme with $\boldsymbol{d}_h^\star = \boldsymbol{d}_h^{n-1}$ this dissipation is superfluous. Yet, for $\boldsymbol{d}_h^\star = \boldsymbol{d}_h^n + \tau \dot{\boldsymbol{d}}_h^{n-1}$ and under the $\frac{4}{3}$-CFL condition (50), the term T_5 can alternatively be bounded from below as follows:*

$$T_5 \geq \frac{\tau^2}{2} \|\dot{\boldsymbol{\xi}}_h^n - \dot{\boldsymbol{\xi}}_h^{n-1}\|_{\mathrm{e}}^2 - \tau \frac{\alpha^3}{2} \|\boldsymbol{\xi}_h^n\|_{\mathrm{e}}^2 - T_{5,1} - T_{5,2},$$

where the second term of the right-hand side can be controlled via Lemma 4.1 and (70), so that the use of the numerical dissipation is avoided. $\diamond$

We define the energy-norm of the error, at time level $n \geq 1$, as

$$\mathcal{Z}_h^n \overset{\text{def}}{=} (\rho^{\mathrm{f}})^{\frac{1}{2}} \|\boldsymbol{u}^n - \boldsymbol{u}_h^n\|_{0,\Omega} + \left(\sum_{m=1}^n \tau \|\boldsymbol{u}^m - \boldsymbol{u}_h^m\|_{\boldsymbol{V}}^2 \right)^{\frac{1}{2}} + \left(\sum_{m=1}^n \tau |p_h^m|_{s_h}^2 \right)^{\frac{1}{2}}$$

$$+ (\rho^{\mathrm{s}}\epsilon)^{\frac{1}{2}} \|\dot{\boldsymbol{d}}^n - \dot{\boldsymbol{d}}_h^n\|_{0,\Sigma} + \|\boldsymbol{d}^n - \boldsymbol{d}_h^n\|_{\mathrm{e}},$$

for which we have the following a priori estimate.

Corollary 5.4 *Under the assumptions of Theorem 5.2, for $n \geq 1$ and $n\tau \leq T$, there holds*

$$\mathcal{Z}_h^n \lesssim c^\star \left(\tilde{c}_1 h^k + c_2 h^{\tilde{l}} + c_3 \tau + e_\tau^\star \right) \quad (86)$$

with

$$\tilde{c}_1 \overset{\text{def}}{=} c_1 + (\rho^{\mathrm{f}})^{\frac{1}{2}} h \left(c_\mu \mu^{\frac{1}{2}} \|\boldsymbol{u}\|_{L^\infty(0,T;H^{k+1}(\Omega))} + \tilde{c}_\mu \|\boldsymbol{u}\|_{L^\infty(0,T;H^{k+1}(\Sigma))} \right)$$

$$+ (\rho^{\mathrm{s}}\epsilon)^{\frac{1}{2}} h \|\boldsymbol{u}\|_{L^\infty(0,T;H^{k+1}(\Sigma))} + (\beta^{\mathrm{e}})^{\frac{1}{2}} \|\boldsymbol{d}\|_{L^\infty(0,T;H^{k+1}(\Sigma))}$$

and $c^\star$, c_1, c_2, c_3, $e_\tau^\star$ given by Theorem 5.2.

Proof. It is a direct consequence of (57)-(58), Theorem 5.2, Lemma 5.1 and the estimates (13), (51) and (52). $\diamondsuit$

Following Remark 4.4, and for further reference in Section 6, we provide an error estimate for Algorithm 2, which follows from the proofs of Theorem 5.2 and Corollary 5.4.

Corollary 5.5 *Let* $(\boldsymbol{u}, p, \boldsymbol{d}, \dot{\boldsymbol{d}})$ *be the solution of* (5) *and*

$$\left\{ (\boldsymbol{u}_h^n, p_h^n, \boldsymbol{d}_h^n, \dot{\boldsymbol{d}}_h^n) \right\}_{n \geq 1} \subset \boldsymbol{V}_h \times Q_h \times \boldsymbol{W}_h \times \boldsymbol{W}_h$$

be given by Algorithm 2, with discrete initial data (59). *Suppose that the exact solution has the regularity* (55), *and that* (54) *holds. Then, following error estimate holds, for* $n \geq 1$ *and* $n\tau \leq T$,

$$\mathcal{Z}_h^n \lesssim c^\star \left(\tilde{c}_1 h^k + c_2 h^{\tilde{l}} + c_3 \tau \right), \tag{87}$$

with $\tilde{c}_1$, c_2, c_3 *given by Corollary 5.4 and*

$$c^\star = \exp \left(\frac{T}{T - \tau} \right).$$

Proof. Thanks to $(28)_1$, we can test (64) with

$$(\boldsymbol{v}_h, q_h) = \tau(\boldsymbol{\theta}_h^n, y_h^n), \quad \boldsymbol{w}_h = \tau \dot{\boldsymbol{\xi}}_h^n,$$

so that (70) holds with $T_5 = T_6 = T_7 = 0$. The discrete error estimate (60) is hence inferred with $e_\tau^\star = 0$. We then conclude as in the proof of Corollary 5.4. $\diamondsuit$

Corollary 5.4 shows that, for regular enough solutions, the displacement-correction schemes reported in Algorithm 5 converge to the solution of (5). The analysis predicts a sub-optimal $\mathcal{O}(\tau^{\frac{1}{2}})$ time-convergence rate for the non-incremental variant in the energy-norm. This is due to the low-order consistency $(61)_1$ of the perturbed kinematic constraint (39) when $\boldsymbol{d}_h^\star = \boldsymbol{0}$. On the contrary, for $\boldsymbol{d}_h^\star = \boldsymbol{d}_h^{n-1}$ and $\boldsymbol{d}_h^\star = \boldsymbol{d}_h^{n-1} + \tau \dot{\boldsymbol{d}}_h^{n-1}$, the consistency $(61)_{2,3}$ of the perturbations scale as $\mathcal{O}(\tau)$ and $\mathcal{O}(\tau^2)$, respectively. Therefore, an overall optimal convergence-rate $\mathcal{O}(h^k + h^{\tilde{l}} + \tau)$ is recovered with the proposed incremental displacement-correction schemes. In particular, for $\boldsymbol{d}_h^\star = \boldsymbol{d}_h^{n-1}$, it is worth noting that this optimality is obtained without any condition between the discretization parameters and the polynomial order. This is a significant progress with respect to the stabilized explicit coupling scheme reported in [7, 9] (see Section 3.2.1 above). Indeed, overall first-order optimal accuracy $\mathcal{O}(h)$ can only be guaranteed under a parabolic-CFL condition $\tau = \mathcal{O}(h^2)$ and piece-wise affine approximations ($k = 1$), unless enough defect-correction iterations are performed.

Remark 5.6 *It is worth mentioning that a somewhat similar non-incremental/incremental convergence behavior has been observed in the pressure error estimates of projection methods for incompressible flow (see, e.g., [28, Section 3]).*

Remark 5.7 *According to Corollary 5.5, the overall time-accuracy of the implicit scheme is here* $\mathcal{O}(h^k + h^{\tilde{l}} + \tau)$. *As a result, the second-order extrapolation* $\boldsymbol{d}_h^\star = \boldsymbol{d}_h^{n-1} + \tau \dot{\boldsymbol{d}}_h^{n-1}$ *in Algorithm 5 is superfluous in terms of convergence rate. An alternative could be to consider Algorithm 5 with second-order time-marching in the fluid and in the structure (see Remarks 4.3 and 5.3). This is an interesting point, but that lies out of the scope of the present paper.* $\diamondsuit$

Remark 5.8 *Note that the constant of the consistency rate (61) is proportional to*

$$\beta^{\mathrm{e}} \, (\rho^{\mathrm{s}} \epsilon)^{-\frac{1}{2}} = \omega^{\mathrm{e}} (\beta_{\mathrm{e}})^{\frac{1}{2}}.$$

Hence, from (62) and by comparing the estimates (86) and (87), we infer that the accuracy of the displacement-correction schemes is sensitive to the magnitude of the maximum solid elastic wave-speed ω^{e}. In other words, for a fixed time-step size $\tau > 0$, decreasing ω^{e} reduces the impact of the consistency rate perturbation (61) in the global error estimate (60), while increasing ω^{e} should degrade the accuracy of Algorithm 5. Yet, owing to (61), this degradation is expected to be less important with the proposed incremental variants. $\diamondsuit$

Remark 5.9 *According to Theorem 5.2, the error estimate (60) involves a multiplicative constant that, for $\boldsymbol{d}_h^\star = \boldsymbol{0}$ and $\boldsymbol{d}_h^\star = \boldsymbol{d}_h^{n-1}$, scales linearly in $T^{\frac{1}{2}}$. However, with the second-order extrapolation this dependence becomes exponential. $\diamondsuit$*

6   Numerical experiments

In order to illustrate the stability and accuracy of the proposed schemes, we consider a slightly simplified version of the fluid-structure benchmark used in [29]. We couple the 2D Stokes equations with an undamped 1D generalized string model (see, e.g., [23]), hence, in (2) we take

$$\boldsymbol{d} = \begin{pmatrix} 0 \\ d_y \end{pmatrix}, \quad \boldsymbol{L}^{\mathrm{e}} \boldsymbol{d} = \begin{pmatrix} 0 \\ -\lambda_1 \partial_{xx} \boldsymbol{d}_y + \lambda_0 \boldsymbol{d}_y \end{pmatrix},$$

with

$$\lambda_1 \stackrel{\mathrm{def}}{=} \frac{E\epsilon}{2(1+\nu)}, \quad \lambda_0 \stackrel{\mathrm{def}}{=} \frac{E\epsilon}{R^2(1-\nu^2)}. \tag{88}$$

As usual, here E denotes the Young modulus and ν the Poisson ratio of the solid. All the quantities will be given in the CGS system. The fluid domain and the fluid-solid interface are, respectively,

$$\Omega = [0, L] \times [0, R], \quad \Sigma = [0, L] \times \{R\},$$

with $L = 6$ and $R = 0.5$. At $x = 0$ we impose a sinusoidal pressure of maximal amplitude 2×10^4 during 5×10^{-3} seconds, corresponding to half a period. Zero pressure is enforced at $x = 6$ and a symmetry condition is applied on the lower wall $y = 0$. The solid is clamped at its extremities, $x = 0, L$. The fluid physical parameters are given by

$$\rho^{\mathrm{f}} = 1.0, \quad \mu = 0.035,$$

while for the solid we have

$$\rho^{\mathrm{s}} = 1.1, \quad \epsilon = 0.1, \quad E = 0.75 \times 10^6, \quad \nu = 0.5. \tag{89}$$

For the discretization in space we have considered two finite element formulations entering the framework of the above analysis. The first is made of continuous piece-wise affine approximations for both the fluid and the structure, $k = l = 1$ in (6), with the following pressure stabilization operator (see, e.g., [6]):

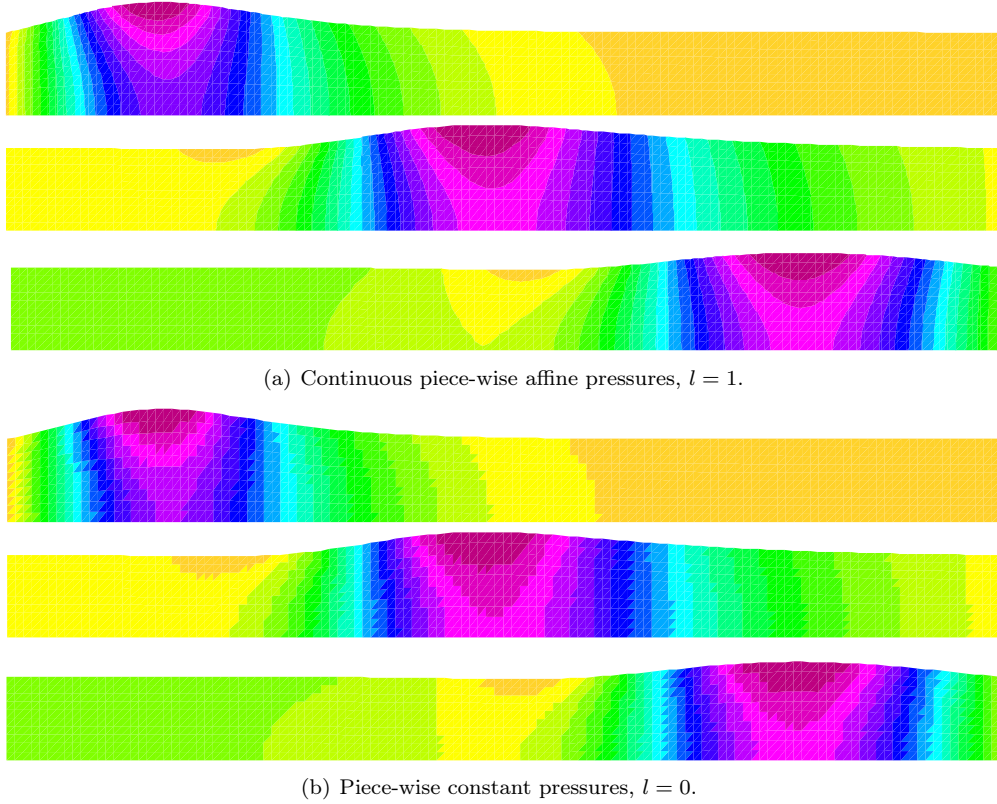$$s_h(p_h, q_h) = \frac{\gamma h^2}{\mu} (\boldsymbol{\nabla} p_h, \boldsymbol{\nabla} q_h),$$

(a) Continuous piece-wise affine pressures, $l = 1$.

(b) Piece-wise constant pressures, $l = 0$.

Figure 1: Snapshots of the pressure at $t = 0.005, 0.01\,0.015$ (from top to bottom). Algorithm 5 with $\boldsymbol{d}_h^\star = \boldsymbol{d}_h^{n-1}$, $\tau = 10^{-4}$ and $h = 0.05$. Fluid domain in deformed configuration (amplified).

where $\gamma = 10^{-3}$. In the second formulation, the pressure is approximated using piece-wise constants functions, so that $k = 1$ and $l = 0$ in (6) and the pressure stabilization (see, e.g., [34]) is given by

$$s_h(p_h, q_h) = \frac{\gamma h}{\mu} \sum_{K \in \mathcal{T}_h} \int_{\partial K \backslash \partial \Omega} [\![p_h]\!][\![q_h]\!],$$

with $\gamma = 10^{-3}$. Here, $[\![q_h]\!]$ denotes the jump of q_h over the inter-element boundaries. These two pressure stabilizations satisfy the criteria of Section 3.1.1 with $\tilde{l} = 1$ (see, e.g., [8, Section 3.1.1]) and, therefore, are optimal for the considered approximation spaces.

For illustrations purposes, we have reported in Figure 1 a few snapshots of the pressure field obtained using Algorithm 5, with $\boldsymbol{d}_h^\star = \boldsymbol{d}_h^{n-1}$, $\tau = 10^{-4}$ and $h = 0.05$. All the computations have been performed with FreeFem++ [40]. The fluid domain has been displayed in deformed configuration (amplified by a factor 5), so that we can visualize the displacement of the interface as well. The numerical solution remains stable, as predicted by Theorem 4.2, and a propagating pressure-wave is observed (see, e.g., [29]). Both finite element approximations give similar results.

We now turn our attention to the accuracy of the schemes reported in Algorithms 3 and 5. To this aim, a reference solution has been generated using Algorithm 2, with $k = l = 1$ and a high grid resolution ($\tau = 10^{-6}$ and $h = 3.125 \times 10^{-3}$). We have first refined both in time and in
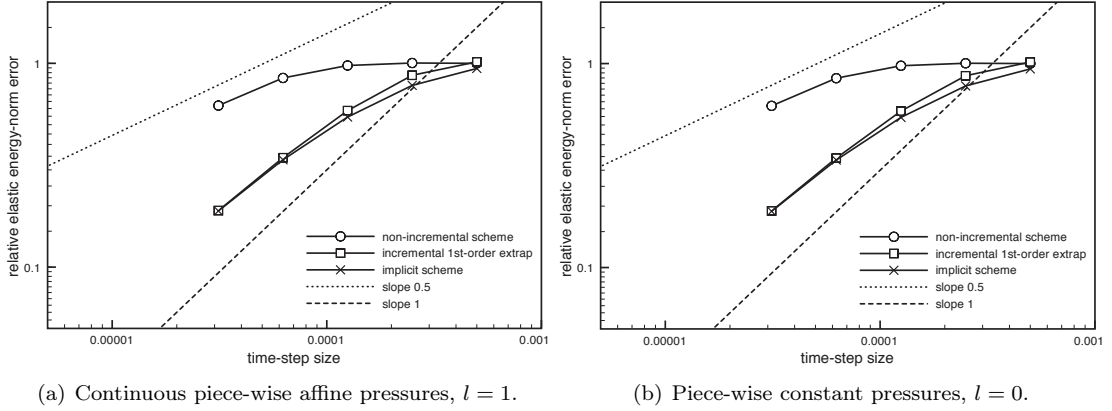
(a) Continuous piece-wise affine pressures, $l = 1$.   (b) Piece-wise constant pressures, $l = 0$.

Figure 2: Time-convergence history of the displacement at $t = 0.015$, with $h = \mathcal{O}(\tau)$.

space at the same rate, with the following set of discrete parameters:

$$(\tau, h) \in \left\{ \left(\frac{5 \times 10^{-4}}{2^i}, \frac{10^{-1}}{2^i} \right) \right\}_{i=0}^{4}. \tag{90}$$

Note that this allows to highlight the h-uniformity of the convergence in time. Figure 2 reports the corresponding time-convergence history of the solid displacement at time $t = 0.015$, in the relative elastic energy-norm, for the non-incremental scheme (Algorithm 5 with $\boldsymbol{d}_h^\star = \boldsymbol{0}$ or, Algorithm 3), the incremental scheme (Algorithm 5 with $\boldsymbol{d}_h^\star = \boldsymbol{d}_h^{n-1}$) and the implicit scheme (Algorithm 2). The incremental and the implicit schemes yield an overall $\mathcal{O}(\tau)$ optimal accuracy, while a sub-optimal $\mathcal{O}(\tau^{\frac{1}{2}})$ rate is observed with the non-incremental scheme. Thus, in agreement with the error estimations of Corollaries 5.4 and 5.5. Indeed, since $k = 1$, $\tilde{l} = 1$ and, from (90), $h = \mathcal{O}(\tau)$, the error estimations (86) and (87) yield the observed time-convergence rates.

(a) Continuous piece-wise affine pressures, $l = 1$.   (b) Piece-wise constant pressures, $l = 0$.
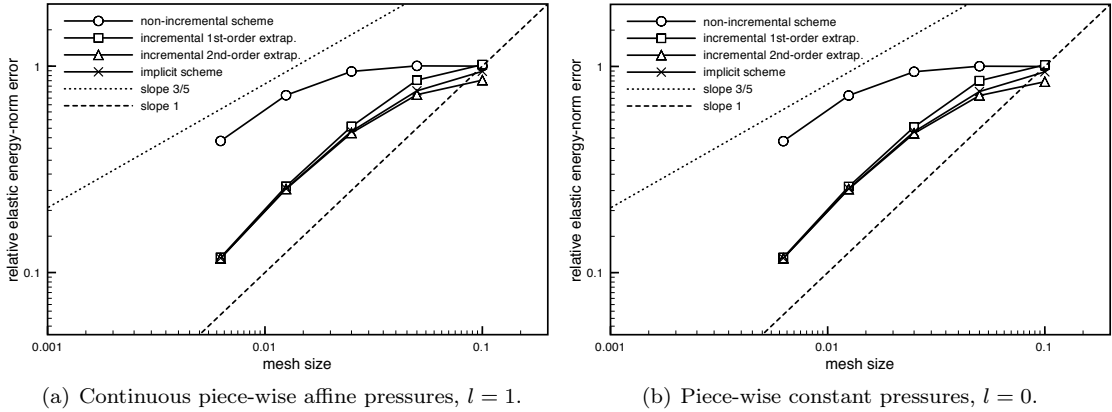
Figure 3: Space-convergence history of the displacement at $t = 0.015$, with $\tau = \mathcal{O}(h^{\frac{6}{5}})$.

In order to guarantee the stability of the approximations provided by the incremental scheme with the second-order extrapolation (Algorithm 5 with $\boldsymbol{d}_h^\star = \boldsymbol{d}_h^{n-1} + \tau \dot{\boldsymbol{d}}_h^{n-1}$), we now consider

the following set of discrete parameters:

$$(\tau, h) \in \left\{ \left(\frac{5 \times 10^{-4}}{2^{\frac{6}{5}i}}, \frac{10^{-1}}{2^i} \right) \right\}_{i=0}^{4}, \tag{91}$$

for which the $\frac{6}{5}$-CFL condition (43) holds. Figure 3 shows the corresponding space-convergence history with Algorithms 2, 3 and 5. Note that, since $k = 1$, $\tilde{l} = 1$ and, from (91), $\tau = \mathcal{O}(h^{\frac{6}{5}})$, the error estimates provided by Corollaries 5.4 and 5.5 predict an overall $\mathcal{O}(h)$ optimal accuracy for the incremental and the implicit schemes, while a sub-optimal $\mathcal{O}(h^{\frac{3}{5}})$ is expected for the non-incremental scheme. These theoretical convergence rates are in agreement with those observed numerically in Figure 3.

(a) $i = 0$.

(b) $i = 1$.

(c) $i = 2$.

(d) $i = 3$.
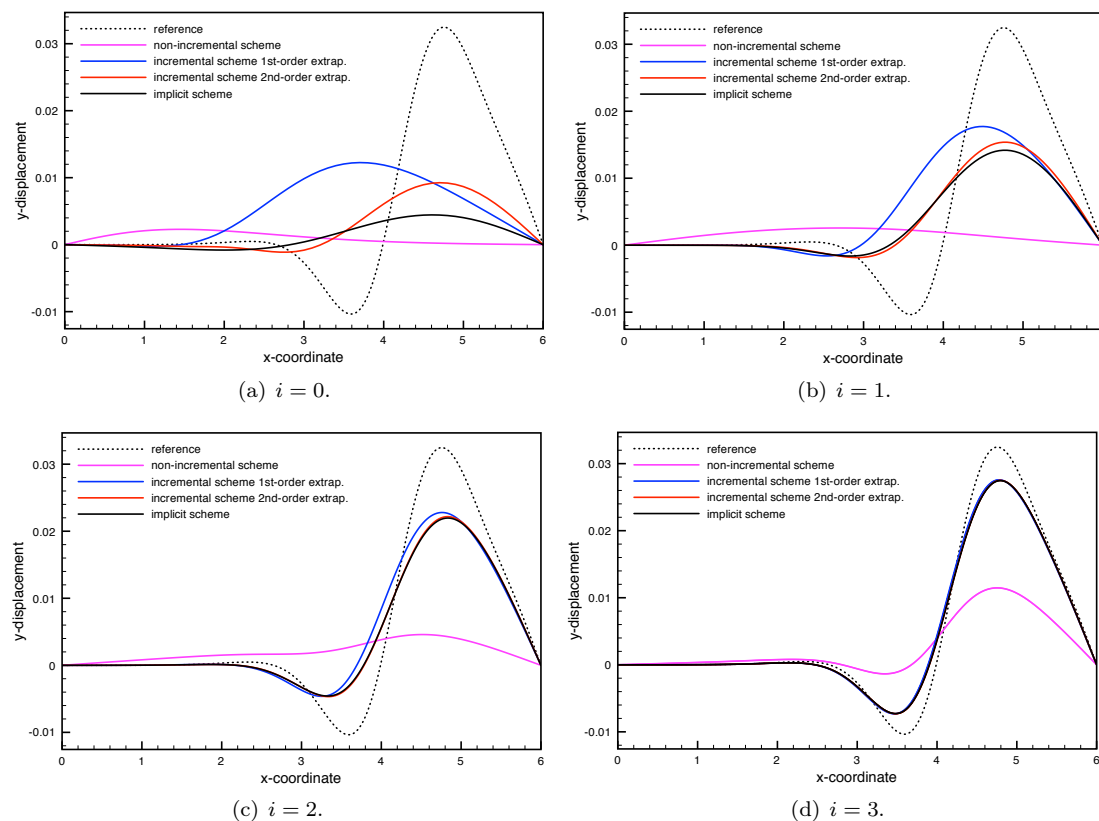
Figure 4: Comparison of the displacements at $t = 0.015$, obtained with $k = l = 1$ and different levels of (τ, h)-refinement, given by (91) with $i = 0, \ldots, 3$.

The superior accuracy of the incremental schemes, with respect to the original non-incremental variant, is also clearly visible in Figure 4, where we have displayed the interface displacements associated to Figure 3(a) (first four points of each curve). For comparison purposes, the reference displacement is also shown. Observe that, even with the smallest time-steps sizes (e.g., Figure 4(d)), the non-incremental scheme provides a rather poor approximation. On the contrary, the two incremental variants are able to retrieve the accuracy of the implicit coupling scheme. It is also worth noting that, though superfluous in terms of overall convergence rate (see Figure 3 and

(a) $E = \frac{E_{\text{ref}}}{5}$ and $\rho^{\text{s}} = \rho^{\text{s}}_{\text{ref}}$.

(b) $E = E_{\text{ref}}$ and $\rho^{\text{s}} = \rho^{\text{s}}_{\text{ref}} \times 5$.
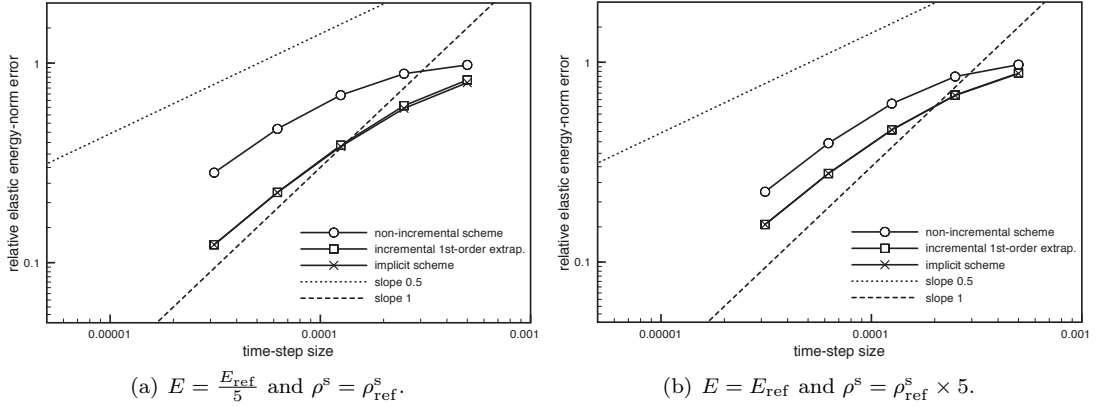
Figure 5: Displacement energy-error convergence history in time for a lower ω^{e}.

Remark 5.7), the second-order extrapolation does improve the accuracy in practice, as we can observe in Figure 4, particularly for the coarsest grid resolutions. This is not surprising since, according to Theorem 5.2, the choice $\boldsymbol{d}_h^{\star} = \boldsymbol{d}_h^{n-1} + \tau \dot{\boldsymbol{d}}_h^{n-1}$ yields the highest consistency in the perturbed kinematic condition (39).

(a) $E = E_{\text{ref}} \times 5$ and $\rho^{\text{s}} = \rho^{\text{s}}_{\text{ref}}$.

(b) $E = E_{\text{ref}}$ and $\rho^{\text{s}} = \frac{\rho^{\text{s}}_{\text{ref}}}{5}$.
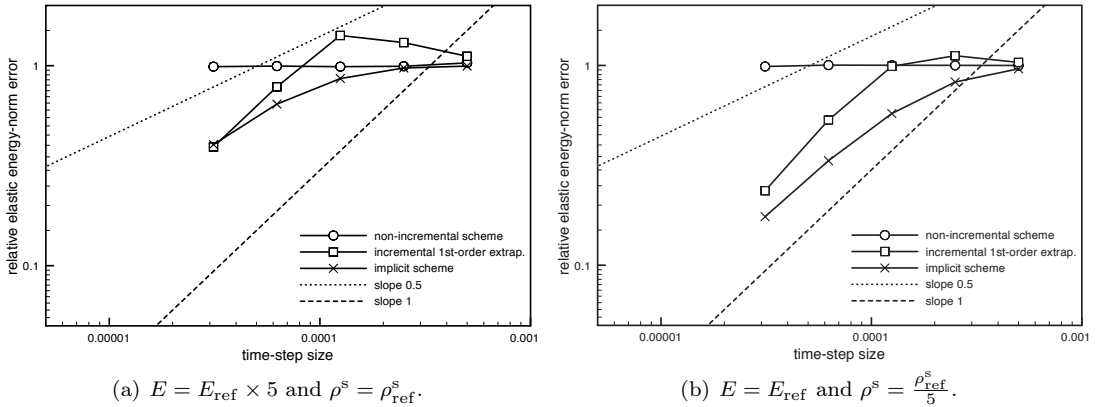
Figure 6: Displacement energy-error convergence history in time for a higher ω^{e}.

In line with the discussion of Remark 5.8, we now investigate the sensitivity of the displacement-correction approximations to the magnitude of the solid elastic wave-speed ω^{e}. Note that, from (45) and (88), it follows that

$$\omega^{\text{e}} \approx \left(\frac{E}{\rho^{\text{s}}} \right)^{\frac{1}{2}}.$$

Thus, we have reran the simulations of Figure 2(a) with different values of the Young modulus and of the solid density:

$$E \in \left\{ E_{\text{ref}} \times 5^i \right\}_{i=-1,0,1}, \quad \rho^{\text{s}} \in \left\{ \rho^{\text{s}}_{\text{ref}} \times 5^i \right\}_{i=-1,0,1},$$

where E_{ref} and $\rho^{\text{s}}_{\text{ref}}$ are given by (89). The convergence histories corresponding to the lowest elastic wave-speed are displayed in Figure 5. The comparison with Figure 2(a) (i.e., $E = E_{\text{ref}}$

and $\rho^{\mathrm{s}} = \rho^{\mathrm{s}}_{\mathrm{ref}}$) shows that the accuracy of both the non-incremental and the incremental schemes is enhanced when we lower ω^{e}. Note, in particular, that the amount of this impact is much more striking for the non-incremental variant. Conversely, the accuracy of the displacement-correction schemes deteriorates when we increase ω^{e}, as shown in Figure 6 (see also Remark 5.8). Observe that the non-incremental variant is unable to show the expected sub-optimal convergent behavior towards the reference solution (i.e., further τ-refinement is needed), whereas the incremental scheme still retrieves the optimal convergence rate.

7 Conclusion

We have introduced and analyzed a class of incremental displacement-correction schemes for the explicit coupling of a thin-structure with an incompressible fluid. A salient feature of this work is that the non-incremental, incremental and implicit schemes are cast into a unified analysis framework, for a wide variety of interface-matching finite element discretizations in space.

We have shown that the displacement-correction schemes are a particular class of Robin-Neumann explicit coupling schemes. In particular, they can be seen as explicit variants of the Robin-Neumann iterative procedures reported in [2], for a particular choice of the Robin-parameter and of the initialization. These schemes can also be interpreted as interface kinematic perturbations of an underlying implicit coupling scheme. The magnitude of this perturbation depends on the time-step size, τ, and it is proportional to the solid elastic wave-speed. Their stability properties are independent of the added-mass effect. The analysis shows that the proposed incremental schemes yield an optimal $\mathcal{O}(\tau)$ time-accuracy in the energy-norm, while a sub-optimal $\mathcal{O}(\tau^{\frac{1}{2}})$ convergence rate is expected for the original non-incremental variant. Numerical tests in a benchmark confirmed these theoretical findings.

Extensions of this work can explore various directions. We can address, for instance, the development of second-order time-accurate schemes (see Remark 5.7) and the derivation of pressure estimates. A further valuable extension of the present explicit coupling paradigm is to consider the case of thick-solid models. A preliminary study in this direction can be found in [21]. Finally, ongoing work focuses on the formulation of these displacement-correction schemes within a nonlinear fluid-structure framework involving, for instance, nonlinear shell models.

Acknowledgement

A Proof of Lemma 3.2

The first inequality follows by simply noting that, from (17), we get

$$\|\boldsymbol{\pi}_h^{\mathrm{e}} \boldsymbol{w}\|_{\mathrm{e}}^2 = a^{\mathrm{e}}\big(\boldsymbol{w}, \boldsymbol{\pi}_h^{\mathrm{e}} \boldsymbol{w}\big) \leq \|\boldsymbol{w}\|_{\mathrm{e}} \|\boldsymbol{\pi}_h^{\mathrm{e}} \boldsymbol{w}\|_{\mathrm{e}}.$$

On the other hand, for $\boldsymbol{w} \in \boldsymbol{D}^{\mathrm{e}}$, and thanks to (16) and (4), we have

$$\|\boldsymbol{L}_h^{\mathrm{e}} \boldsymbol{w}\|_{0,\Sigma}^2 = a^{\mathrm{e}}(\boldsymbol{w}, \boldsymbol{L}_h^{\mathrm{e}} \boldsymbol{w}) = (\boldsymbol{L}^{\mathrm{e}} \boldsymbol{w}, \boldsymbol{L}_h^{\mathrm{e}} \boldsymbol{w})_{\Sigma},$$

which yields (19). For the identity (20) if suffices to observe that, for all $\boldsymbol{w}_h \in \boldsymbol{W}_h$, we have

$$\big(\boldsymbol{L}_h^{\mathrm{e}} \boldsymbol{\pi}_h^{\mathrm{e}} \boldsymbol{w}, \boldsymbol{w}_h\big)_{\Sigma} = a^{\mathrm{e}}\big(\boldsymbol{\pi}_h^{\mathrm{e}} \boldsymbol{w}, \boldsymbol{w}_h\big) = a^{\mathrm{e}}\big(\boldsymbol{w}, \boldsymbol{w}_h\big) = \big(\boldsymbol{L}_h^{\mathrm{e}} \boldsymbol{w}, \boldsymbol{w}_h\big)_{\Sigma}.$$

Using (3) and a standard inverse estimate (see, e.g., [16, Section 1.7]), for all $\boldsymbol{w}_h \in \boldsymbol{W}_h$, we have

$$\|\boldsymbol{w}_h\|_{\mathrm{e}}^2 = a^{\mathrm{e}}(\boldsymbol{w}_h, \boldsymbol{w}_h) \le \beta^{\mathrm{e}} \|\boldsymbol{w}_h\|_{1,\Sigma}^2 \le \frac{\beta^{\mathrm{e}} C_{\mathrm{inv}}^2}{h^2} \|\boldsymbol{w}_h\|_{0,\Sigma}^2,$$

so that (21) holds. At last, by using this estimate, we get

$$
\begin{aligned}
\|\boldsymbol{L}_h^{\mathrm{e}} \boldsymbol{w}_h\|_{\mathrm{e}}^2 &\le \frac{\beta^{\mathrm{e}} C_{\mathrm{inv}}^2}{h^2} \|\boldsymbol{L}_h^{\mathrm{e}} \boldsymbol{w}_h\|_{0,\Sigma}^2 = \frac{\beta^{\mathrm{e}} C_{\mathrm{inv}}^2}{h^2} \big(\boldsymbol{L}_h^{\mathrm{e}} \boldsymbol{w}_h, \boldsymbol{L}_h^{\mathrm{e}} \boldsymbol{w}_h\big)_{\Sigma} = \frac{\beta^{\mathrm{e}} C_{\mathrm{inv}}^2}{h^2} a^{\mathrm{e}}\big(\boldsymbol{w}_h, \boldsymbol{L}_h^{\mathrm{e}} \boldsymbol{w}_h\big) \\
&\le \frac{\beta^{\mathrm{e}} C_{\mathrm{inv}}^2}{h^2} \|\boldsymbol{w}_h\|_{\mathrm{e}} \|\boldsymbol{L}_h^{\mathrm{e}} \boldsymbol{w}_h\|_{\mathrm{e}},
\end{aligned}
$$

which yields (22). In particular, the estimate (23) follows by noting that

$$\|\boldsymbol{L}_h^{\mathrm{e}} \boldsymbol{w}_h\|_{0,\Sigma}^2 = a^{\mathrm{e}}(\boldsymbol{w}_h, \boldsymbol{L}_h^{\mathrm{e}} \boldsymbol{w}_h) \le \|\boldsymbol{w}_h\|_{\mathrm{e}} \|\boldsymbol{L}_h^{\mathrm{e}} \boldsymbol{w}_h\|_{\mathrm{e}} \le \frac{\beta^{\mathrm{e}} C_{\mathrm{inv}}^2}{h^2} \|\boldsymbol{w}_h\|_{\mathrm{e}}^2,$$

which completes the proof.

B Error analysis of the fluid-projection operator

We consider the following steady Stokes problem with inhomogeneous Dirichlet boundary conditions on Σ, homogeneous Dirichlet boundary conditions on Γ^{d} and Neumann boundary conditions on Γ^{n}: find $(\boldsymbol{u}, p) \in \boldsymbol{V} \times Q$ such that

$$
\begin{cases}
\boldsymbol{u}|_{\Sigma} = \boldsymbol{g}, \\
a(\boldsymbol{u}, \boldsymbol{v}) + b(p, \boldsymbol{v}) = l(\boldsymbol{v}) \quad \forall \boldsymbol{v} \in \boldsymbol{V}_{\Sigma}, \\
b(q, \boldsymbol{u}) = 0 \quad \forall q \in Q,
\end{cases}
\tag{92}
$$

where $\boldsymbol{g} \in \{\boldsymbol{v}|_{\Sigma} / \boldsymbol{v} \in \boldsymbol{V}\}$ stands for the boundary data on Σ and $l : \boldsymbol{V} \to \mathbb{R}$ is a given continuous linear form into $\boldsymbol{V}$. The estimates stated in Lemma 5.1 can be inferred from the error analysis of the following finite element approximation of (92): find $(\boldsymbol{u}_h, p_h) \in \boldsymbol{V}_h \times Q_h$ such that

$$
\begin{cases}
\boldsymbol{u}_h|_{\Sigma} = \boldsymbol{g}_h, \\
a(\boldsymbol{u}_h, \boldsymbol{v}_h) + b(p_h, \boldsymbol{v}_h) = l(\boldsymbol{v}_h) \quad \forall \boldsymbol{v}_h \in \boldsymbol{V}_{\Sigma,h}, \\
b(q_h, \boldsymbol{u}_h) = s_h(p_h, q_h) \quad \forall q_h \in Q_h,
\end{cases}
\tag{93}
$$

where $\boldsymbol{g}_h \in \{\boldsymbol{v}_h|_{\Sigma} / \boldsymbol{v}_h \in \boldsymbol{V}_h\}$ stands for a given approximation of $\boldsymbol{g}$ and s_h is a pressure stabilization operator entering the framework of Section 3.1.1. The convergence analysis of the finite element approximation (93) involves the generalization of some of the results reported in [31], to the case of symmetric pressure stabilizations and Neumann boundary conditions on Γ^{n}.

We first prove the following generalized inf-sup condition, by combining the arguments involved in the proofs of [8, Lemma 3.1] and [25, Lemma 3.3].

Lemma B.1 *There holds*

$$\|q_h\|_Q \lesssim \sup_{\boldsymbol{v}_h \in \boldsymbol{V}_{\Sigma,h}} \frac{b(q_h, \boldsymbol{v}_h)}{\|\boldsymbol{v}_h\|_{\boldsymbol{V}}} + |q_h|_{s_h} \tag{94}$$

for all $q_h \in Q_h$.

Proof. We first split $q_h \in Q_h$ as $q_h = \bar{q}_h + q_h^*$, with $\bar{q}_h \stackrel{\text{def}}{=} (q_h, 1)/|\Omega|$ and $q_h^* \in L_0^2(\Omega)$. Note that, in particular, we have

$$\|q_h\|_Q^2 = \|\bar{q}_h\|_Q^2 + \|q_h^*\|_Q^2. \tag{95}$$

On the other hand, from [27, Corollary 2.4], there exists $\boldsymbol{v}^* \in [H_0^1(\Omega)]^d$ such that

$$\text{div}\boldsymbol{v}^* = -\frac{q_h^*}{\mu}, \quad \|\boldsymbol{v}^*\|_{\boldsymbol{V}} \lesssim \|q_h^*\|_Q. \tag{96}$$

Hence, using (15), we have

$$\begin{aligned} \|q_h^*\|_Q^2 &= b(q_h^*, \boldsymbol{v}^*) \\ &= b(q_h^*, \boldsymbol{v}^* - \boldsymbol{\mathcal{F}}_h \boldsymbol{v}^*) + b(q_h^*, \boldsymbol{\mathcal{F}}_h \boldsymbol{v}^*) \\ &\lesssim |q_h^*|_{s_h} \|\boldsymbol{v}^*\|_{\boldsymbol{V}} + b(q_h^*, \boldsymbol{\mathcal{F}}_h \boldsymbol{v}^*) = |q_h|_{s_h} \|\boldsymbol{v}^*\|_{\boldsymbol{V}} + b(q_h, \boldsymbol{\mathcal{F}}_h \boldsymbol{v}^*). \end{aligned}$$

Note that the last identity follows from the consistency of s_h (estimate (13)) and the fact that $(\boldsymbol{\mathcal{F}}_h \boldsymbol{v}^*)|_{\partial\Omega} = \boldsymbol{0}$. As a result, from (96), we infer that

$$\|q_h^*\|_Q \lesssim \frac{b(q_h, \boldsymbol{\mathcal{F}}_h \boldsymbol{v}^*)}{\|\boldsymbol{v}^*\|_{\boldsymbol{V}}} + |q_h|_{s_h}. \tag{97}$$

On the other hand (see [25, Lemma 3.3] or [15, Lemma 3.3]), there exists $0 \neq \boldsymbol{z}_h \in \boldsymbol{V}_{\Sigma,h}$ such that

$$\|\bar{q}_h\|_Q \lesssim \frac{b(\bar{q}_h, \boldsymbol{z}_h)}{\|\boldsymbol{z}_h\|_{\boldsymbol{V}}}. \tag{98}$$

Therefore, setting $\boldsymbol{v}_h \stackrel{\text{def}}{=} \|\boldsymbol{v}^*\|_{\boldsymbol{V}}^{-1} \boldsymbol{\mathcal{F}}_h \boldsymbol{v}^* + \delta \|\boldsymbol{z}_h\|_{\boldsymbol{V}}^{-1} \boldsymbol{z}_h \in \boldsymbol{V}_{\Sigma,h}$, with $\delta > 0$ sufficiently small, and using (97), (98) and (95), yields

$$\begin{aligned} b(q_h, \boldsymbol{v}_h) &= \frac{b(q_h, \boldsymbol{\mathcal{F}}_h \boldsymbol{v}^*)}{\|\boldsymbol{v}^*\|_{\boldsymbol{V}}} + \delta \frac{b(q_h, \boldsymbol{z}_h)}{\|\boldsymbol{z}_h\|_{\boldsymbol{V}}} \\ &= \frac{b(q_h, \boldsymbol{\mathcal{F}}_h \boldsymbol{v}^*)}{\|\boldsymbol{v}^*\|_{\boldsymbol{V}}} + \delta \frac{b(\bar{q}_h, \boldsymbol{z}_h)}{\|\boldsymbol{z}_h\|_{\boldsymbol{V}}} + \delta \frac{b(q_h^*, \boldsymbol{z}_h)}{\|\boldsymbol{z}_h\|_{\boldsymbol{V}}} \\ &\gtrsim \|q_h^*\|_Q - |q_h|_{s_h} + \delta \|\bar{q}_h\|_Q - \delta \|q_h^*\|_Q \\ &\gtrsim \|q_h\|_Q - |q_h|_{s_h}. \end{aligned}$$

The inequality (94) then follows, from (15), by noting that $\|\boldsymbol{v}_h\|_{\boldsymbol{V}} \lesssim 1 + \delta$. $\diamond$

We then have the following error estimate, valid for arbitrary approximations $\boldsymbol{g}_h$ of $\boldsymbol{g}$.

Lemma B.2 *Let $(\boldsymbol{u}, p)$ and $(\boldsymbol{u}_h, p_h)$ be the solutions of (92) and (93), respectively. Then, there holds*

$$\begin{aligned} \|\boldsymbol{u} - \boldsymbol{u}_h\|_{\boldsymbol{V}} + |p_h|_{s_h} + \|p - p_h\|_Q &\lesssim \inf_{\widehat{\boldsymbol{u}}_h \in \boldsymbol{V}_h, \widehat{\boldsymbol{u}}_h|_\Sigma = \boldsymbol{g}_h} \left\{ \|\boldsymbol{u} - \widehat{\boldsymbol{u}}_h\|_{\boldsymbol{V}} \right\} \\ &\quad + \inf_{\widehat{p}_h \in Q_h} \left\{ \|p - \widehat{p}_h\|_Q + |\widehat{p}_h|_{s_h} \right\}. \end{aligned} \tag{99}$$

Proof. By subtracting (93) from (92), we have that

$$\begin{cases} a(\boldsymbol{u} - \boldsymbol{u}_h, \boldsymbol{v}_h) + b(p - p_h, \boldsymbol{v}_h) = 0, \\ \quad -b(q_h, \boldsymbol{u} - \boldsymbol{u}_h) = s_h(p_h, q_h) \end{cases}$$

for all $(\boldsymbol{v}_h, q_h) \in \boldsymbol{V}_{\Sigma,h} \times Q_h$. We now consider the following discrete space

$$\boldsymbol{Z}_h \stackrel{\text{def}}{=} \big\{ (\widehat{\boldsymbol{u}}_h, \widehat{p}_h) \in \boldsymbol{V}_h \times Q_h \,/\, b(q_h, \widehat{\boldsymbol{u}}_h) = s_h(\widehat{p}_h, q_h) \; \forall q_h \in Q_h \big\}.$$

Hence, for $(\widehat{\boldsymbol{u}}_h, \widehat{p}_h) \in \boldsymbol{Z}_h$ with $\widehat{\boldsymbol{u}}_h|_\Sigma = \boldsymbol{g}_h$ it follows that

$$a(\boldsymbol{u}_h - \widehat{\boldsymbol{u}}_h, \boldsymbol{v}_h) + b(p_h - \widehat{p}_h, \boldsymbol{v}_h) = a(\boldsymbol{u} - \widehat{\boldsymbol{u}}_h, \boldsymbol{v}_h) + b(p - \widehat{p}_h, \boldsymbol{v}_h) \tag{100}$$

for all $\boldsymbol{v}_h \in \boldsymbol{V}_{\Sigma,h}$, and that

$$-b(q_h, \widehat{\boldsymbol{u}}_h - \boldsymbol{u}_h) = -b(q_h, \boldsymbol{u} - \widehat{\boldsymbol{u}}_h) - s_h(p_h, q_h) = -s_h(p - \widehat{p}_h, q_h) \tag{101}$$

for all $q_h \in Q_h$. As a result, since $(\boldsymbol{u}_h - \widehat{\boldsymbol{u}}_h) \in \boldsymbol{V}_{\Sigma,h}$, by taking $\boldsymbol{v}_h = \boldsymbol{u}_h - \widehat{\boldsymbol{u}}_h$ in (100) and $q_h = p_h - \widehat{p}_h$ in (101), we get the identity

$$2\mu \|\boldsymbol{\epsilon}(\widehat{\boldsymbol{u}}_h - \boldsymbol{u}_h)\|_{0,\Omega}^2 + |\widehat{p}_h - p_h|_{s_h}^2 = a(\boldsymbol{u} - \widehat{\boldsymbol{u}}_h, \widehat{\boldsymbol{u}}_h - \boldsymbol{u}_h) + b(p - \widehat{p}_h, \widehat{\boldsymbol{u}}_h - \boldsymbol{u}_h).$$

Hence, using Korn's inequality,

$$\|\widehat{\boldsymbol{u}}_h - \boldsymbol{u}_h\|_{\boldsymbol{V}} + |\widehat{p}_h - p_h|_{s_h} \lesssim \|\boldsymbol{u} - \widehat{\boldsymbol{u}}_h\|_{\boldsymbol{V}} + \|p - \widehat{p}_h\|_Q. \tag{102}$$

A triangle inequality thus yields

$$\|\boldsymbol{u} - \boldsymbol{u}_h\|_{\boldsymbol{V}} \lesssim \|\boldsymbol{u} - \widehat{\boldsymbol{u}}_h\|_{\boldsymbol{V}} + \|p - \widehat{p}_h\|_Q,$$
$$|p_h|_{s_h} \lesssim \|\boldsymbol{u} - \widehat{\boldsymbol{u}}_h\|_{\boldsymbol{V}} + \|p - \widehat{p}_h\|_Q + |\widehat{p}_h|_{s_h}$$

for all $(\widehat{\boldsymbol{u}}_h, \widehat{p}_h) \in \boldsymbol{Z}_h$ with $\widehat{\boldsymbol{u}}_h|_\Sigma = \boldsymbol{g}_h$. On the other hand, from (100), Lemma B.1 and (102), it follows that

$$\begin{aligned}
\|p - p_h\|_Q &\leq \|p - \widehat{p}_h\|_Q + \|\widehat{p}_h - p_h\|_Q \\
&\lesssim \|p - \widehat{p}_h\|_Q + \|\boldsymbol{u} - \widehat{\boldsymbol{u}}_h\|_{\boldsymbol{V}} + \|\widehat{\boldsymbol{u}}_h - \boldsymbol{u}_h\|_{\boldsymbol{V}} + |\widehat{p}_h - p_h|_{s_h} \\
&\lesssim \|p - \widehat{p}_h\|_Q + \|\boldsymbol{u} - \widehat{\boldsymbol{u}}_h\|_{\boldsymbol{V}}
\end{aligned}$$

for all $(\widehat{\boldsymbol{u}}_h, \widehat{p}_h) \in \boldsymbol{Z}_h$ with $\widehat{\boldsymbol{u}}_h|_\Sigma = \boldsymbol{g}_h$. Therefore,

$$\begin{aligned}
\|\boldsymbol{u} - \boldsymbol{u}_h\|_{\boldsymbol{V}} + \|p - p_h\|_Q &\lesssim \inf_{(\widehat{\boldsymbol{u}}_h, \widehat{p}_h) \in \boldsymbol{Z}_h, \, \widehat{\boldsymbol{u}}_h|_\Sigma = \boldsymbol{g}_h} \big\{ \|\boldsymbol{u} - \widehat{\boldsymbol{u}}_h\|_{\boldsymbol{V}} + \|p - \widehat{p}_h\|_Q \big\}, \\
|p_h|_{s_h} &\lesssim \inf_{(\widehat{\boldsymbol{u}}_h, \widehat{p}_h) \in \boldsymbol{Z}_h, \, \widehat{\boldsymbol{u}}_h|_\Sigma = \boldsymbol{g}_h} \big\{ \|\boldsymbol{u} - \widehat{\boldsymbol{u}}_h\|_{\boldsymbol{V}} + \|p - \widehat{p}_h\|_Q + |\widehat{p}_h|_{s_h} \big\}.
\end{aligned} \tag{103}$$

We will now show how to relax the constraint $(\widehat{\boldsymbol{u}}_h, \widehat{p}_h) \in \boldsymbol{Z}_h$ in (103). To this aim, we take arbitrarily $(\boldsymbol{z}_h, r_h) \in \boldsymbol{V}_h \times Q_h$ with $\boldsymbol{z}_h|_\Sigma = \boldsymbol{g}_h$ and denote by $(\boldsymbol{x}_h, y_h) \in \boldsymbol{V}_{\Sigma,h} \times Q_h$ the solution of the following pressure stabilized discrete Stokes-problem with homogeneous Dirichlet boundary conditions on Σ:

$$\begin{cases} a(\boldsymbol{x}_h, \boldsymbol{v}_h) + b(y_h, \boldsymbol{v}_h) = 0, \\ b(q_h, \boldsymbol{x}_h) = s_h(y_h, q_h) + b(q_h, \boldsymbol{u} - \boldsymbol{z}_h) - s_h(r_h, q_h) \end{cases} \tag{104}$$

for all $(\boldsymbol{v}_h, q_h) \in V_{\Sigma,h} \times Q_h$. By taking $(\boldsymbol{v}_h, q_h) = (\boldsymbol{x}_h, y_h)$ in (104) we have

$$\|\boldsymbol{x}_h\|_{\boldsymbol{V}}^2 + |y_h|_{s_h}^2 \lesssim \|y_h\|_Q \|\boldsymbol{u} - \boldsymbol{z}_h\|_{\boldsymbol{V}} + |r_h|_{s_h}^2. \tag{105}$$

On the other hand, from $(104)_1$ and Lemma B.1, it follows that

$$\|y_h\|_Q \lesssim \|\boldsymbol{x}_h\|_{\boldsymbol{V}} + |y_h|_{s_h},$$

which, in combination with (105), yields the estimate

$$\|\boldsymbol{x}_h\|_{\boldsymbol{V}} + |y_h|_{s_h} + \|y_h\|_Q \lesssim \|\boldsymbol{u} - \boldsymbol{z}_h\|_{\boldsymbol{V}} + |r_h|_{s_h}. \tag{106}$$

We now set

$$\widehat{\boldsymbol{u}}_h \overset{\text{def}}{=} \boldsymbol{x}_h + \boldsymbol{z}_h, \quad \widehat{p}_h \overset{\text{def}}{=} y_h - r_h. \tag{107}$$

Since $\mathrm{div}\boldsymbol{u} = 0$, from $(104)_2$ it follows that

$$b(q_h, \widehat{\boldsymbol{u}}_h) = s_h(\widehat{p}_h, q_h) \quad \forall q_h \in Q_h,$$

so that $(\widehat{\boldsymbol{u}}_h, \widehat{p}_h) \in \boldsymbol{Z}_h$. Moreover, since $\boldsymbol{x}_h \in \boldsymbol{V}_{\Sigma,h}$, we have $\boldsymbol{x}_h|_\Sigma = \boldsymbol{z}_h|_\Sigma = \boldsymbol{g}_h$. Hence, from (103), it follows that that

$$\begin{aligned}
\|\boldsymbol{u} - \boldsymbol{u}_h\|_{\boldsymbol{V}} + \|p - p_h\|_Q &\lesssim \|\boldsymbol{u} - \widehat{\boldsymbol{u}}_h\|_{\boldsymbol{V}} + \|p - \widehat{p}_h\|_Q, \\
|p_h|_{s_h} &\lesssim \|\boldsymbol{u} - \widehat{\boldsymbol{u}}_h\|_{\boldsymbol{V}} + \|p - \widehat{p}_h\|_Q + |\widehat{p}_h|_{s_h}.
\end{aligned} \tag{108}$$

On the other hand, from the definitions (107) and the estimate (106), we have

$$\begin{aligned}
\|\boldsymbol{u} - \widehat{\boldsymbol{u}}_h\|_{\boldsymbol{V}} &\leq \|\boldsymbol{u} - \boldsymbol{z}_h\|_{\boldsymbol{V}} + \|\boldsymbol{x}_h\|_{\boldsymbol{V}} \lesssim \|\boldsymbol{u} - \boldsymbol{z}_h\|_{\boldsymbol{V}} + |r_h|_{s_h}, \\
\|p - \widehat{p}_h\|_Q &\leq \|p - r_h\|_Q + \|y_h\|_Q \lesssim \|p - r_h\|_Q + \|\boldsymbol{u} - \boldsymbol{z}_h\|_{\boldsymbol{V}} + |r_h|_{s_h}, \\
|\widehat{p}_h|_{s_h} &\leq |y_h|_{s_h} + |r_h|_{s_h} \lesssim \|\boldsymbol{u} - \boldsymbol{z}_h\|_{\boldsymbol{V}} + |r_h|_{s_h}.
\end{aligned}$$

The estimate (99) follows by inserting these inequalities in (108) and by using the arbitrariness of $(\boldsymbol{z}_h, r_h). \diamondsuit$

Remark B.3 *For inf-sup stable velocity/pressure pairs and $\Gamma^{\mathrm{n}} = \emptyset$, Lemma B.2 yields the error estimate reported in [31, Proposition 8]. Indeed, in this case the inequality (94) holds with $|\cdot|_{s_h} = 0$ (see Remark 3.1).* $\diamondsuit$

The next result follows by a simple adaption of the Aubin-Nistche argument reported in [31, Proposition 9] and the estimate of Lemma B.2 with $\boldsymbol{g} = \boldsymbol{g}_h = \boldsymbol{0}$.

Lemma B.4 *Let $(\boldsymbol{u}, p)$ and $(\boldsymbol{u}_h, p_h)$ the solutions of (92) and (93), respectively. Assume that (54) holds. Then, we have*

$$\|\boldsymbol{u} - \boldsymbol{u}_h\|_{0,\Omega} \lesssim c_{1,\mu} h\big(\|\boldsymbol{u} - \boldsymbol{u}_h\|_{\boldsymbol{V}} + |p_h|_{s_h} + \|p - p_h\|_Q\big) + c_{2,\mu}\|\boldsymbol{g} - \boldsymbol{g}_h\|_{0,\Sigma}.$$

We finally consider the case in which $\boldsymbol{g}_h$ is chosen as the Lagrange interpolant of the boundary data (see, e.g., [22]). The corresponding error estimates are stated in the next theorem.

Theorem B.5 *Let $(\boldsymbol{u}, p)$ be the solution of (92) and $(\boldsymbol{u}_h, p_h)$ be the solution of (93) with $\boldsymbol{g}_h = \boldsymbol{\mathcal{I}}_h \boldsymbol{g}$. Assume that $(\boldsymbol{u}, p) \in [H^{k+1}(\Omega)]^d \times H^{\tilde{l}}(\Omega)$. Then, there holds*

$$\|\boldsymbol{u} - \boldsymbol{u}_h\|_{\boldsymbol{V}} + |p_h|_{s_h} + \|p - p_h\|_Q \lesssim \mu^{\frac{1}{2}} h^k \|\boldsymbol{u}\|_{k+1,\Omega} + \mu^{-\frac{1}{2}} h^{\tilde{l}} \|p\|_{\tilde{l},\Omega}. \tag{109}$$

If, in addition, $\boldsymbol{u}|_\Sigma \in [H^{k+1}(\Sigma)]^d$ and the regularity estimate (54) holds, we have

$$\|\boldsymbol{u} - \boldsymbol{u}_h\|_{0,\Omega} \lesssim c_\mu \big(\mu^{\frac{1}{2}} h^{k+1} \|\boldsymbol{u}\|_{r,\Omega} + \mu^{-\frac{1}{2}} h^{\tilde{l}+1} \|p\|_{\tilde{l},\Omega}\big) + \tilde{c}_\mu h^{k+1} \|\boldsymbol{u}\|_{k+1,\Sigma}. \tag{110}$$

Proof. The estimate (109) follows from Lemma B.2, standard interpolation theory and the consistency estimate (13). At last, (110) can be inferred from Lemma B.4, the estimate (109) and standard interpolation theory. $\diamondsuit$

References

[1] M. Astorino and C. Grandmont. Convergence analysis of a projection semi-implicit coupling scheme for fluid-structure interaction problems. *Numer. Math.*, 116:721–767, 2010.

[2] S. Badia, F. Nobile, and C. Vergara. Fluid-structure partitioned procedures based on Robin transmission conditions. *J. Comp. Phys.*, 227:7027–7051, 2008.

[3] S. Badia, A. Quaini, and A. Quarteroni. Splitting methods based on algebraic factorization for fluid-structure interaction. *SIAM J. Sci. Comput.*, 30(4):1778–1805, 2008.

[4] R. Becker and M. Braack. A finite element pressure gradient stabilization for the Stokes equations based on local projections. *Calcolo*, 38(4):173–199, 2001.

[5] D. Braess. *Finite elements.* Cambridge University Press, 2007.

[6] F. Brezzi and J. Pitkäranta. On the stabilization of finite element approximations of the Stokes equations. In *Efficient solutions of elliptic systems (Kiel, 1984)*, volume 10 of *Notes Numer. Fluid Mech.*, pages 11–19. Vieweg, 1984.

[7] E. Burman and M.-A. Fernández. Stabilized explicit coupling for fluid-structure interaction using Nitsche's method. *C. R. Math. Acad. Sci. Paris*, 345(8):467–472, 2007.

[8] E. Burman and M.-A. Fernández. Galerkin finite element methods with symmetric pressure stabilization for the transient Stokes equations: stability and convergence analysis. *SIAM J. Numer. Anal.*, 47(1):409–439, 2008.

[9] E. Burman and M.-A. Fernández. Stabilization of explicit coupling in fluid-structure interaction involving fluid incompressibility. *Comput. Methods Appl. Mech. Engrg.*, 198(5-8):766–784, 2009.

[10] E. Burman and P. Hansbo. Edge stabilization for the generalized Stokes problem: a continuous interior penalty method. *Comput. Methods Appl. Mech. Engrg.*, 195(19-22):2393–2410, 2006.

[11] P. Causin, J.-F. Gerbeau, and F. Nobile. Added-mass effect in the design of partitioned algorithms for fluid-structure problems. *Comput. Methods Appl. Mech. Engrg.*, 194(42–44):4506–4527, 2005.

[12] P.G. Ciarlet. *Mathematical elasticity. Vol. I*, volume 20 of *Studies in Mathematics and its Applications.* North-Holland, 1988.

[13] R. Codina and J. Blasco. A finite element formulation for the Stokes problem allowing equal velocity-pressure interpolation. *Comput. Methods Appl. Mech. Engrg.*, 143(3-4):373–391, 1997.

[14] Q. Du, M. D. Gunzburger, L. S. Hou, and J. Lee. Analysis of a linear fluid-structure interaction problem. *Discrete Contin. Dyn. Syst.*, 9(3):633–650, 2003.

[15] Q. Du, M.D. Gunzburger, L.S. Hou, and J. Lee. Semidiscrete finite element approximations of a linear fluid-structure interaction problem. *SIAM J. Numer. Anal.*, 42(1):1–29, 2004.

[16] A. Ern and J.-L. Guermond. *Theory and practice of finite elements*, volume 159 of *Applied Mathematical Sciences.* Springer, 2004.

[17] M.-A. Fernández. Coupling schemes for incompressible fluid-structure interaction: implicit, semi-implicit and explicit. *SēMA J.*, (55):59–108, 2011.

[18] M.-A. Fernández. Incremental displacement-correction schemes for the explicit coupling of a thin structure with an incompressible fluid. *C. R. Math. Acad. Sci. Paris*, 349(7-8):473–477–104, 2011.

[19] M.-A. Fernández, J.-F. Gerbeau, and C. Grandmont. A projection algorithm for fluid-structure interaction problems with strong added-mass effect. *C. R. Math. Acad. Sci. Paris*, 342(4):279–284, 2006.

[20] M.-A. Fernández, J.F. Gerbeau, and C. Grandmont. A projection semi-implicit scheme for the coupling of an elastic structure with an incompressible fluid. *Int. J. Num. Meth. Engrg.*, 69(4):794–821, 2007.

[21] M.-A. Fernández and J. Mullaert. Displacement-velocity correction schemes for incompressible fluid-structure interaction. *C. R. Math. Acad. Sci. Paris*, 349(17-18):1011–1015, 2011.

[22] G.J. Fix, M.D. Gunzburger, and J.S. Peterson. On finite element approximations of problems having inhomogeneous essential boundary conditions. *Comput. Math. Appl.*, 9(5):687–700, 1983.

[23] L. Formaggia, A. Quarteroni, and A. Veneziani, editors. *Cardiovascular Mathematics. Modeling and simulation of the circulatory system*, volume 1 of *Modeling, Simulation and Applications*. Springer, 2009.

[24] C. Förster, W.A. Wall, and E. Ramm. Artificial added mass instabilities in sequential staggered coupling of nonlinear structures and incompressible viscous flows. *Comput. Methods Appl. Mech. Engrg.*, 196(7):1278–1293, 2007.

[25] L.P. Franca and R. Stenberg. Error analysis of Galerkin least squares methods for the elasticity equations. *SIAM J. Numer. Anal.*, 28(6):1680–1697, 1991.

[26] M. Gee, E. Ramm, and W.-A. Wal. Parallel multilevel solution of nonlinear shell structures. *Comput. Methods Appl. Mech. Engrg.*, 194(21-24):2513–2533, 2005.

[27] V. Girault and P.-A. Raviart. *Finite element methods for Navier-Stokes equations.* Springer, 1986.

[28] J. L. Guermond, P. Minev, and J. Shen. An overview of projection methods for incompressible flows. *Comput. Methods Appl. Mech. Engrg.*, 195(44-47):6011–6045, 2006.

[29] G. Guidoboni, R. Glowinski, N. Cavallini, and S. Canic. Stable loosely-coupled-type algorithm for fluid-structure interaction in blood flow. *J. Comp. Phys.*, 228(18):6916–6937, 2009.

[30] G. Guidoboni, R. Glowinski, N. Cavallini, S. Canic, and S. Lapin. A kinematically coupled time-splitting scheme for fluid-structure interaction in blood flow. *Appl. Math. Lett.*, 22(5):684–688, 2009.

[31] M.D. Gunzburger and S.L. Hou. Treating inhomogeneous essential boundary conditions in finite element methods and the calculation of boundary stresses. *SIAM J. Numer. Anal.*, 29(2):390–424, 1992.

[32] P. Hansbo. Nitsche's method for interface problems in computational mechanics. *GAMM-Mitt.*, 28(2):183–206, 2005.

[33] J.G. Heywood and R. Rannacher. Finite-element approximation of the nonstationary Navier-Stokes problem. IV. Error analysis for second-order time discretization. *SIAM J. Numer. Anal.*, 27(2):353–384, 1990.

[34] T.J.R. Hughes, L.P. Franca, and M. Balestra. A new finite element formulation for computational fluid dynamics. V. Circumventing the Babuška-Brezzi condition: a stable Petrov-Galerkin formulation of the Stokes problem accommodating equal-order interpolations. *Comput. Methods Appl. Mech. Engrg.*, 59(1):85–99, 1986.

[35] P. Le Tallec and S. Mani. Numerical analysis of a linearised fluid-structure interaction problem. *Numer. Math.*, 87(2):317–354, 2000.

[36] P. Le Tallec and J. Mouro. Fluid structure interaction with large structural displacements. *Comput. Meth. Appl. Mech. Engrg.*, 190:3039–3067, 2001.

[37] D.P. Mok, W.A. Wall, and E. Ramm. Partitioned analysis approach for the transient, coupled response of viscous fluids and flexible structures. In W. Wunderlich, editor, *Proceedings of the European Conference on Computational Mechanics*. ECCM'99, TU Munich, 1999.

[38] F. Nobile and C. Vergara. An effective fluid-structure interaction formulation for vascular dynamics by generalized Robin conditions. *SIAM J. Sci. Comput.*, 30(2):731–763, 2008.

[39] S. Piperno and P.E. Bournet. Numerical simulations of wind effects on flexible civil engineering structures. *Rev. Eur. Élém. Finis*, 8(5–6):659–687, 2001.

[40] O. Pironneau, F. Hecht, A. Le Hyaric, and J. Morice. Freefem++, `www.freefem.org/ff++`.

[41] A. Quaini and A. Quarteroni. A semi-implicit approach for fluid-structure interaction based on an algebraic fractional step method. *Math. Models Methods Appl. Sci.*, 17(6):957–983, 2007.

[42] A. Quarteroni and A. Valli. *Numerical Approximation of Partial Differential equations*. Springer, 1997.

Contents